التحليل اللاخطي للأعتاب الخرسانية المسبقة الجهد تحت تأثير الأحمال المركبة لقوى القص والالتواء

رسالة

مقدمة إلى كلية الهندسة في جامعة بابل و هي جزء من متطلبات

نيل درجة ماجستير علوم في الهندسة المدنية

من قبل

أمير طعمه كمال بيعي

بكالوريوس هندسة مدنية ٢٠٠٢

إشراف

أ.م.د. مصطفى بلاسم داود

أ.م.د. نمير عبد الأمير علوش

كانون الأول

٢٠٠٥

Nonlinear Analysis of Prestressed Concrete Beams Subjected to Combined Shear and Torsion

A Thesis

Submitted to the College of Engineering of University of Babylon

in Fulfillment of Partial the Requirements for the Degree of

Master of Science in Civil Engineering

by

Amir Toama Kemal Baiee

B.Sc. in Civil Engineering (٢٠٠٢)

supervised by

Asst. Prof. Dr. Mustafa B. Dawood

Asst. Prof. Dr. Nameer A. Alwash

December

٢٠٠٥

الخلاصة

خصصت هذه الدراسة لبحث سلوك الأعتاب الخرسانية مسبقة الجهد والمعرضة إلى عزوم اللي والأحمال المركبة من قوى القص,الانحناء والالتواء باستخدام نموذج التحليل اللاخطي ثلاثي الأبعاد باستخدام طريقة العناصر المحددة.

تم تمثيل الخرسانة باستخدام عناصر طابوقية ثلاثية الأبعاد ذات العشرين عقدة، أما قضبان التسليح المسبقة الجهد والاعتيادية فقد تم تمثيلها كعناصر محورية مطمورة داخل العنصر الطابوقي للخرسانة، مع فرض وجود ترابط تام بين الخرسانة وحديد التسليح. تأثير الإجهاد المسبق على الخرسانة ادخل على شكل إجهاد وانفعال فعال في نقاط حديد التسليح المسبق الجهد. سلوك الخرسانة تحت تأثير اجهادات الانضغاط تم تمثيله بنموذج مرن - لدن يتبعه تصرف لدن تام ينتهي عند بداية تهشم الخرسانة. بينما سلوك الخرسانة تحت تأثير اجهادات الشد فقد مثل باستخدام نموذج الشق المنتشر والذي يكون عموديا على محاور الإجهاد الرئيسية مع اعتماد نموذج تصلب الشد لتمثيل الاجهادات المتبقية، نموذج بقاء القص لتمثيل تدهور مقاومة القص نتيجة التشقق، ونموذج التطرية لتمثيل الانخفاض الحاصل في مقاومة الخرسانة نتيجة التشققات المتعامدة.

تم حل معادلات التوازن اللاخطية باستخدام طريقة تزايدية - تكرارية اعتمادا على طريقة نيوتن - رافسون المعدلة. تمت التكاملات العددية باستخدام قاعدة التكامل المختزلة ذات الخمسة عشر نقطة.

تم تحليل العديد من الأعتاب الخرسانية المسبقة الجهد المعرضة إلى عزوم اللي والأحمال المركبة من قوى القص, الانحناء والالتواء. أظهرت نتائج التحليل توافق جيد مع النتائج العملية بالنسبة لعزم اللي بفارق يتراوح بين (% ٠.٥- %٨.٤). تم إجراء دراسات لبحث تأثير معاملات مختلفة على سلوك الأعتاب. كذلك تم دراسة تأثير كمية حديد التسليح المسبق الجهد والاعتيادي الطولي والعرضي و تأثير الحمل المركز(P) على سعة عزم اللي (T). بينت النتائج أن لا تأثير للحمل المركز (P) على السعة القصوى لعزم اللي (T) عندما تكون نسبة الحمل المركز إلى عزم اللي (T/P) اكبر أو تساوي (٢).

Abstract

This study is conducted to investigate the behavior of prestressed concrete beams subjected to pure torsion and combined loads of shear, bending and torsion using three dimensional nonlinear finite element analysis. The concrete was modeled by ٢٠-noded isoparametric brick elements, while the prestressing and ordinary bars were modeled as axial members embedded within the brick element of concrete, with assuming a perfect bond between the concrete and reinforcement. The effect of prestressing is introduced as effective stress and strain at the sampling points of prestressing steel.

An elasto-plastic work hardening model followed by a perfectly plastic response, which terminated at the onset of crushing has been considered to simulate the behavior of concrete in compression. The behavior of concrete in tension is simulated by a smeared crack model with fixed orthogonal cracks in connection with using a tension stiffening model to account for the retained post-cracking stresses, shear retention model to account for the reduced shear modulus, and a softening model to account for the reduction in compressive strength due to orthogonal cracks.

An incremental-iterative technique based on the modified Newton-Raphson method has been considered to solve the nonlinear equations of equilibrium. The numerical integration has been carried out using the reduced integration ١٥b-point Gaussian rule.

Many prestressed concrete beams subjected to pure torsion and combined shear, bending and torsion loads have been analyzed. The results of the analysis shows a good agreement with the available experimental results with difference (٠.٥٪ - ٨.٤٪) for ultimate torque.

Parametric studies are implemented to study the effect of some important finite element and material parameters. Also, the effect of amount of prestressing, longitudinal, and transverse steel and the torque (T) to transverse load (P) ratio are carried out. The results explain that the effect of transverse load (P) on the ultimate torque capacity (T) is negligible for (T/P) ratio equal to or above (٢).

Acknowledgement

I would like to express my sincere thanks and gratitude to my supervisors ***Dr. Mustafa B. Dawood*** and ***Dr. Nameer A. Alwash*** for their valuable advices, and guidance throughout the research work. Thanks are also expressed for the head of civil engineering department ***Dr. Ammar Y. Ali*** and the staff of civil engineering department for their appreciable assistance.

Special thanks are also extended for ***Dr. Ihsan A. Al-Shaarbaf*** for his useful information and consistent help.

Finally, special thanks are devoted to ***my family*** for their care, encouragement and assistance during this work.

Amir Toama Kemal Baiee

٢٠٠٥

CONTENT

Chapter Three : Finite Element Method and Nonlinear Solution Technique

Chapter Four : Modeling of Material Properties

Chapter Five : Applications, Results, and Discussion

Chapter Six : Conclusions and Recommendations for Future Works

NOTATION AND SYMBOLS

The major part of the symbols used in the text is listed below, others are defined with their equations where they first appear.

General Symbols

$[A]^T$,$\{a\}^T$	Transpose of matrix [A] and vector {a}.
$[A]^{-1}$	Inverse of matrix [A].
d, ∂	Differential symbols.
$\|\ \|$, det	Determinate of matrix or absolute value.
Δ	Denotes incremental quantity.
{ }	Vector.
[ ]	Matrix.

Scalar

A_l	Area of ordinary longitudinal reinforcing steel bar.
A_{ps}	Area of prestressing steel.
A_o	Area enclosed by the shear flow path.
A_v	Area of ordinary transverse reinforcing steel bar.
C_p	Plasticity coefficient.
$d\lambda$	Plastic multiplier.
E_c	Modulus of elasticity of concrete.
E_{ps}	Modulus of elasticity of prestressing steel.
E_s	Modulus of elasticity of ordinary steel bar.
f	Function.
f_c'	Uniaxial compressive strength of concrete.
f_{py}	Yield strength of prestressing bar.
f_r	Modulus of rupture of concrete.
f_t	Uniaxial tensile strength of concrete.
f_y	Yield strength of ordinary steel bar.
G	Shear modulus of concrete.

H'	Hardening parameter.
I_1	First stress invariant.
I_1'	First strain invariant.
J	Jacobian.
J_2	Second deviatoric stress invariant.
J_2'	Second deviatoric strain invariant.
l, m, n	Direction cosine of principal stresses.
k_1	Concrete compressive strength reduction parameter.
q	Shear flow path.
p	Perimeter of the center line of the stirrups.
P	Concentrated applied load.
S, C	Direction cosine of in-plane principal stresses.
s	Spacing of transverse reinforcement.
T	Applied torque.
T_c	Torsional moment contributed by concrete.
T_{cr}	Cracking torsional moment of concrete.
T_s	Torsional moment contributed by reinforcement bars.
T_n	Nominal torsional strength.
u, v, w	Displacement components.
V	Volume.
W	Weight of a sampling point.
X, Y, Z	Global coordinate system.
x, y, z	Local coordinate system.
x_1, y_1	Smaller and longer length of the stirrups.
α	Material parameter.
α_1, α_2	Tension stiffening parameters.
β	Shear retention factor or material constant.
γ	Shear strain.
$\gamma_1, \gamma_2, \gamma_3$	Shear retention parameters.
ε	Strain.

ε_{cu}	Ultimate strain of concrete.
ε_e	Elastic strain.
ε_o	Strain corresponding to peak Uniaxial concrete compressive stress.
$\boldsymbol{\varepsilon_o'}$	Total strain corresponding to the parabolic part of uniaxial compressive strength stress-strain curve.
ε_p	Plastic strain.
ε_{cr}	Uniaxial cracking strain.
$\lambda_١$	Compression strength reduction factor of concrete.
υ	Poisson's ratio.
σ	Stress.
$\boldsymbol{\sigma_o}$	Effective stress at onset of plastic deformation.
$\bar{\boldsymbol{\sigma}}$	Effective stress.
τ	Shear stress.
ξ,η,ζ	Natural coordinates system.

Matrices

[A]	Displacement gradient matrix of concrete element.
[B]	Strain-displacement matrix.
[D]	Material constitutive matrix.
[D$'$]	Constitutive matrix for steel bar.
[J]	Jacobian matrix.
[K]	Stiffness matrix of concrete element.
[K$'$]	Stiffness matrix of bar element.
[N]	Shape function of concrete element.
[T]	Transformation matrix.

Vectors

{a}	Nodal displacement or flow vector.
{B'}	Strain-displacement vector of the bar element.
{b}	Body forces.
{f}	External nodal forces.
{P}	Internal load vector.
{r}	Residual load vector.
{t}	Surface traction.
{u}	Displacement vector.
$\{\sigma\}$	Stress vector.
$\{\varepsilon\}$	Strain vector.

Subscripts and superscripts

c	Concrete.
cr	Cracking.
e	Elastic component.
ep	Elasto-plastic.
n	Number.
n`	Normal.
p	Plastic component.
s	Steel.
T	Tangential.
t	Tension.
y	Yielding.
x,y,z	Denotes Cartesian coordinate.
١,٢,٣	Denotes the principal directions.

Appendix A

This appendix presents the modifications in (**P٣DNFEA**) program that used to introduce the effect of prestressing and calculating the combination loads.

١.) Introduce the Effect of Prestressing :

```
C   READING THE INFORMATION OF PRESTRESSING TO INTRODUCED THE EFFECT
C     OF PRESTRESSING.
C   INPUT PRESTRESSING INDICATOR (PREST), WHEN (PREST) EQUAL ١ INPUT THE
C     EFFECT OF PRESTRESSING.
C     INPUT NUMBER OF G.P OF TENDONS (IGP).
C     INPUT NUMBER OF  INCREMENTS OF TENDONS STRESSES (INOT).
      READ (NIN,*) IGP, INOT , PREST
       WRITE (*,*) IGP, INOT , PREST
C     INPUT THE EFFECTIVE STRESS (FSE) OF PRESTRESSING TENDONS.
C     INPUT THE MODULUS OF ELASTICITY (EPS) OF PRESTRESSING TENDONS.
      READ (NIN,*) FSE, EPS
       WRITE (*,*) FSE, EPS
      DO ١٠ I = ١, IGP
      READ (NIN,*) GPOT(I)
       WRITE (*,*) GPOT(I)
١٠   CONTINUE

C     INPUT THE EFFECT OF PRETRESSING.
      IF (PREST .EQ. ١.٠) THEN
      DO ٩٥ I = ١, INOT
      IF (IINCS .EQ. I) THEN
      DO ١٠٠ K = ١,TOTGAS
      DO ١١٠ J = ١,IGP
      IF (K .EQ .GPOT(J)) THEN
       A١ = FSE
      STRSG (١,K) = A١*I
      B١ = A١*I / EPS
      STRNG (١,K) = B١
      ENDIF
       WRITE (*,*) ' STRSG = ' STRSG (١,K) , ' STRNG = ' STRNG (١,K)
١١٠   CONTINUE
```

```
١٠٠  CONTINUE
     ENDIF
٩٥   CONTINUE
     ENDIF
```

٢.) Calculating the Combination Loads :

```
C     INPUT THE LOADS APPLIED ON THE PRESTRESED CONCRETE BEAM.
C    INPUT THE INDICATOR OF TORSION (ITOR), WHEN (ITOR) EQUAL ١ CALCULATED
C     THE TORSION MOMENT (TTOR).
C    INPUT THE INDICATOR OF CONCENTRATED LOAD (ICON), WHEN (ICON) EQUAL ١
C     CALCULATED THE CONCENTRATED LOAD (PLOD).
C     INPUT THE INITIAL VALUE OF TORSION MOMENT (TOR).
C     INPUT THE INITIAL VALUE OF CONCENTRATED LOAD (CONP).
      READ (NIN,*) ITOR , TOR , ICON , CONP
      INOT١ = INOT + ١.٠
      DO ١١٢٠ K = ١,TOTDOF
      IF (IINCS.LT. INOT١) THEN
      LOADS(K) = FACT(١) * ORLOAD(K)
      INLOAD(K) = NLOAD(K) + LOADS(K)
      ELSEIF (IINCS .LT. ٦٠) THEN
      LOADS(K) = FACT(٢) * ORLOAD(K)
      INLOAD(K) = INLOAD(K) + LOADS(K)
      ELSEIF (IINCS .LT. ١٠٠٠٠) THEN
      LOADS(K) = FACT(٣) * ORLOAD(K)
      INLOAD(K) = INLOAD(K) + LOADS(K)
      ENDIF
١١٢٠ CONTINUE

C     CALCULATED THE TORSION MOMENT  (TTOR).
      IF (ITOR .EQ. ١.٠) THEN
      IF (IINCS.LT. INOT١) THEN
      DTOR =FACT(١) * TOR
       TTOR = TTOR + DTOR
      ELSEIF (IINCS .LT. ٦٠) THEN
      DTOR = FACT(٢) * TOR
       TTOR = TTOR + DTOR
      ELSEIF (IINCS .LT. ١٠٠٠٠) THEN
      DTOR = FACT(٣) * TOR
       TTOR = TTOR + DTOR
```

```
      ENDIF
      ENDIF

C     CALCULATED THE CONCENTRATED LOAD (PLOD).
      IF (ICON .EQ. ١٠) THEN
      IF(IINCS .LT. INOT١)THEN
      TOT = FACT(١) * CONP
      TOTO = TOTO + TOT
      ELSEIF (IINCS .LT. ٦٠) THEN
      TOT = FACT(٢) * CONP
      TOTO = TOTO + TOT
      ELSEIF (IINCS .LT. ١٠٠٠٠) THEN
      TOT = FACT(٣) * CONP
      TOTO = TOTO + TOT
     ENDIF
      ENDIF
```

Certificate

We certify that this thesis titled ***"Nonlinear Analysis of Prestressed Concrete Beams Subjected to Combined Shear and Torsion"***, was prepared by ***Amir Toama Kemal Baiee*** under our supervision at University of Babylon as a fulfillment of the partial requirements for the Degree of Master of Science in Civil Engineering.

Supervisor

Signature :

Name : Dr. Mustafa B. Dawood

Date : / /٢٠٠٥

Supervisor

Signature :

Name: Dr. Nameer A. Alwash

Date : / /٢٠٠٥

Certification

We certify that we have read this thesis, titled ***"Nonlinear Analysis of Prestressed Concrete Beams Subjected to Combined Shear and Torsion"***, and as an examining committee examined the student ***Amir Toama Kemal Baiee*** in its contents and in what is considered with it, and that in our opinion it meets the standared of thesis for the Degree of Master of Science in Civil Engineering (Structure).

Signature :
Name : ***Asst. Prof. Dr. Mustafa B. Dawood***
Date : / / ٢٠٠٥
(Supervisor)

Signature :
Name : ***Asst. Prof. Dr. Nameer A. Alwash***
Date : / / ٢٠٠٥
(Supervisor)

Signature :
Name : ***Asst. Prof. Dr. Ammar Y. Ali***
Date : / / ٢٠٠٥
(Member)

Signature :
Name : ***Asst. Prof. Abdul Ridah Saleh***
Date : / / ٢٠٠٥
(Member)

Signature :
Name : ***Prof. Dr. Hisham M. Al-Hassani***
Date : / /
(Chairman)

Approval of Civil Engineering Department
Head of the Civil Engineering Department

Signature :
Name : ***Asst. Prof. Dr. Ammar Y. Ali***
Date : / / ٢٠٠٥

Approval of the Deanery of the College Engineering
Dean of the College Engineering

Signature :
Name :
Date : / / ٢٠٠٦

Chapter One

Introduction

١.١ General

Concrete is essentially a compression material. Its strength in tension is much lower than that in compression. The original concept of prestressing concrete is to introduce sufficient axial pre-compression in member so that all tension in concrete is eliminated in member at service load. Therefore, prestressing can be defined in general terms as the pre-loading of a structure before application of service loads, so as to improve its performance in specific ways [٣٨].

The amount of prestressing may be sufficient to complete elimination of tensile stresses in members at service load, this is defined as fully prestressing. The intermediate solution between fully prestressed concrete and ordinary reinforced concrete is partially prestressed concrete, in which the tensile stresses are not complete elimination but reduced at full service load. This permits some cracks to occur, thus ordinary steel must be used to control cracking. This type of prestressing reduces the initial camber (upward deflection) and also, reduces the cracks which may occur at the end zone of post-tensioned members and is more economical. All prestressed concrete members can be placed in one of two categories which are either pre-tensioned or post-tensioned [٣٨].

Torsion has a primary influence in many types of structures such as curved beam, spandrel beam, curved bridges and spiral staircase. Beams in practice are rarely loaded in torsion alone. If torsional moments exist, they generally accompany bending and shearing forces.

Interaction between torsion and shear occurs because both torsion and shear produce diagonal tension stresses in concrete beams. These stresses are additive on one face of the beam and subtractive on the other. Therefore, when a beam is subjected to both torsion and shear, diagonal tension cracking will generally occur at a torque less than the diagonal tension cracking in pure torsion, and at shear less than that which causes diagonal tension cracking if shear and moment only acted on the beam [٣٥].

For reinforced concrete members which fail in torsion or shear modes, the softening phenomenon of concrete compressive strength plays an important role on the overall behavior and ultimate capacity of these members. This phenomenon implies a reduction in the concrete compressive strength in presence of transverse strains [١٥].

The development of digital computers and numerical techniques made the finite element method a powerful analytical tool to investigate the behavior of prestressed concrete structures under different types of loading. In this method many aspects of behavior in prestressed concrete structures can be modeled rationally. These aspects include the nonlinear multiaxial material properties, changes in material properties after cracking, steel-concrete interface behavior, yielding of prestressing and ordinary steel bars and many other properties.

١.٢ Objectives and Scope

This study is devoted to investigate the behavior of prestressed concrete beams subjected to torsion and combined shear and torsion loads, using finite element method. To achieve this aim, modifications have been done on the finite element computer program **P٣DNFEA** (Program of ٣-Dimensional Nonlinear Finite Element Analysis), which was originally developed by Al-Shaarbaf [٧], to be applicable for analyzing prestressed concrete beams subjected to torsion and combined shear, bending and torsion loads. In the present study the material nonlinearity is considered while the geometrical nonlinearity is neglected. The cracking and crushing of concrete, plastic flow of concrete, steel-concrete interface, the degradation in compressive strength of concrete due to orthogonal cracks and yielding of reinforcement, have been considered.

Many applications have been considered to demonstrate the applicability of the adopted models by comparing the predicted results with the available experimental results. Parametric studies to investigate the effect of some important material properties and geometrical parameters are also considered.

١.٣ Layout of the Thesis

The thesis consists of ***six chapters***. A general introduction describing the prestressed concrete members under the torsional with shear load and the objective and scope of this thesis are presented in ***chapter one***.

Chapter two reviews the theories of torsion, and the previous investigation about the experimental and nonlinear finite element analysis of reinforced and prestressed concrete members under different types of loading.

The basic concepts of the finite element method and the derivation of the governing equilibrium equations using the principle of virtual displacements are presented in ***chapter three***. The ٢٠-noded brick element, the representation of concrete and steel, the integration rules, the incremental-iterative Newton-Raphson methods and nonlinear solution techniques are also presented in this chapter.

Chapter four deals with the material constitutive relationships of concrete, the concrete model which used to represent the behavior of concrete through different stages of loading, and the steel model.

The results of the analysis of prestressed concrete beams under pure torsion and combined shear and torsion, and the comparison with the available experimental results are presented in ***chapter five***. Parametric studies to investigate the effect of some important material properties and geometrical parameters are also presented in this chapter.

Chapter six summarizes the conclusions drawn from this research and the recommendations for future work.

Chapter Two

Review of Literature

٢.١ Introduction

This chapter reviews the theories of torsion used to predict the torsional strength of concrete beams. The previous experimental works of prestressed concrete beams subjected to flexural, torsion, and combined shear, bending and torsion loads were presented in this chapter.

The nonlinear finite element analysis of prestressed concrete beams subjected to flexural and torsion loads were also reviewed.

٢.٢ Torsion Theories

٢.٢.١ Skew Bending Theory

This theory that was initially proposed by **Lessig** in ١٩٥٩, had been widely used to compute the torsional capacity of reinforced concrete members. The basic characteristic of this approach is the formation of the skew failure surface which was initiated by a helical crack along three faces of the member. The ends of the helical crack were connected by a compression zone near the fourth face. The skew failure surface intersects both the closed stirrups and the longitudinal steel.

The assumption of this theory were, both stirrups and longitudinal steel yield at failure, the tensile strength of concrete was neglected, the spacing of the stirrups was constant within the failure zone, no external loads were presented within the failure zone, the effect of steel near the compression zone was neglected, and the shape of shear-compression zone was rectangular. Based on these assumptions the torsional strength can be determined by taking equilibrium of the free body about the axis of twist (internal torque equal to the external torque). The components of the internal torsion moment were the axial forces of the stirrups, the shear-compression face of concrete and the dowel forces of the longitudinal bars as shown in figure (٢-١).

The theory was extended and modified by **Hsu**, **Zia**, and **Gesund**. In ١٩٦٨, **Hsu** made a major contribution experimentally to the development of the skew bending theory as it stand in the **ACI ٣١٨-٨٩ code**. Hsu proposed the following expression to calculate the ultimate torque for the rectangular section :

$$T_n = T_c + \alpha_t \frac{x_1 . y_1}{s} A_t . f_{sy} \qquad \text{---------- (٢-١)}$$

$$\alpha_t = \frac{1}{3}\left(2 + \frac{y_1}{x1}\right) \quad \leq 1.5 \qquad \text{---------- (٢-٢)}$$

where :

T_c : Torque resisted by concrete.

α_t : Coefficient accounts for crack geometry.

x_1 : Shortest length of the stirrups.

y_1 : Longest length of the stirrups.

A_t : Area of transverse steel.

f_{sy} : Yield stress of transverse steel.

s : Spacing of stirrups.

(T_c) was taken equal to (٠.٤) of cracking torque (T_{cr}) [٣٩] hence :

$$T_c = 0.4\frac{x^2.y}{3}(0.85)f_r \qquad \text{---------- (٢-٣)}$$

where :

f_r : Modulus of rupture of concrete.

x,y : The cross sectional dimensions of concrete members.

For prestressed concrete members subjected to torsion, limited tests showed that the ultimate torsional strength can be expressed as the sum of the strengths contributed by the concrete and the web reinforcement, just as for non-prestressed members. The effect of prestress was to increase the contribution of the concrete to the ultimate torsional strength, while the contribution of the reinforcement remains unchanged. Then the ultimate torque for prestressed members can be expressed as [٣٨] :

$$T_n = T_c' + T_s \qquad \text{---------- (٢-٤)}$$

$$T_s = \alpha_t \frac{x_1.y_1}{s} A_t.f_y \qquad \text{---------- (٢-٥)}$$

where the terms of (T_s) were exactly as defined earlier for non-prestressed members, and (T_c`) is the torsional resistance of the concrete after cracking which can be expressed by the following expression :

$$T_c' = (\eta.x^2.y).6\sqrt{f_c'}\left(\sqrt{1+\frac{10f_{cc}}{f_c'}}-k\right) \qquad \text{---------- (٢-٦)}$$

$$k = (1-\frac{T_c}{T_{cr}}) = (1-\frac{0.133}{\eta}) \qquad \text{---------- (٢-٧)}$$

$$\eta = \frac{0.35}{0.75+(x/y)} \qquad \text{---------- (٢-٨)}$$

where :

η : Shape factor based on measured cracking torque.

f_{cc} : The average longitudinal prestress (P_e/A_c).

Then the total nominal resisting torque (T_n)for a rectangular prestressed member with web reinforcement is [٣٨] :

$$T_c = (\eta.x^2.y).6\sqrt{f_c'}(\sqrt{1+\frac{10\,f_{cc}}{f_c'}}-k)+\alpha_t.\frac{x_1.y_1}{s}A_t.f_y \qquad \text{---------- (٢-٩)}$$

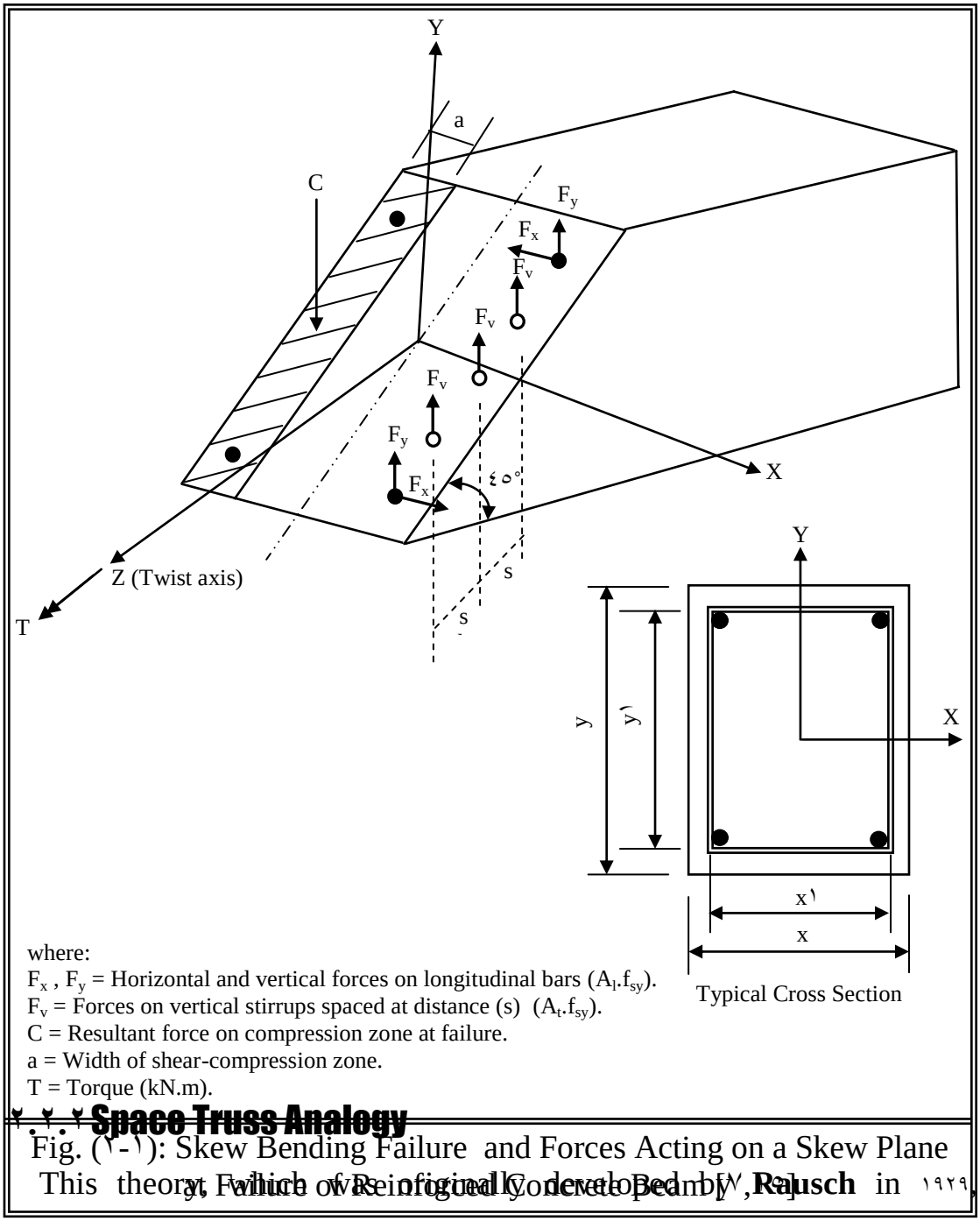

where:
F_x , F_y = Horizontal and vertical forces on longitudinal bars ($A_l.f_{sy}$).
F_v = Forces on vertical stirrups spaced at distance (s) ($A_t.f_{sy}$).
C = Resultant force on compression zone at failure.
a = Width of shear-compression zone.
T = Torque (kN.m).

Fig. (٢-١): Skew Bending Failure and Forces Acting on a Skew Plane of Failure of Reinforced Concrete Beam [٣٨].

٢.٢.٢ Space Truss Analogy

This theory, which was originally developed by **Rausch** in ١٩٢٩, assumed that a member with arbitrary solid cross-section was assumed to

act like a tube, so that the external torsional moment was resisted by circulatory shear flow in the wall of the tube. Each wall segment of the tube was assumed to act like a plane truss where the longitudinal bars served as a chord members while the stirrups and the concrete within the segment served as the web members. After cracking the concrete is separated by ٤٥-degrees cracks into a series of helical members. These helical concrete members were assumed to interact with the longitudinal and hoop steel bars to form a space truss as shown in figure (٢-٢). This figure illustrates that the torsion is resisted by the tangential component of the diagonal compression which produced a shear flow (q), around the perimeter. This shear flow (q) was related to the applied torque (T) by the equilibrium equation :

$$T = 2A_o.q \qquad \text{---------- } (٢\text{-}١٠)$$

where (A_o) is the area enclosed by the shear flow path (q).
The longitudinal component of the diagonal compression is balanced by tension in the longitudinal bars.

Lampert and **Thurlimann** in ١٩٦٨ proposed two modifications to the Rauschs approach. The first modification was that the crack inclination (θ) which was assumed equal to ٤٥-degrees by **Rausch** was assumed to be variable, hence the model is called the variable – angle truss model. Secondly, assumed that the perimeter connecting the centeriod of the corner longitudinal bars represent the centerline of the shear flow.

Collins and **Mitchell**, in ١٩٨٠ suggested thin-walled tube approach which represents an extension to the space truss analogy. This approach assume that the concrete cover outside the centerline of the stirrups provides the resistance of torsion by the outer skin of the cross section

roughly centered on the closed stirrups as shown in figure (٢-٣). The new **ACI ٣١٨M-٠٢ code** adopted the thin walled tube space truss analogy.

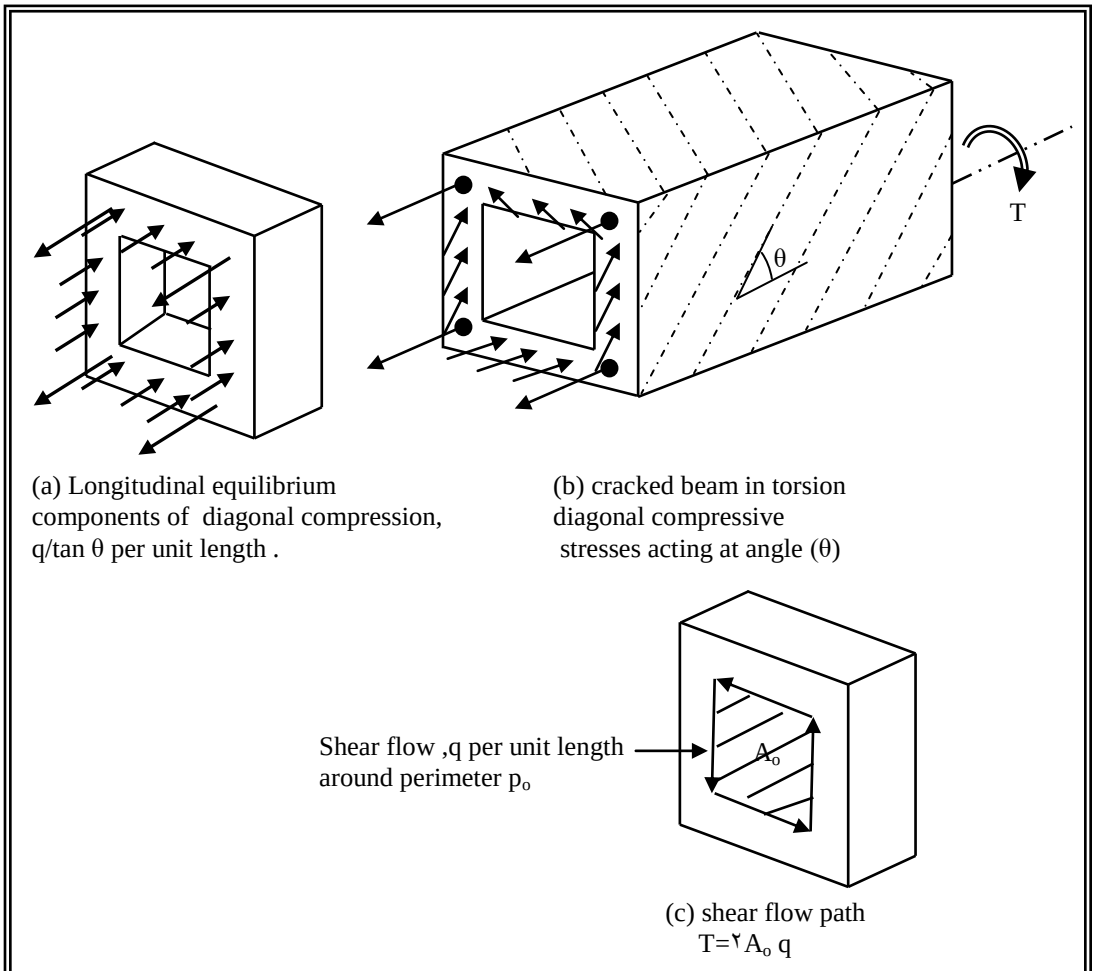

Fig. (٢-٢): Space Truss Model for Hollow Rectangular Reinforced Concrete Beam [١٢]

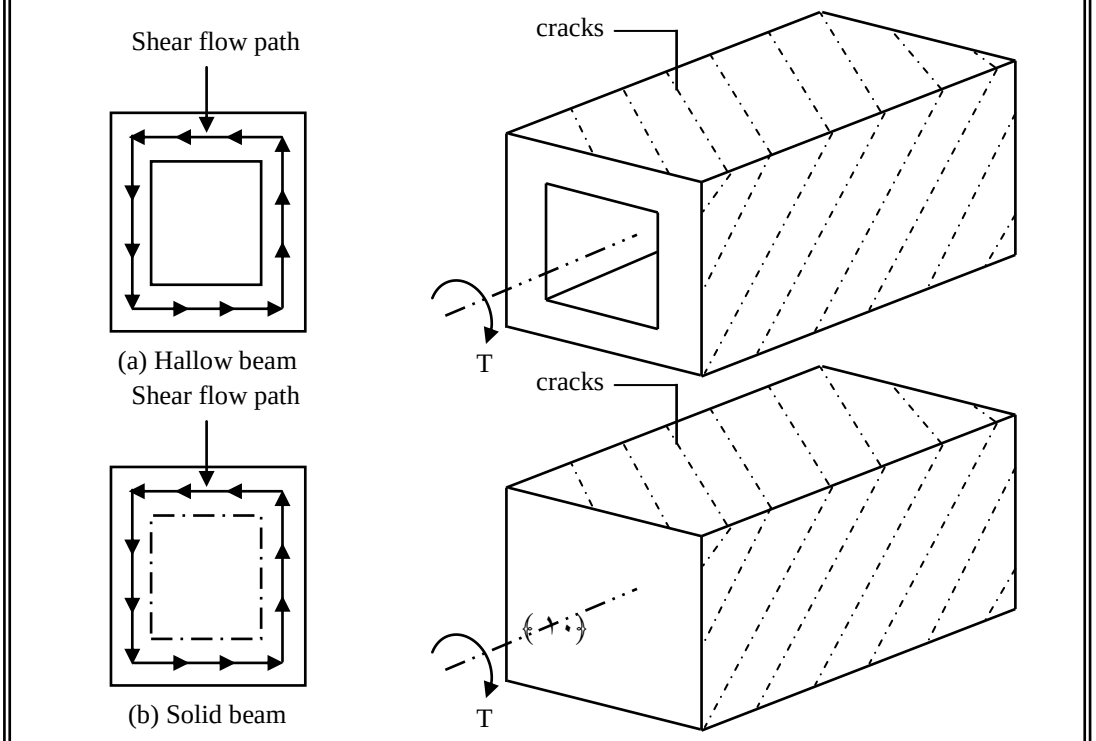

٢.٣ Experimental Works on Prestressed Concrete beams under Flexural Loads

In ١٩٥٦, **Janney et al.**, tested (١٩) rectangular beams, involving three pre-tension, three post-tensioned grouted, five post-tensioned unbonded, three post-tensioned unbonded with deformed bars and five conventional deformed bar reinforcement under flexural loads. The investigators concluded that the strengths of pretension and the corresponding post-tensioned bonded beams were nearly equal, and were (٢٠ to ٤٠) percent greater than the strength of the corresponding unbonded post – tensioned beams. It was believed that this increasing in strength is due to the bonding which varied with reinforcement percentage, magnitude of prestressing steel, beam span to depth ratio, and type of loading.

Study of the effects of non-prestressed steel on the behavior of prestressed concrete beams represented by **Shaikh and Branson** in ١٩٧٠. Effects of camber, loss of prestressing force, cracking, and deflection were included. Analytical results were compared with the observed results. Twelve rectangular simply supported pre-tension, prestressed concrete beams were tested, ten of which contained non tensioned steel. The study presented that the effect of non-prestressed steel in reducing time-dependent camber of prestressed concrete beams was similar to the effect of compressive reinforcement in reducing long-time deflections of ordinary reinforced concrete members.

A study of the structural performances of CFRP (Carbon Fiber Reinforced Polymer) tendon fully and partially prestressed beams were presented by **Yan et.al** in ٢٠٠٠. The study consist of testing five simply supported prestressed concrete beams with rectangular cross section under symmetrical two-points loading. The objectives of these tests to investigate the flexural behavior of these specimens and to compare the experimental results with the predicted values to validate the analytical model, and to give recommendations for (CFRP) prestressing design optimization by correlating different behavior of specimens sections, number of tendons (one or two layers), and prestressing patterns. Simple parametric study was performed to study the sensitivity of the model to change parameters and to determine the most efficient way to use the material.

٢.٤ Experimental Works on Prestressed Concrete beams under Pure Torsion

Humphreys, in ١٩٥٧, tested in pure torsion, (٩٤) rectangular prestressed concrete members of varying width to depth ratio from ١ to ٤, and without web reinforcement. Ninety of the specimens were prestressed by an unbonded central bar while the remain were eccentrically prestressed. The applied compression varied between specimens from zero to about ٧٥ percent of the cylinder compression strength f_c`. The results explain that

the torsional strength of prestressed concrete increased beyond the strength of plain concrete.

In ١٩٦١, **Zia**, reported tests on (٦٨) prestressed concrete members of rectangular T and I sections with and without web reinforcement, all beams tested in pure torsion and some of specimens were eccentrically prestressed. The results explain that under short time loads the ultimate torque capacity (T_c) of prestressed concrete members without web reinforcement was the same as that causing the formation of the first crack, and the ultimate torsional strength of prestressed members with web reinforcement was equal to the sum of the concrete torsional moment (T_c) and the torque resisted by the web reinforcement (T_s).

Six rectangular beams all with the same amount of hoop reinforcement but with varying amounts and types of longitudinal reinforcement the beams were tested in pure torsion by **Mitchell and Collins** in ١٩٧٨. The degree of prestressing of the tested beams ranging from zero (non-prestressed) to fully prestressed concrete beams. These tests study the effect of the longitudinal prestressing steel on the torsion response. The study presented that the thick-walled hollow prestressed members have the same torsional response as solid prestressed members. Otherwise, identical properties and the addition of longitudinal prestressing steel did not affect the pre-cracking torsional stiffness but it caused a significant increase in the post cracking torsional stiffness.

Hsu (١٩٨٥), tested (٨) prestressed concrete beams under pure torsion with various properties and presented a new theory to predict the ultimate torque of non-prestressed concrete members, and indicated that this theory can be broaden to include uniformly prestressed concrete by using

the concept of the decompression of concrete. This generalized theory was used to predict the torsional strength of prestressed concrete beams under pure torsion.

In ١٩٨٨**, Abul-Hasanat et al.**, carried out an experimental program on prestressed concrete beams containing a small circular transverse opening under torsion. Based on the familiar skew-bending model, strength equations were developed for axially and eccentrically prestressed beams with and without web reinforcement. Test result of ١٤ axially and eccentrically prestressed beams with two different opening diameter were presented. Introduction of web reinforcement in prestressed beams changes its brittle failure characteristic torque to ductile one and improves this torsional strength. Comparison of test results of axially and eccentrically prestressed beams shows that eccentric prestressing is more economical than axial prestressing.

٢.٥ Experimental Works on Prestressed Concrete beams under Combined Shear, Bending and Torsion

Cowan and Armstrong (١٩٥٧), reported tests on (١٢) rectangular beams without web reinforcements, post-tensioned by four unbounded bars, tested under different combinations of torsion, bending and shear. Three of the beams were non-prestressed, three uniformly prestressed and six eccentrically prestressed. It was concluded that for prestressed beams with relatively low bending moment / torque ratios, the cracking load

coincided with the ultimate load. Also, concluded that with higher bending moment / torque ratios the ultimate load was higher than that causing the formation of the first cracks.

Reported tests on (٤٢) T-beams without web reinforcement subjected to combined bending and torsion has been done by **Reeves** (١٩٦٢). The beams had constant height but varied flange width. Beams eccentrically post-tensioned by bonded (٥٠ mm) diameter wire. The results show that the ultimate twisting strength increased with the bending moment up to the cracking bending moment. Beyond this moment the twisting strength decreased but did not drop below the pure twisting strength until approximately ٨٠ percent of the ultimate bending moment is applied. The study illustrated that the variation of the torque and moment capacities by interaction diagram curves which given the relation between combined ultimate torque and moment and the pure ultimate moment and torque capacities.

Bishara, In ١٩٦٩, presented an experimental investigation on the behavior and ultimate capacity of prestressed concrete beams of rectangular, I and T cross sections, with web reinforcement, subjected to the combined action of torsion, bending, and shear. The elastic and the rupture criteria defined. Neither the cracking load nor the ultimate capacity could be satisfactorily predicted by Saint Venant`s elastic torsion theory and the principal stress criterion. The variation in the ultimate capacity for each group of beams having the same cross section was illustrated using non dimensional interaction curves. An empirical expression for calculating the pure torsional strength of prestressed

concrete members had been developed. For sections were the bending moment / shear value is constant an empirical expression have been developed to define the relation between torque and bending moment, torque and the shear at ultimate capacities.

Mukherjee and Warwaruk (١٩٧١), tested two sets of prestressed concrete beams each set grouped into four series within each series the beams had identical properties, and among series, only the prestress and its eccentricity were varied. The first set consisted of (٢٨) beams tested under different combinations of torsion and bending loads, while the second set consisted of (٢٤) beams tested under different combinations of shear, bending and torsion loads. It was concluded that the torsional reinforcement, composed of rectangular ties and longitudinal bars at the corners prevents a brittle type failure in prestressed concrete beams, and the initial torsional stiffness is practically unaffected by the level of prestressing, torque moment ratio and flexural shear.

Henry and Zia In ١٩٧٤, reported a tests of (٣٢) rectangular prestressed concrete beams with closed stirrups and longitudinal steel, under combined torsion, bending and shear loads. The beams grouped into four series, within each series four beams, with various torque to bending moment ratios and torque to shear ratios. The tests were carried out to find the load deflection and torque twist curve, failure modes, crack pattern, and the non dimensional interaction diagrams for both torque-bending and torque – shear. The results presented that prestressed concrete beams that subjected to torsion, bending and shear tend to fail in

one of two modes of skew bending. These were torsion mode and bending mode.

In ١٩٧٨**, Mattock and Wyss**, reported a tests of nine eccentrically prestressed concrete I-girders without web reinforcement, with the same cross sectional dimensions, and the magnitude of prestressing steel subjected to combined torsion, shear, and bending. The beams were divided into two groups according to bending moment to shear ratio (M/V). The primary objective of the tests were to determine the influence of the bending moment to shear ratio on the torsion-shear interaction relationship for diagonal tension cracking in I-section prestressed concrete girders. The results presented that the torsional and flexural stiffness of uncracked girder were not reduced in combined loading , and may be calculated with reasonable accuracy on the basis of the elastic theory.

٢.٦ Non-Linear Finite Element Analysis of Prestressed Concrete Beams under Flexural Load

In ١٩٨٠**, Young-Jan and Alexander**, presented a numerical method based on the finite element method for the material and geometric nonlinear analysis of plane prestressed concrete frames, including the time dependent effects of concrete and relaxation of prestressing steel. These models were capable of predicting the behavior of prestressed concrete frames, throughout service load history as well as throughout

elastic, inelastic and ultimate load range in one computer analysis. It was concluded that a Parabolic stress-strain curves were capable to simulate the behavior of concrete. While the behavior of reinforcing and prestressing steel can simulated by a bilinear and multi linear stress – strain curve.

Abdul- Rahman and Hinton (١٩٨٦), analyzed reinforced and prestressed concrete cellular slabs based on slab model by using linear and nonlinear two dimensional finite element models. The basic idea of this work was the separation of the cellular plate into main components, a hallow plate, representing the upper and lower flanges and stiffening beams representing the vertical webs between the voids. The voided slab cross sections were represented as different layered elements with assuming that the plane sections before deformation remain plane after deformation. The study presented that the load – deflection curves of both experimental and numerical tests were favorable, and good agreement exist between the measured and analytical values of the first cracking load.

A study on the behavior of reinforced and prestressed three dimensional multi-planer system were presented by **Ghalib** (١٩٩٠). The concrete was represented by assemblage of a set of isoparamertic layered ٨-noded flat shell elements. The behavior of concrete in compression was modeled as an elastic-plastic material with hardening and as elastic-brittle fracture in tension. A generally curved bonded/unbonded prestressing strand element embedded in the general ٨-noded shell element has been developed. An iterative incremental technique was adopted in the study to suit the nonlinear path-dependent response.

Harlt and Engamal in ٢٠٠٠, developed a finite element formulation based on three dimensional solid elements for concrete with embedded one dimensional elements in order to represent the reinforcement and tendons. The concrete is modeled as a plastic material, steel reinforcement and tendons were allowed to intersect the mesh in any arbitrary direction and their contribution to the stiffness matrix is superimposed on the respective parent elements. Prestress is considered with an iterative procedure by utilizing the load balancing concept. The bond slip or tendon sliding was modeled by introducing supplementary interface elements after the displacement field has been computed. It was concluded that the ordinary and prestressed concrete structures can be analyzed in two dimensional and three dimensional. in the two dimensional case, the program was limited to plane stress or plane strain problems.

In ٢٠٠٢**, Tawfieq**, used a three dimensional nonlinear finite element model for the analysis of fully and partially rectangular, I, and T prestressed concrete beams under flexure. The ٢٠-noded isoparametric brick element have been used to model the concrete, while the reinforcement was modeled as axial members embedded within the brick element assuming perfect bond between concrete and reinforcement. The behavior of concrete in compression was simulated by elasto-plastic work hardening model followed by perfectly plastic response which terminated at the onset of crushing. Fixed smeared crack model has been used to simulate the behavior of concrete in tension. The prestressing effect was

introduced as effective stresses and strains at sampling points of tendons and as an external prestressing forces at the ends of beam. The study presented that when the area of prestressing steel increased from (١٠٠ mm^2) to (١٦٠mm^2), the ultimate load capacity is increased by a bout (٢١.٨ %).

٢.٧ Non-Linear Finite Element Analysis of Prestressed Concrete beams under pure torsion

Shuber in ٢٠٠٢, investigated the behavior of prestressed concrete beams under pure torsion using a nonlinear three dimensional finite element model. A ٢٠-noded isoparametric brick elements have been used to model the concrete, while the reinforcing bars were idealized as axial members embedded within the concrete element. An elasto-plastic work hardening followed by perfect plastic response which terminated at the onset of crushing was proposed to simulate the behavior of concrete in compression while the behavior in tension was simulated by smeared crack model. The prestressing effect was introduces as an external prestressing forces at the ends of beam. It was concluded that the prestressed concrete beams without web reinforcement have a little ductility, and failure is sudden and violent. The introduce of web reinforcement improves ductility, as well as torsional strength.

From the previous sections, many investigations had been carried out to study the behavior of reinforced and prestressed concrete members under flexural loads or pure torsion. These studies had been based on either experimental work or numerical techniques. Little experimental works on studying the behavior of prestressed concrete beams subjected

to combined shear and torsion have been considered, as a compared with the experimental works of beams under flexural or pure torsion. Because these experimental tests were expensive, complex and involve two main problems; the difficulty in accounting for flexure and difficulty in eliminating the effect of local disturbances due to loads and supports [٤٠].

In the present study, three dimensional non-linear finite element analysis using ٢٠-noded brick element with three degrees of freedom at each node (u, v, w) to model the concrete and one dimensional element to model reinforcement, with assuming perfect bond between reinforcement and concrete have been considered to study the behavior of prestressed concrete beams subjected to pure torsion and combined shear and torsion. The effect of prestressing is introduced as an effective stress and strain at the sampling points of tendons, while **Shuber** introduced the effect of prestressing as external prestressing forces at the ends of the beam.

Chapter Three

Finite Element Method and Nonlinear Solution Technique

٣.١ Introduction

In finite element method, the continuum of infinite degrees of freedom is replaced by mathematical model which is an assembly of subdivisions of finite number of degrees of freedom called finite elements. These elements are connected together by a finite number of joints called nodes. The external loading is also transformed into equivalent forces applied at the nodes [١٥].

The nonlinear finite element approach can be used to predict the behavior of prestressed concrete structures at different stages of loading. This approach can be considered as a theoretical or more accurately a numerical laboratory to test the prestressed concrete members. The accuracy of this approach depends mainly on the suitable modeling of material properties of concrete and prestressing steel individually and on the shape, size, and number of elements. In the present study, ٢٠-noded isoparametric brick elements are used to idealize the concrete, while the reinforcement is idealized as axial one dimensional element embedded within the brick concrete element, assuming a perfect bond between concrete and reinforcement.

The formulation of the finite element, material representations, numerical integration and nonlinear solution techniques are presented in this chapter.

٣.٢ Finite Element Formulation

The governing equations of static equilibrium can be established by using the principle of virtual displacement. Consider a three –dimensional body subjected to external forces. These forces cause a displacement having components *u*, *v*, and *w* in the *x*, *y*, and *z* directions respectively.
The displacement vector at any point within the element $\{u\}^e$ can be expressed as :

$$\{u\}^e = [N] \ . \ \{a\}^e \qquad \text{---------- (٣-١)}$$

where *[N]* is a matrix containing the interpolation functions which relate the displacement $\{u\}^e$, to the nodal displacements, $\{a\}^e$, where $\{u\}^e$ is given by :

$$\{u\}^e = [u \quad v \quad w]^e \qquad \text{---------- (٣-٢)}$$

The corresponding strains, $\{\varepsilon\}^e$, are obtained by differentiation of the displacements :

$$\{\varepsilon\}^e = [A] \ \{u\}^e \qquad \text{---------- (٣-٣)}$$

where *[A]* is a matrix which contains the differential operators.

Substitution of equation (٣-١) into equation (٣-٣) yields :

$$\{\varepsilon\}^e = [B] \ \{a\}^e \qquad \text{---------- (٣-٤)}$$

where *[B]* is the strain-displacement matrix given by :

$$[B] = [A][N] \qquad \text{---------- (٣-٥)}$$

The stress-strain relationship is usually given by :

$$\{\sigma\}^e = [D]\{\varepsilon\}^e \qquad \text{---------- (٣-٦)}$$

where *[D]*, is the constitutive matrix, $\{\sigma\}^e$ is the stress vector and given by :

$$\{\sigma\}_e^{\mathrm{T}} = \begin{bmatrix} \sigma_x & \sigma_y & \sigma_z & \tau_{xy} & \tau_{yz} & \tau_{zx} \end{bmatrix} \qquad \text{---------- (٣-٧)}$$

and the $\{\varepsilon\}^{\mathrm{e}}$ is the strains vector given by :

$$\{\varepsilon\}^e = \begin{Bmatrix} \varepsilon_x \\ \varepsilon_y \\ \varepsilon_z \\ \gamma_{xy} \\ \gamma_{yz} \\ \gamma_{zx} \end{Bmatrix} = \begin{Bmatrix} \partial u/\partial x \\ \partial v/\partial y \\ \partial w/\partial z \\ \dfrac{\partial u}{\partial y} + \dfrac{\partial v}{\partial x} \\ \dfrac{\partial v}{\partial z} + \dfrac{\partial w}{\partial y} \\ \dfrac{\partial u}{\partial z} + \dfrac{\partial w}{\partial x} \end{Bmatrix} \qquad \text{---------- (٣-٨)}$$

substitution of equation (٣-٤) into equation (٣-٦) yields the stress-displacement relationship,

$$\{\sigma\}^e = [D][B]\{a\}^e \qquad \text{---------- (٣-٩)}$$

The principle of virtual displacements which has been used in the study states that , ***"a deformable body is in equilibrium if the total work done by all external forces minus the total work done by all internal forces during any kinematically admissible virtual displacement is zero"*** [١٤] . By considering the external work, W_{ext}, and the internal work, W_{int}, the principle can be written as :

$$\delta W_{int} - \delta W_{ext} = ٠ \qquad \text{---------- (٣-١٠)}$$

where δW_{int} is the internal work, and δW_{ext} is the external work.

By considering a system of volume (V) and surface area (S) subjected to body forces $\{b\}$ and surface forces $\{t\}$, the external work is expressed as :

$$\delta W_{ext} = \int_V \partial\{u\}^T \{b\}\, dV + \int_S \partial\{u\}^T \{t\}\, dS \qquad \text{---------- (٣-١١)}$$

the internal work can be expressed as :

$$\delta W_{\text{int}} = \int_V \partial\{\varepsilon\}^T \{\sigma\} dV \qquad \text{---------- (٣-١٢)}$$

substituting of equation (٣-٦) into equation (٣-١٢) yields :

$$\delta W_{\text{int}} = \int_V \partial\{\varepsilon\}^T [D]\{\varepsilon\} dV \qquad \text{---------- (٣-١٣)}$$

by substituting equation (٣-١١) and (٣-١٣) into equation (٣-١٠) yields :

$$\int_V \partial\{\varepsilon\}^T [D]\{\varepsilon\} dV - \int_V \partial\{u\}^T \{b\} dV - \int_S \partial\{u\}^T \{t\} dS = \{0\} \qquad \text{---------- (٣-١٤)}$$

this expression represents the equation of static equilibrium for a general body.

Substituting equation (٣-١) and (٣-٤) in equation (٣-١٤) yields :

$$\partial\{a\}^T \left[\sum_n \int_{V^e} [B]^T [D]\ [B] dV^e \{a\}^e - \sum_n \int_{V^e} [N]^T \{b\}^e dV^e - \sum_n \int_{S^e} [N]^T \{t\}^e dS^e \right] = \{0\}$$

(٣.١٥)

where (n) is the total number of elements of discrete system.

since, $\partial\{\mathrm{a}\}^{\mathrm{T}}$ is arbitrary, thus it may be canceled from both two sides of equation (٣-١٥) and yields the following expression :

$$\{\mathrm{f}\} = [\mathrm{K}]\ \{\mathrm{a}\} \qquad \text{---------- (٣-١٦)}$$

where, *[K]* is the stiffness matrix of the element assemblage which is formed by systematic addition of the element stiffness matrices, and is given by :

$$[K]=\sum_{n}\int_{V^e}[B]^T[D]\ [B]dV^e \qquad \text{---------- (٣-١٧)}$$

{a} is the corresponding element assemblage nodal displacement vector, and *{f}* is the element assemblage of external nodal force vector. The body force vector and the surface traction vector are calculated by direct addition of element body forces vector and the element surface traction vectors as shown in the following expression [٧].

$$\{f\}=\sum_{n}\int_{V^e}[N]^T\{b\}^e dV^e+\sum_{n}\int_{S^e}[N]^T\{t\}^e dS^e \qquad \text{---------- (٣-١٨)}$$

٣.٣ Material Representation

In the present study, concrete is simulated by isoparametric ٢٠-noded brick elements, while the prestressing steel bars and ordinary reinforcement are modeled by using one-dimensional bar elements.

٣.٣.١ Concrete Idealization

In this study concrete is modeled by using ٢٠-noded isoparametric brick element as shown in figure (٣-١a); the major advantage of using ٢٠-noded brick element is that the warping displacement of the beam cross section can be adequately approximated with fewer elements. The element sides are defined in the local coordinate system by ($\xi=\pm١$, $\zeta=\pm١$,

and $\eta=\pm$١) and the origin of the local coordinate system is the center of the element as shown in figure (٣-١b) [٧].

Each nodal point has three degrees of freedom of movement (*u, v,* and *w*) along the Cartesian coordinates (*x, y,* and *z*), respectively. The element coordinate and displacement field within the element is defined in terms of the shape functions and displacement values at the nodes.

The displacement field is given by :

$$\left.\begin{aligned} u(\xi,\eta,\zeta) &= \sum_{i=1}^{20} N_i(\xi,\eta,\zeta).u_i \\ v(\xi,\eta,\zeta) &= \sum_{i=1}^{20} N_i(\xi,\eta,\zeta).v_i \\ w(\xi,\eta,\zeta) &= \sum_{i=1}^{20} N_i(\xi,\eta,\zeta).w_i \end{aligned}\right\} \qquad \text{---------- (٣-١٩)}$$

where *Ni (ξ,η,ζ)* represents the shape function in the local coordinates ξ, η, and ζ at the node (*i*) at which the nodal displacements at (*x, y,* and *z*) coordinates are u_i, v_i and w_i respectively. The value of (*i*) range from one to twenty. The shape functions of the ٢٠-noded brick element, are given in Table (٣-١).

The global coordinates in terms of the natural coordinates are given by :

$$\left.\begin{aligned} x(\xi,\eta,\zeta) &= \sum_{i=1}^{20} N_i(\xi,\eta,\zeta).x_i \\ y(\xi,\eta,\zeta) &= \sum_{i=1}^{20} N_i(\xi,\eta,\zeta).y_i \\ z(\xi,\eta,\zeta) &= \sum_{i=1}^{20} N_i(\xi,\eta,\zeta).z_i \end{aligned}\right\} \qquad \text{---------- (٣-٢٠)}$$

where x_i, y_i and z_i are the nodal coordinates.

By substituting equation (٣-١٩) into equation (٣-٨), the strain fields vector $\{\varepsilon\}$ can be expressed by the following expression :

$$\begin{Bmatrix} \varepsilon_x \\ \varepsilon_y \\ \varepsilon_z \\ \gamma_{xy} \\ \gamma_{yz} \\ \gamma_{zx} \end{Bmatrix} = \sum_{i=1}^{20} \begin{bmatrix} \frac{\partial N_i}{\partial x} & 0 & 0 \\ 0 & \frac{\partial N_i}{\partial y} & 0 \\ 0 & 0 & \frac{\partial N_i}{\partial z} \\ \frac{\partial N_i}{\partial y} & \frac{\partial N_i}{\partial x} & 0 \\ 0 & \frac{\partial N_i}{\partial z} & \frac{\partial N_i}{\partial y} \\ \frac{\partial N_i}{\partial z} & 0 & \frac{\partial N_i}{\partial x} \end{bmatrix} \begin{Bmatrix} u_i \\ v_i \\ w_i \end{Bmatrix} \quad \text{---------- (٣-٢١)}$$

The shape functions, (N_i) can be expressed in either local or global coordinate systems . The derivatives of the brick shape functions can be given by the usual chain rule :

$$\begin{bmatrix} \frac{\partial N_i}{\partial \xi} \\ \frac{\partial N_i}{\partial \eta} \\ \frac{\partial N_i}{\partial \zeta} \end{bmatrix} = \begin{bmatrix} \frac{\partial x}{\partial \xi} & \frac{\partial y}{\partial \xi} & \frac{\partial z}{\partial \xi} \\ \frac{\partial x}{\partial \eta} & \frac{\partial y}{\partial \eta} & \frac{\partial z}{\partial \eta} \\ \frac{\partial x}{\partial \zeta} & \frac{\partial y}{\partial \zeta} & \frac{\partial z}{\partial \zeta} \end{bmatrix} \cdot \begin{bmatrix} \frac{\partial N_i}{\partial x} \\ \frac{\partial N_i}{\partial y} \\ \frac{\partial N_i}{\partial z} \end{bmatrix} \quad \text{---------- (٣-٢٢)}$$

$$\begin{bmatrix} \frac{\partial N_i}{\partial \xi} \\ \frac{\partial N_i}{\partial \eta} \\ \frac{\partial N_i}{\partial \zeta} \end{bmatrix} = [J] \cdot \begin{bmatrix} \frac{\partial N_i}{\partial x} \\ \frac{\partial N_i}{\partial y} \\ \frac{\partial N_i}{\partial z} \end{bmatrix} \quad \text{---------- (٣-٢٣)}$$

where *[J]* is known as the Jacobean matrix.

Then, the shape function derivatives with respect to (*x, y,* and *z*) can be obtained by :

$$\begin{Bmatrix} \partial N_i/\partial x \\ \partial N_i/\partial y \\ \partial N_i/\partial z \end{Bmatrix} = [J]^{-1} \begin{Bmatrix} \partial N_i/\partial \xi \\ \partial N_i/\partial \eta \\ \partial N_i/\partial \zeta \end{Bmatrix} \qquad \text{---------- (٣-٢٤)}$$

Hence the element stiffness matrix in terms of local coordinates can be written as :

$$[k]^e = \int_{-1}^{1}\int_{-1}^{1}\int_{-1}^{1} [B]^T.[D].[B]|J|.d\xi.d\eta.d\zeta \qquad \text{---------- (٣-٢٥)}$$

The element stiffness matrix $[K]^e$ can be evaluated numerically by the numerical integration.

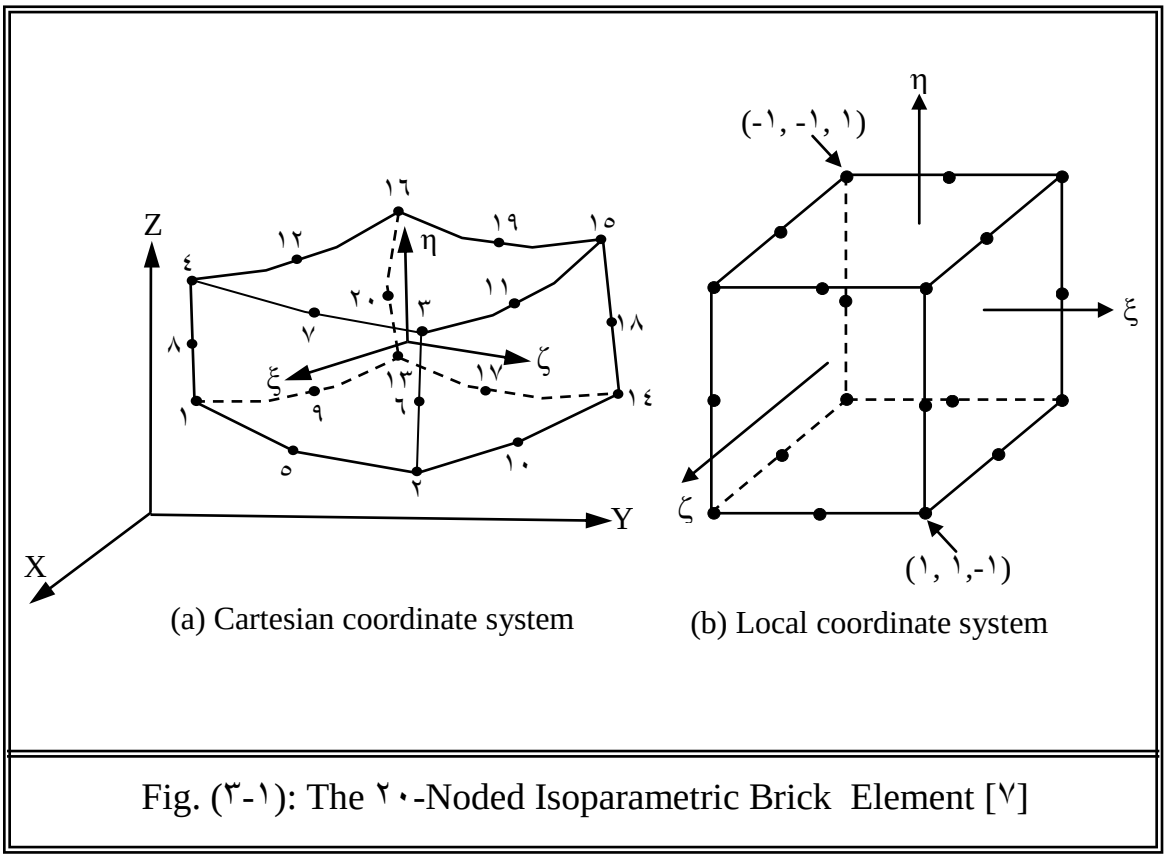

(a) Cartesian coordinate system (b) Local coordinate system

Fig. (٣-١): The ٢٠-Noded Isoparametric Brick Element [٧]

Table (٣-١) Shape Functions for the ٢٠-Nodded Brick Element [٧,١٥]

Nodes	***Shape function*** $N_i(\xi,\eta,\zeta)$
Corner nodes $\xi_i = \pm1, \eta_i = \pm1, \zeta_i = \pm1$	$\frac{1}{8}(1+\xi\xi_i)(1+\eta\eta_i)(1+\zeta\zeta_i)(\xi\xi_i+\eta\eta_i+\zeta\zeta_i-2)$
Mid side nodes $\xi_i = 0, \eta_i = \pm1, \zeta_i = \pm1$	$\frac{1}{4}(1-\xi^2)(1+\eta\eta_i)(1+\zeta\zeta_i)$
Mid side nodes $\xi_i = \pm1, \eta_i = 0, \zeta_i = \pm1$	$\frac{1}{4}(1+\xi\xi_i)(1-\eta^2)(1+\zeta\zeta_i)$
Mid side nodes $\xi_i = \pm1, \eta_i = \pm1, \zeta_i = 0$	$\frac{1}{4}(1+\xi\xi_i)(1+\eta\eta_i)(1-\zeta^2)$

ξ_i, η_i, ζ_i denote the coordinates of i-th node.

٣.٣.٢ Reinforcement Idealization

The analysis of prestressed concrete members by using the finite element method requires a simple representation to simulate the prestressing and ordinary bars in the finite element model. Three alternative representations for steel bars which have been usually used are discrete, distributed, and embedded representation [١٦].

In discrete representation the steel bars are replaced by a truss element that are connected to the concrete elements at the nodes. This approach allows to slip bar within the parent element and can use linkage element with this representation to account for the slip. However, this increases the number of degrees of freedom per element.

In distributed representation the bars are assumed as a two-dimensional membrane layer of equivalent thickness. The bars are assumed to resist axial force only in the bar direction and assumed a perfect bond between steel and concrete. This representation is suitable for homogenous distributed reinforcement.

The current study adopts the embedded representation in which the bar element is assumed to be built in the parent brick element so that the displacement of two types of element (concrete and steel) are to be consistent, the steel bars are capable to transmitting axial force only with assumed perfect bond between concrete and reinforcement. The major advantage of this representation is that the steel bars can be placed in their correct positions without imposing any restrictions on mesh choice, and hence the finite element analysis can be carried out with a smaller number of elements, as compared to the discrete representation. The three types of reinforcement representation are shown in figure (٣-٢).

Assuming a bar element is embedded in the brick element, as shown in figure (٣-٢c), parallel to ξ and has a position $\eta = \eta_i$ and $\zeta = \zeta_i$, the shape function of the brick element can be used to represent the displacement of the bar element as follows [٧] :

$$\left.\begin{aligned} u &= \sum_{i=1}^{20} N_i(\xi) u_1 \\ v &= \sum_{i=1}^{20} N_i(\xi) v_1 \\ w &= \sum_{i=1}^{20} N_i(\xi) w_1 \end{aligned}\right\} \qquad \text{---------- (٣-٢٦)}$$

where (i) is equal to ١ and ٢ in the embedded steel representation. Since, the bar is capable of transmitting axial forces only, one component of strain contributes to the strain energy [٨]. The strain-displacement relationship is given by [٧,٨] :

$$\{\varepsilon\} = \sum_{i=1}^{20} \left[\frac{1}{h^2} \begin{bmatrix} c_1 & c_2 & c_3 \\ c_2 & c_4 & c_5 \\ c_3 & c_5 & c_6 \end{bmatrix} \cdot \begin{bmatrix} \frac{\partial N_i}{\partial x} \\ \frac{\partial N_i}{\partial y} \\ \frac{\partial N_i}{\partial z} \end{bmatrix} \right] \cdot \begin{bmatrix} u_i \\ v_i \\ w_i \end{bmatrix} \quad \text{---------- (٣-٢٧)}$$

where :

$$C_1 = (\partial x/\partial \xi)^2, C_2 = (\partial x/\partial \xi)(\partial y/\partial \xi),$$
$$C3 = (\partial x/\partial \xi)(\partial z/\partial \xi), C_4 = (\partial y/\partial \xi)^2,$$
$$C_5 = (\partial y/\partial \xi)(\partial z/\partial \xi), C_6 = (\partial z/\partial \xi)^2$$

$$\mathrm{h} = \sqrt{\mathrm{C}_1^2 + \mathrm{C}_4^2 + \mathrm{C}_6^2} \quad \text{---------- (٣-٢٨)}$$

finally, equation (٣-٢٧) may be rewritten in form :

$$\{\varepsilon'\} = [\mathrm{B}'].\{\mathrm{a}\}^{\mathrm{e}} \quad \text{---------- (٣-٢٩)}$$

The stiffness matrix of an axially loaded bar element may be expressed as

$$[K'] = \int_{V^e} [B']^T . [D'][B'] dV \quad \text{---------- (٣-٣٠)}$$

where the constitutive matrix *[D`]* represents the modulus of elasticity of the steel bar.

$$dV^e = A_s \, . \, dx = A_s \, . \, h \, . \, d\xi \quad \text{---------- (٣-٣١)}$$

where (A_s) represents the area of the steel bar.

Substituting equation (٣-٣١) in equation (٣-٣٠), the stiffness matrix of the embedded bar can be expressed as :

$$[k'] = As \int_{-1}^{1} [B']^T . [D'][B'] h . d\xi \quad \text{---------- (٣.٣٢)}$$

a similar derivation can be used for bar parallel to the η and ζ axes .

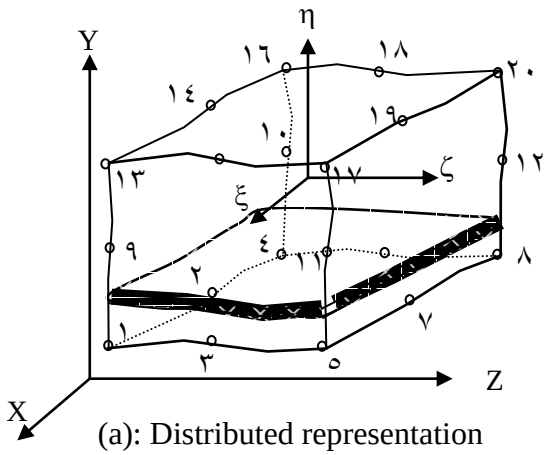

(a): Distributed representation

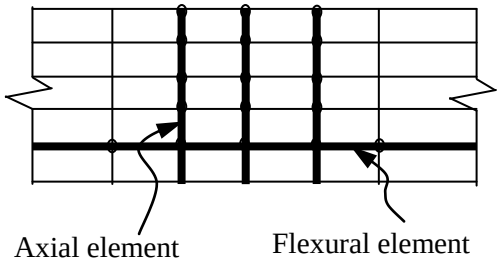

(b): Discrete representation

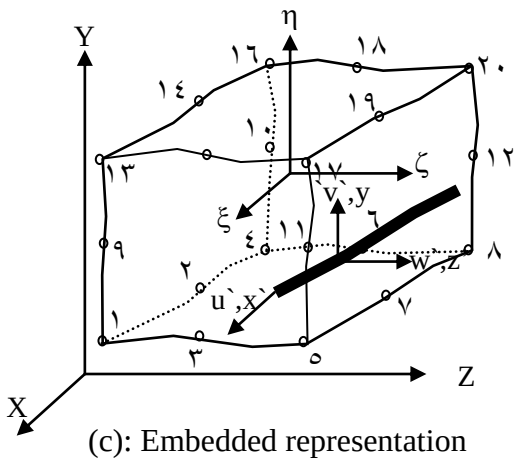

(c): Embedded representation

Fig. (٣-٢): Representation of Steel Reinforcement [٢٣]

٣.٤ Numerical Integration

The evaluation of the element stiffness matrix of concrete brick element and embedded reinforcement element may be very difficult or even impossible. Therefore, an alternative arrangement of numerical integration is used. Usually the Gauss-Legendre scheme is used to perform the integration required to set up the stiffness matrix.

For the isoparametric concrete brick element, the required integration of equation (٣-٢٥) can be expressed by [٧] :

$$I = \int_{-1}^{1}\int_{-1}^{1}\int_{-1}^{1} F(\xi,\eta,\zeta)\,d\xi\,d\eta\,d\zeta \qquad \text{---------- (٣-٣٣)}$$

which can be calculated numerically as :

$$I = \sum_{i=1}^{ni}\sum_{j=1}^{nj}\sum_{k=1}^{nk} W_i.W_j.W_k \;\; F(\xi_i,\eta_j,\zeta_k) \qquad \text{---------- (٣-٣٤)}$$

where *ni, nj,* and *nk* represent the number of Gaussian points in the *ξ, η,* and *ζ* direction respectively, and *wi, wj,* and *wk* are the weight factor of *ith, jth,* and *kth* integration point . The function *F(ξi, ηj, ζk)* represents the matrix multiplication $[[B]^T.[D][B]|J|]$ in equation (٣-٢٥).

Generally the number of integration points are taken equal in the three directions. In a similar manner the integration of the stiffness matrix of the embedded reinforcement can be written as :

$$I = \int_{-1}^{1} F(\xi).d\xi \cong \sum_{i=1}^{ni} Wi.F(\xi i) \qquad \text{---------- (٣-٣٥)}$$

In which, *F(ξi)* represents the matrix multiplication $[[B']^T.[D'][B']]$ in equation (٣.٣٢). It is necessary to choose a suitable integration rule that minimizes the computation time with sufficient accuracy. The ٢٧ (٣x٣x٣) and ١٥-point Gauss-Quadrature integration rule has been used in this investigation. While for steel bars the one dimensional ٢-points Gauss integration rule has been used. Figure (٣-٣) shows the distribution of the sampling points and the corresponding weights and locations are tabulated in table (٣-٢).

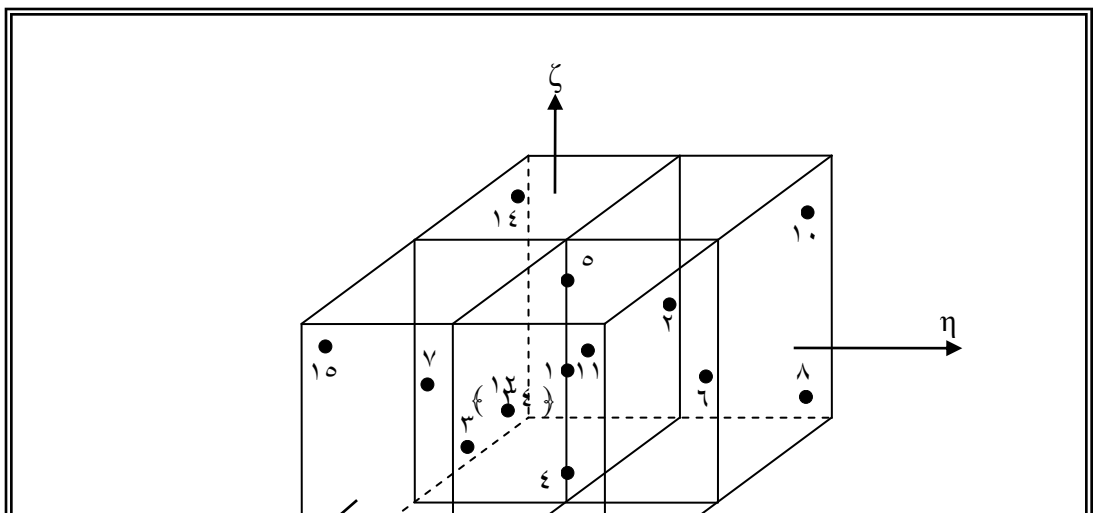

Table (٣-٢) Weights and Locations of Sampling Points for The ١٥ and ٢٧ – Point Integration Rules [٧,١٥]

Integration rule	***Sampling Point***	***Load Coordinates***			***Weight***
		ξ	η	ζ	
١٥a	١	٠	٠	٠	١.٥٦٤٤٤
	٢,٣	±١	٠	٠	٠.٣٥٥٥٥
	٤,٥	٠	٠	±١	٠.٣٥٥٥٥
	٦,٧	٠	±١	٠	٠.٣٥٥٥٥

	٨ to ١٥	±٠.٦٧١٤	±٠.٦٧١٤	±٠.٦٧١٤	٠.٥٣٧٧٧
١٥b	١	٠	٠	٠	٠.٧١٢١٣
	٢,٣	±٠.٨٤٨٤١٨	٠	٠	٠.٦٨٦٢٢
	٤,٥	٠	٠	±٠.٨٤٨٤١٨	٠.٦٨٦٢٢
	٦,٧	٠	±٠.٨٤٨٤١٨	٠	٠.٦٨٦٢٢
	٨ to ١٥	±٠.٧٢٧٦٦٢	±٠.٧٢٧٦٦٢	±٠.٧٢٧٦٦٢	٠.٣٩٦٣١
٢٧	١,٣,٥,٧,١٩,٢١,٢٣,٢٥	±٠.٥٧٧٣٥	±٠.٥٧٧٣٥	±٠.٥٧٧٣٥	٠.١٧١٤٦
	٢,٤,٦,٨,١٠,١٢,١٤,١٦,٢٠,٢٢,٢٦	±٠.٧٧٤٦	±٠.٧٧٤٦	±٠.٧٧٤٦	٠.٢٧٤٣٤
	٩,١١,١٣,١٥,١٧,٢٧	±٠.٧٧٤٦	±٠.٧٧٤٦	±٠.٧٧٤٦	٠.٤٣٨٩٥
	١٨	٠	٠	٠	٠.٧٠٢٣٣

٣.٥ Nonlinear Solution Techniques

The nonlinear behavior of concrete structures may be due to the material or geometrical nonlinearities. The material nonlinear behavior results from cracking and crushing of concrete, yielding of reinforcement and plastic deformation of concrete and reinforcement. The geometrical nonlinearity is related to the large deformations and, in many cases, this nonlinearity is neglected as a result of early onset of the material nonlinearity in reinforced concrete structures [٧]. Thus, the material nonlinearity is only considered in the present study.

The general form of the set of algebraic equations which describes the nonlinearity is of the system is given by [٧] :

$$\{r(a)\} = \{p(a)\} - \{f\} \qquad \text{---------- (٣-٣٦)}$$

where *{r(a)}*, is the out of balance residual force vector, *{a}* is the vector of the nodal displacements, *{f}* is the vector of external loads and {p(a)} is the internal nodal loads vector which is given by :

$$\{p(a)\} = \int_V [B]^T . \{\sigma\} . dV \qquad \text{---------- (٣-٣٧)}$$

where *{σ}* is the stress vector. The solution of the set of equilibrium equations (٣-٣٦) is based on obtaining a balance between the external and the internal load vectors such that residual forces approach zero. The solution of nonlinear problems is usually performed by three basic techniques, these techniques are the incremental technique, iterative technique, and the incremental-iterative technique.

In the incremental approach figure (٣-٤a), the external load is applied as sequence of small increments. Because the purely incremental technique does not account for the redistribution of forces during the application of loading increments; this technique suffers from continuous drift from the true equilibrium path. While, in the iterative technique figure (٣-٤b), the load is applied in a single increment. An initial estimate of the vector of unknown nodal displacement is obtained. Then, for each estimation, the internal forces are calculated, and after that the out of balance forces are obtained to check the convergence. The purely iterative technique unable to trace out the overall behavior throughout the entire range of loading.

The incremental-iterative technique, figure (٣-٤c), implies the subdivision of the total external load into smaller increments, within each increment of loading, iterative cycles are performed in order to obtain a converged solution corresponding to the stage of loading under

consideration. The progress of the iterative procedure is monitored with reference to specified convergence criterion [٧].

The main approaches of incremental-iterative technique are [١٥] :

١.) The Standard Newton – Raphson Method :

In this method, the tangential stiffness matrix is updated and a new system of equations are solved for each iteration. This method is an expensive computational procedure as shown in figure (٣-٤d).

٢.) The Modified Newton – Raphson Method [KT١]:

In this method, the tangential stiffness matrix is updated at the first iteration of each increment of loading as shown in figure (٣-٤e).

٣.) The Modified Newton – Raphson Method [KT٢]:

In this method, the tangential stiffness matrix is updated at the second iteration of each increment of loading.

٤.) The Modified Newton – Raphson Method [KT١a]:

In this method, the tangential stiffness matrix is updated at the ١st, ٦th, ١١th, ….. Iteration of each increment of loading, figure (٣-٤f).

٥.) The Modified Newton – Raphson Method [KT٢a]:

In this method , the tangential stiffness matrix is updated at the ٢nd, ١٢th, ٢٢th,…. Iteration of each increment of loading. This method adopted by searchers [٥,٦,١٥,٤٤,٤٦] who tested beams under torsion and under flexural load, for this work, this method has been used in the analysis.

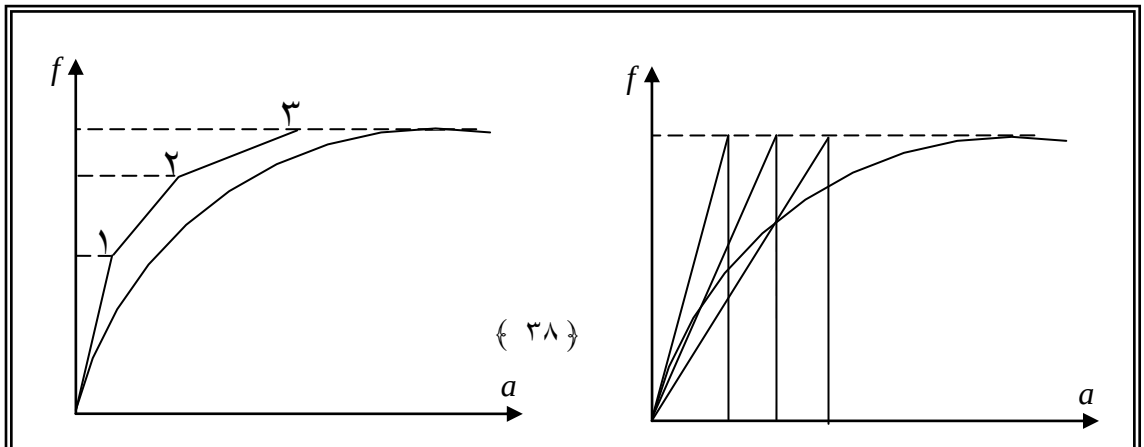

٣.٦ Convergence Criteria

When the difference between the external and internal forces becomes negligibly small, the convergence is assumed to occur and then the

iterative process is terminated. The accuracy of the approximate solution is usually specified by selection of a suitable convergence tolerance.

In general, the main types of convergence criteria for nonlinear structural analysis are the force, displacement and internal work convergence criteria. The force convergence criterion has been considered in the present work, which is based on out of balance forces and can be expressed in the form [٧] :

$$\frac{\sqrt{\{r(a)\}^T.\{r(a)\}}}{\sqrt{\{f\}^T.\{f\}}} \leq \text{convergence tolerance} \qquad \text{---------- (٣-٣٨)}$$

where *r{a}* represent the residual forces and *{f}* is the applied loads for each increment.

٣.٧ Equivalent Nodal Forces

Generally, in the finite element analysis, any external loads must be represented by an equivalent set of forces applied at the nodes. In the case of applying an external torque these forces should be distributed amongst the nodes of the free end to provide the same configuration of shear stresses as those induced by the original torque. When applying the nodal loads in proportions other than the correct one, this will lead to an incorrect distribution of stresses especially in the region adjacent to the loaded section.

An iterative scheme can be used to determine the proper distribution of nodal loads corresponding to elastic pure torque. This approach that was proposed by Al-Shaarbaf [٧], is based on the fact that the reaction forces at the nodes of the restrained ends, represent better estimate of the correct loads than obtained from the corresponding nodal forces applied at the free end. In this iterative scheme, a set of nodal loads is applied at the free end such that they produce a torque moment equivalent to the external

applied torque. The reactions corresponding to the applied nodal loads at the fixed end are found using the finite element analysis within the elastic stage. Then, the obtained reactions are assumed to be a new set of nodal loads at the free end. This procedure is repeated until the difference between the applied forces and the reactions is negligible. The nodal forces represent the equivalent forces that are applied at the ends of the beams under torsion.

٣.٨ Outline of the Computer Program

In the present study, the computer program **P٣DNFEA** (Program of ٣-Dimensional Nonlinear Finite Element Analysis) which was originally developed by Al-Shaarbaf [٧], has been used. This program was coded in FORTRAN-٧٧ Language to analyze ordinary reinforced concrete members under general three – dimensional state of loading up to failure.

The computer program has been modified to be capable to analyze prestressed concrete beams subjected to torsion and combined shear, bending and torsion. The modifications include introducing the effect of prestressing and the combination loads of shear, bending and torsion. The effect of prestressing has been introduced to the concrete beams as effective stress (f_{se}) which represents the stress remaining in prestressing steel after losses have occurred, and strain at sampling points along the prestressing tendons in a sufficient number of increments in order to avoid the crushing of concrete during introducing the effective stress of prestressing (f_{se}) .

When the stress of prestressing has been fully introduced, the external vertical loads and torsion moments are then applied at non-uniform increments. Large increments were used for the first stages of loading, while for stages close to the ultimate capacity small increments were

used. The external torsion moment is applied to the concrete beams as an equivalent set of forces applied at the nodes according to equivalent nodal forces approach which was proposed by Al-Shaarbaf [٧].

The modified computer program was implemented on Pentium (٤) computer with ١٢٨ MB RAM, compiler with F٧٧L – EM ٣٢ FORTRAN ٧٧ and operated by using the Microsoft Fortran Power Station Development System version (٤.٠).

The modifications in the (P٣DNFEA) program to introduce the effect of prestressing and the combination loads are presented in Appendix A.

Chapter Four

Modeling of Material Properties

٤.١ Introduction

The efficiency and accuracy of the nonlinear finite element approach in the analysis of reinforced concrete structures depends mainly on the suitable modeling of material properties. The modeling implies choosing the suitable element type, simulation of the actual behavior of the material properties, choosing of sufficient number of the sampling points and selection of the proper integration technique [١٥].

The information required in any three-dimensional nonlinear finite element analysis of reinforced concrete structures are the material constitutive relationships, which describe the multi-dimensional stress-strain relations that govern the behavior of the structures. The prestressed concrete is a complicated composite material therefore its behavior can not be obtained without considering the constitutive relations of its constituents (concrete, prestressing tendons, and ordinary steel bars) independently. Perfect bond between concrete and steel bars has been assumed to exist throughout the present study.

This chapter deals with the observed behavior of concrete and the modeling of constitutive material properties of concrete, prestressing steel, and ordinary reinforcement.

٤.٢ The Observed Behavior of Concrete

One of the most important characteristics of concrete is its low tensile strength, which results in tensile cracking at very low stress compared with compressive stresses. The tensile cracking reduces the stiffness of the concrete and is usually the major contributor to the nonlinear behavior of reinforced concrete structures [١١].

٤.٢.١ Unixial Behavior of Concrete

٤.٢.١.١ Behavior of Concrete under Unixial Compression

A typical stress – strain relationship for concrete subjected to unixial compression stress is shown in figure (٤-١). The stress- strain curve has a nearly linear-elastic behavior up to ٣٠ percent of its unixial compressive strength, f_c. This level of stress $(0.3f'_c)$ has been termed onset of localized cracking and has been proposed as the limit of elasticity [١١]. For stresses greater than $(0.3f_c)$, the curve shows a gradual increase in curvature due to form micro cracks at the mortar – coarse aggregate interfaces and propagate through the mortar upon further stresses. At a stress level of about $(0.75f'_c)$, the rate of crack propagation increases rapidly and the stress – strain curve bends sharply until the peak stress level is reached. Beyond the peak stress level, concrete shows a softening response, which is presented by the descending portion of the stress-strain curve. This softening response is terminated when crushing failure occurs at some ultimate strain ε_u [٢٠].

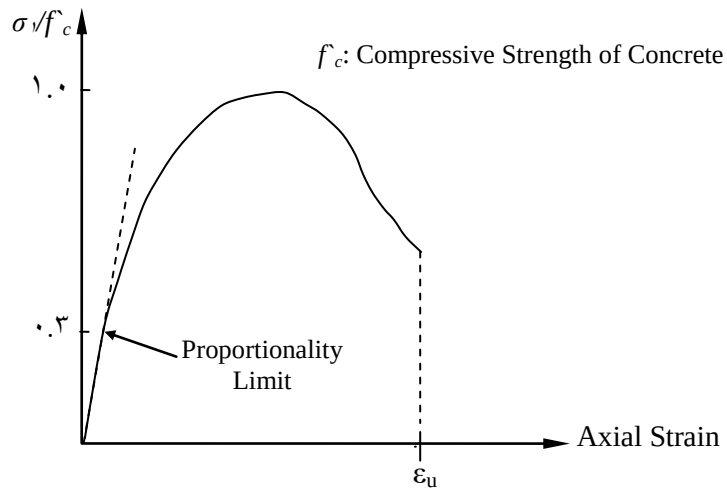

Fig.(٤-١): Typical Unixial Stress-Strain Curve for Concrete in Compression [٤٧]

٤.٢.١.٢ Behavior of Concrete Under Unixial Tension

The stress – strain curve of concrete in uniaxial tension, figure (٤-٢), shows many similarities to the uniaxial compressive curve. For stresses less than about ٦٠ percent of the uniaxial tensile strength f_t, the creation of new micro cracks is negligible. Thus, this stress level will correspond to limit of elasticity; above this level the bond micro cracks start to grow and the nonlinearity of the curve start to increase as the stress level increases until peak stress is reached [١١].

As a result of the difficulties in implementing the direct testing of concrete in pure axial tension, indirect tests are alternatively used to determine the concrete cracking strength. These tests are the modulus of rupture f_r, which is determined from bending test, the splitting strength f_{ct}, which is determined by splitting the concrete cylinder with a line load, and the double punching test for determining concrete cracking strength [١٥]. For normal aggregate concrete, the splitting cylinder strength of concrete is usually between $0.5\sqrt{f_c'}$ and $0.67\sqrt{f_c'}$, where $f`_c$ represents the compressive strength of concrete in (N/mm^2) [٣٨].

According to the ACI- Building Code ٣١٨M-٠٢ [٤], the modulus of rupture of concrete estimated by :

$f_r = 0.7\sqrt{f'_c}$ (N/mm^2) ---------- (٤-١)

where $f`_c$ is the uniaxial compressive strength of concrete in N/mm^2.

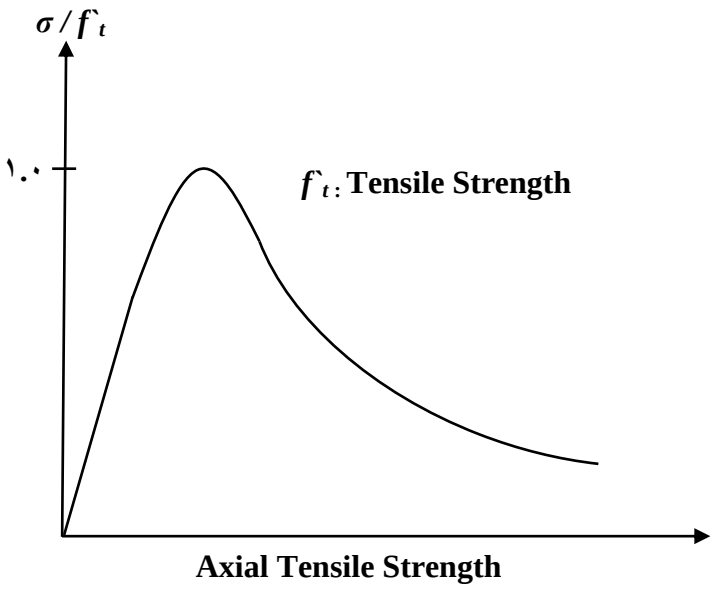

Fig.(٤-٢): Typical Unixial Stress-Strain Curve for Concrete in Tension [٤٧]

٤.٢.٢ Multiaxial Behavior of Concrete

The strength and the stress – strain behavior of concrete under biaxial and triaxial states of stresses are different from that of uniaxial state. The maximum compressive strength increases for the biaxial compression state, and this increase is approximately ٢٥ percent at a stress ratio of (σ_2/σ_1 =٠.٥) and is reduced to about ١٦ percent at an equal biaxial – compression state (σ_2/σ_1 =١.٠), while under biaxial compression – tension, the compressive strength decreases almost linearly as the applied tensile stress is increase and under biaxial tension, the strength is the

same as that of uniaxial tensile strength [٤٥]. Figure (٤-٣) shows a typical biaxial failure envelope of concrete.

Under triaxial compressive stresses, the axial strength of concrete increases with increasing confining pressure. Experimental studies indicate that the three – dimensional failure is the function of the three principal stresses. The elastic limit (onset of stable crack propagation), the onset of unstable crack propagation, and the failure limit can be represented as surfaces in three – dimensional principal stress space as shown in figure (٤-٤) [١١].

٤.٢.٣ The Modulus of Elasticity and Poisson's Ratio of Concrete

The modulus of elasticity of concrete, E_c, may be estimated according to the ACI-Building Code ٣١٨M –٠٢ [٤] as :

$$E_c = W_c^{1.5}.(0.043)\, f_c^{\prime(0.5)} \quad (\text{N/mm}^2) \qquad \text{---------- (٤-٢)}$$

where W_c is the unit weight of concrete in Kg/m^3. For normal strength concrete, equation (٤-٣) can be expressed in the following form :

$$E_c = 4700\sqrt{f_c'} \qquad (\text{N/mm}^2) \qquad \text{---------- (٤-٣)}$$

Poisson's ratio (υ) for concrete under uniaxial compressive loading ranges from about (٠.١٥ to ٠.٢٢). the ratio (υ) remains constant until approximately ٨٠ percent of $f`_c$, at which stress the apparent Poisson's ratio begins to increase [١١].

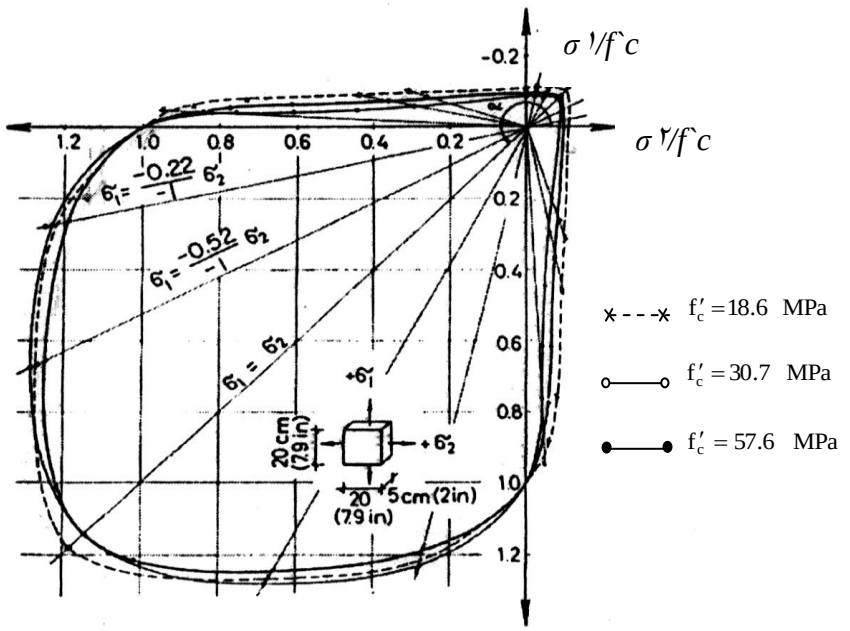

Fig. (٤-٣): Failure Envelope of Concrete in Biaxial Stress Space [١١]

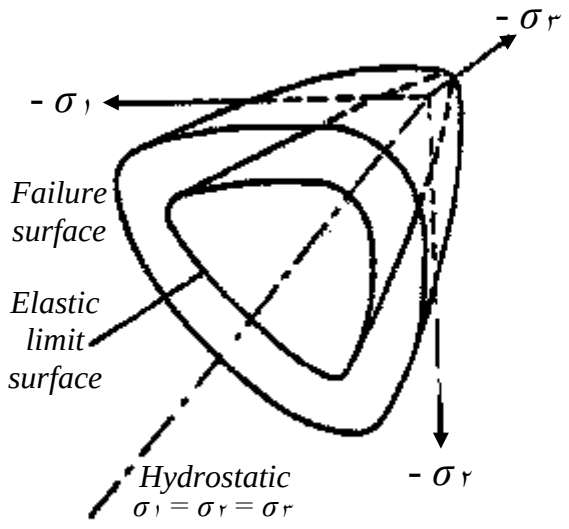

Fig.(٤-٤): Typical Traixial Failure Envelope of Concrete [١١]

٤.٣ Numerical Modeling of Concrete

Prestressed concrete is one of the composed materials that have a complex behavior due to the cracking of concrete in tension and the nonlinear inelastic behavior in compression. Hence the mathematical modeling of concrete behavior is complicated.

In the finite element analysis, the numerical models of concrete should cover the overall behavior of prestressed concrete members within sufficient degree of accuracy and at the same time these models must be kept as simple as possible for easy implementation in the finite element program.

٤.٢.١ Modeling of Concrete in Compression

The plasticity – based model has been used to describe the nonlinear behavior of concrete in compression. In this approach, the nonlinear deformations occur when concrete is stressed beyond its limit of elasticity. The total strain may be separated into recoverable and irrecoverable parts. The recoverable part represents the framework of elasticity, while the treatment of the irrecoverable part is based on the theory of plasticity. Under triaxial compression, concrete can flow like a ductile material on the yield or failure surfaces before reaching its crushing strains [١١].

In this study, the behavior of concrete in compression is simulated by an elasto-plastic work hardening model followed by a perfectly plastic response, which is terminated at the onset of crushing. The adopted plasticity model will be illustrated in terms of the following constituents :

a) The yield criterion.
b) The hardening rule.

c) The flow rule.

d) The incremental stress – strain relationship.

e) The crushing condition.

٤.٣.١.١ The Yield Criterion

Three stress invariants are necessary to determine the general formulation of the three – dimensional failure surface. Therefore, the yield criterion required to monitor the onset of yield is also dependent on the three stress invariants in its general form. However, many researchers [٧,١٩] showed that a yield criterion can be expressed in terms of two stress invariants only. The yield criterion incorporated in the present model is dependent on two stress invariants (I_1,J_2).

This criterion is expressed as [٧] :

$$f(\{\sigma\}) = f(I_1, J_2) = \sqrt{\alpha I_1 + 3\beta J_2} = \sigma_0 \qquad \text{---------- (٤-٤)}$$

where (α) and (β) are material parameters, and I_1, J_2 are the first stress invariant and the second deviatoric stress invariant, respectively that are given by :

$$I_1 = \sigma_x + \sigma_y + \sigma_z \qquad \text{---------- (٤-٥)}$$

$$J_2 = \frac{1}{3}\left[\left(\sigma_x^2 + \sigma_y^2 + \sigma_z^2\right) - \left(\sigma_x.\sigma_y + \sigma_y.\sigma_z + \sigma_z.\sigma_x\right)\right] + \tau_{xy}^2 + \tau_{yz}^2 + \tau_{zx}^2 \qquad \text{----(٤-٦)}$$

and σ. is the equivalent effective stress at the onset of plastic deformation that can be determined from the uniaxial compression test as :

$$\sigma_0 = C_p.f_c' \qquad \text{---------- (٤-٧)}$$

where C_p is the plasticity coefficient which is used to mark the initiation of the plastic deformation ranging from zero to one. For normal strength concrete, a value of ٠.٣ is usually taken for C_p [٧].

The yield stress for the uniaxial compression state is given by :

$$\sigma_x = -\sigma_0 \qquad \text{---------- (٤-٨)}$$

and for the equal biaxial compression state of stress is given by :

$$\sigma_x = \sigma_y = -\gamma\sigma_0 \qquad \text{---------- (٤-٩)}$$

If the results obtained by **Kupfer** for a failure envelope of plain concrete are employed for initial yielding, the value of the constant (γ) is equal to (١.١٦), and the material constants can be found to be :

$\alpha =$ ٠.٣٥٤٦٨ σ_o and $\beta =$ ١.٣٥٤٦٨

let $C = \dfrac{\alpha}{2\sigma_0} = 0.17734$ ---------- (٤-١٠)

therefore, equation (٤-٥) can be rewritten as :

$$f(\sigma) = \sqrt{2.C.\sigma_0.I_1 + 3\beta J_2} = \sigma_0 \qquad \text{---------- (٤-١١)}$$

solving for σ_o,

$$f(\sigma) = C.I_1 + \sqrt{(C.I_1)^2 + 3\beta J_2} = \sigma_0 \qquad \text{---------- (٤-١٢)}$$

٤.٣.١.٢ The Hardening Rule

The hardening rule is required to describe the evolution of the subsequent loading surfaces during plastic deformation, when a material is stressed beyond its initial yield surface. Three hardening rules are usually used to describe the growth of the subsequent loading surfaces for strain or work – hardening material. These rules are the isotropic hardening, kinematic hardening, and mixed hardening rules [١١].

The kinematic hardening rule assumes that during plastic flow the loading surface is translated as a rigid body in the stress space, maintaining the size and the shape of the initial yield surface. This rule is more appropriate for cyclic types of loading. In the mixed hardening rule

the loading surface undergoes both translation and uniform expansion in all directions [٥].

In the current study, an isotropic hardening rule is adopted, which assumes that the yield surface expands uniformly without distortion as plastic flow occurs, this type of hardening rule mainly implies to monotonic proportional loading [٧,١٥].

From equation (٤-١٢) the subsequent loading function may be expressed as :

$$f(\{\sigma\}) = C.I_1 + \sqrt{(C.I_1)^2 + 3.\beta.J_2} = \bar{\sigma} \qquad \text{---------- (٤-١٣)}$$

Where ($\bar{\sigma}$) represents the stress level at which further plastic deformation will occur, and is known as the effective stress or the equivalent uniaxial stress. In order to define the expansion of the current loading surface, the incremental theory of plasticity implies a relationship between the effective stress and the effective plastic strain to extrapolate the results of a uniaxial state to multi axial situation.

In the present model, a parabolic stress – strain curve is used for the uniaxial stress – strain relationship beyond the limit of elasticity, $(C_p.f`_c)$. This parabolic curve represents the work – hardening stage of behavior. When the peak compressive stress is reached, a perfectly plastic response is assumed to occur [٧]. The equivalent uniaxial stress – strain in various stages of behavior is shown in figure (٤-٥). The relations of these stages are given by :

a.) For $\bar{\sigma} \le C_p.f_c$

$$\bar{\sigma} = E.\varepsilon_c \qquad \text{---------- (٤-١٤)}$$

b.) For $C_p.f_c^{'} \le \bar{\sigma} \le f_c^{'}$

$$\bar{\sigma} = C_p . f_c^{'} + E\left\{\varepsilon_c - \frac{C_p . f_c^{'}}{E}\right\} - \frac{E}{2.\varepsilon_0'}\left[\varepsilon_c - \frac{C_p . f_c'}{E}\right]^2 \qquad \text{---------- (٤-١٥)}$$

where ε_0' represents the total strain corresponding to the peak strain of the parabolic portion of the curve that can be calculated from :

$$\varepsilon_0^{'} = \frac{2.(1.0 - C_p).f_c^{'}}{E} \qquad \text{---------- (٤-١٦)}$$

the total effective plastic strain ε_c is composed of two parts, elastic and plastic components :

$$\varepsilon_c = \varepsilon_e + \varepsilon_p \qquad \text{---------- (٤-١٧)}$$

where ε_e is the elastic strain and given by :

$$\varepsilon_e = \frac{\bar{\sigma}}{E} \qquad \text{---------- (٤-١٨)}$$

By substituting equations (٤-١٧) and (٤-١٨) into equation (٤-١٥), the effective stress – strain are :

$$\bar{\sigma} = C_p . f_c' - E.\varepsilon_p + \sqrt{2.E^2.\varepsilon_0^{'}.\varepsilon_p} \qquad \text{---------- (٤-١٩)}$$

c.) For $\varepsilon_c \geq \varepsilon_0^{'}$

$$\bar{\sigma} = f_c^{'} \qquad \text{---------- (٤-٢٠)}$$

The, differentiation of equation (٤-١٩) with respect to the plastic strain leads to the slope of the tangent of the effective stress – plastic strain which represents the hardening coefficient H`, which required in the formulation of the incremental stress – strain relationship [٧,١٥].

$$H' = \frac{d\bar{\sigma}}{d\varepsilon_p} = E.\left[\sqrt{\frac{\varepsilon_0^{'}}{2.\varepsilon_p}} - 1.0\right] \qquad \text{---------- (٤-٢١)}$$

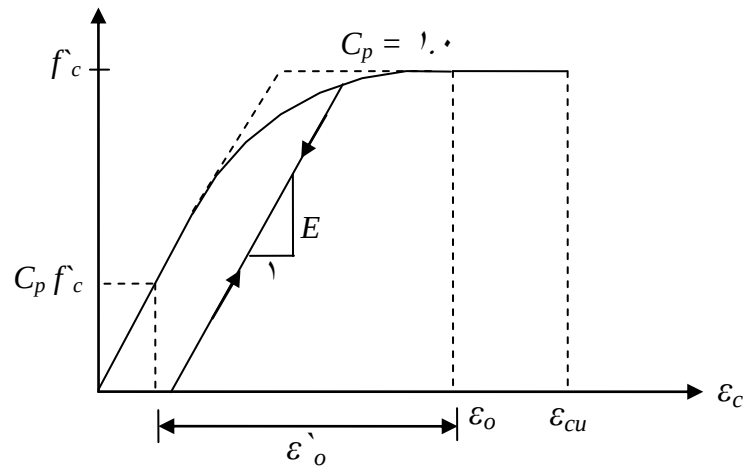

Fig. (٤-٥): Uniaxial Stress-Strain Curve for Concrete [٧]

٤.٣.١.٣ The Flow Rule

In the plasticity – based theory, when the current yield surface is reached, the material become in state of plastic flow upon further loading. The flow rule is usually employed to connect the loading function (*f*) and the stress – strain relation in the plastic range. This rule has been widely used for concrete models because of its simplicity [٧,١١].

The plasticity strain vector will be assumed to be normal to the yield surface , the plastic strain increment is given by :

$$d\{\varepsilon_p\} = d\lambda \frac{\partial f(\{\sigma\})}{\partial \{\sigma\}} \qquad \text{---------- (٤-٢٢)}$$

where $d\lambda$ is a positive scalar hardening parameter which can vary throughout the staining process. The normal to the current loading surface

($\frac{\partial f(\{\sigma\})}{\partial\{\sigma\}}$) is termed as the flow vector, which can be obtained by the derivatives the yield function with respect to the stress components, and given by :

$$\{a\}=\left[\frac{\partial f}{\partial\sigma_x},\frac{\partial f}{\partial\sigma_y},\frac{\partial f}{\partial\sigma_z},\frac{\partial f}{\partial\tau_{xy}},\frac{\partial f}{\partial\tau_{yz}},\frac{\partial f}{\partial\tau_{zx}}\right] \quad \text{---------- (٤-٢٣)}$$

these derivatives can be evaluated from equation (٤-١٣) with the use of equations (٤-٦) and (٤-٧) as :

$$\left.\begin{aligned}
\frac{\partial f}{\partial\sigma_x}&=C+\left[2(C^2+\beta)\sigma_x+(2C^2-\beta)(\sigma_y+\sigma_z)\right]/Q\\
\frac{\partial f}{\partial\sigma_y}&=C+\left[2(C^2+\beta)\sigma_y+(2C^2-\beta)(\sigma_x+\sigma_z)\right]/Q\\
\frac{\partial f}{\partial\sigma_z}&=C+\left[2(C^2+\beta)\sigma_z+(2C^2-\beta)(\sigma_x+\sigma_y)\right]/Q\\
\frac{\partial f}{\partial\tau_{xy}}&=6\,\frac{\beta\tau_{xy}}{Q}\\
\frac{\partial f}{\partial\tau_{yz}}&=6\,\frac{\beta\tau_{yz}}{Q}\\
\frac{\partial f}{\partial\tau_{zx}}&=6\,\frac{\beta\tau_{zx}}{Q}
\end{aligned}\right\} \quad \text{------- (٤-٢٤)}$$

where (C) and (β) are the material constants , and (Q) is given by :

$$Q=2[(C^2+\beta)(\sigma_x^2+\sigma_y^2+\sigma_z^2)+(2C^2-\beta)(\sigma_x\sigma_y+\sigma_y\sigma_z+\sigma_z\sigma_x)+3\beta(\tau_{xy}^2+\tau_{yz}^2+\tau_{zx}^2)]^{0.5}$$

---------- (٤-٢٥)

٤.٣.١.٤ The Incremental Stress – Strain Relationship

The total incremental strain is composed from elastic and plastic strain, therefore :

$$d\{\varepsilon\} = d\{\varepsilon_e\} + d\{\varepsilon_p\} \qquad \text{---------- (٤-٢٦)}$$

Substituting equation (٤-٢٢) in equation (٤-٢٦) yields :

$$d\{\varepsilon\} = d\{\varepsilon_e\} + d\lambda \frac{df(\sigma)}{d(\sigma)} \qquad \text{---------- (٤-٢٧)}$$

The elastic strain increment is related to the stress increment by the elastic constitutive relation given by :

$$d\{\sigma\} = [D]\, d\{\varepsilon_e\} \qquad \text{---------- (٤-٢٨)}$$

Hence :

$$d\{\varepsilon_e\} = [D]^{-1}.d\{\sigma\} \qquad \text{---------- (٤-٢٩)}$$

where *[D]*, is the elastic constitutive matrix given by :

$$[D] = \frac{E}{(1+\nu)(1-2\nu)} \begin{bmatrix} 1-\nu & \nu & \nu & 0 & 0 & 0 \\ \nu & 1-\nu & \nu & 0 & 0 & 0 \\ \nu & \nu & 1-\nu & 0 & 0 & 0 \\ 0 & 0 & 0 & \frac{1-2\nu}{2} & 0 & 0 \\ 0 & 0 & 0 & 0 & \frac{1-2\nu}{2} & 0 \\ 0 & 0 & 0 & 0 & 0 & \frac{1-2\nu}{2} \end{bmatrix} \qquad \text{---- (٤-٣٠)}$$

Substituting equation (٤-٢٩) into equation (٤-٢٧) yields :

$$d\{\varepsilon\} = [D]^{-1}.d\{\sigma\} + d\lambda.\{a\} \qquad \text{---------- (٤-٣١)}$$

Pre-multiplying both sides of equation (٤-٣١) by, *($\{a\}^T$.[D])* and eliminating *($\{a\}^T$.d{σ})*, the following expression for the plastic multiplier, dλ is obtained :

$$d\lambda = \left[\frac{\{a\}^T.[D]}{H' + \{a\}^T.[D].\{a\}} \right].d\{\varepsilon\} \qquad \text{---------- (٤-٣٢)}$$

By substituting equation (٤-٣٣) into equation (٤-٢٩) and pre-multiplying both sides by *[D]*, the complete elasto – plastic incremental stress – strain relationship can be expressed as :

$$d\{\sigma\}=\left[[D]-\frac{\{a\}^T.[D]}{H'+\{a\}^T.[D].\{a\}}\right].d\{\varepsilon\} \qquad \text{---------- (٤-٣٣)}$$

where the second term in the brackets represents stiffness degradation due to the plastic deformation.

٤.٣.١.٥ Crushing Condition

Crushing of concrete indicates the complete rupture and disintegration of the material under compression stress state. After crushing, the current stresses drop rapidly to zero and the concrete is assumed to lose its resistance completely against further deformation.

In the adopted model, the concrete crushing criterion is obtained when the strain reaches the ultimate strain. The crushing criterion is obtained by simply converting the yield criterion in equation (٤-١٢), which is written in terms of stresses directly into strains, thus :

$$C.I_1'+\sqrt{(C.I_1')^2+3\beta.J_2'}=\varepsilon_{cu} \qquad \text{---------- (٤-٣٤)}$$

where ε_{cu} is the ultimate crushing strain of concrete, extrapolated from uniaxial test, I_1' and J_2' are the first strain invariant and the second deviatoric strain invariant that can be obtained by the following equations [٧] :

$$I_1'=\varepsilon_x+\varepsilon_y+\varepsilon_z \qquad \text{---------- (٤-٣٥)}$$

$$J_2=\left(\frac{1}{3}\right)\left[\left(\varepsilon_x^2+\varepsilon_y^2+\varepsilon_z^2\right)-\left(\varepsilon_x\varepsilon_y+\varepsilon_y\varepsilon_z+\varepsilon_z\varepsilon_x\right)\right]+(\gamma_{xy})^2$$
$$+(\gamma_{yz})^2+(\gamma_{zx})^2 \qquad \text{---------- (٤-٣٦)}$$

٤.٣.٢ Behavior of Concrete in Tension

The stress – strain curve of concrete in tension is linear up to about stress level of ٦٠ percent of the uniaxial tensile strength f_t. Above this level, the bond cracks start to grow and the nonlinearity of the curve starts to increase as the stress level increases until the peak stress. The term cracking indicates a partial collapse of the material across the plane of cracking under tensile stress states [١١].

After cracking, concrete changes from isotropic to orthotropic material. In the finite element analysis of concrete structures, three different approaches have been employed for crack modeling [١١] :

١.) Smeared – cracking model.

٢.) Discrete – cracking model.

٣.) Fracture – mechanics model.

The particular cracking model to be selected depends upon the purpose of the analysis [٣٢].

If the overall load – deflection behavior is desired without regard to completely realistic crack patterns and local stresses, the smeared – cracking model is probably the best choice. In this approach the cracked concrete is assumed to remain a continuum, and the concrete becomes orthotropic or transversely isotropic. After the first cracking has occurred, one of the material axes being oriented along the direction of the cracking as shown in figure (٤-٦). For most structural engineering applications, the smeared – cracking modeling is generally used [١١].

The discrete – cracking model represents a continuous smeared – cracking model; this is normally done by disconnecting the displacement at nodal points for adjoining elements as shown in figure (٤-٧). The difficulty in this approach is that the location and orientation of the cracks are not known. This approach is used to obtain details about the local behavior of concrete. While the applicability of fracture – mechanics model to reinforced concrete is still questionable [١١].

In the present study, the behavior of concrete in tension is simulated by linear elastic prior to cracking. The cracking criterion of concrete is expressed in terms of the principal tensile stress or strain. A smeared – cracking model with fixed orthogonal cracks is adopted to represent the fractured concrete.

The adopted model is desired in terms of [٧] :

a.) Cracking criterion.

b.) Post – cracking model.

c.) Shear retention modal.

d.) Compressive strength reduction due to orthogonal crack model.

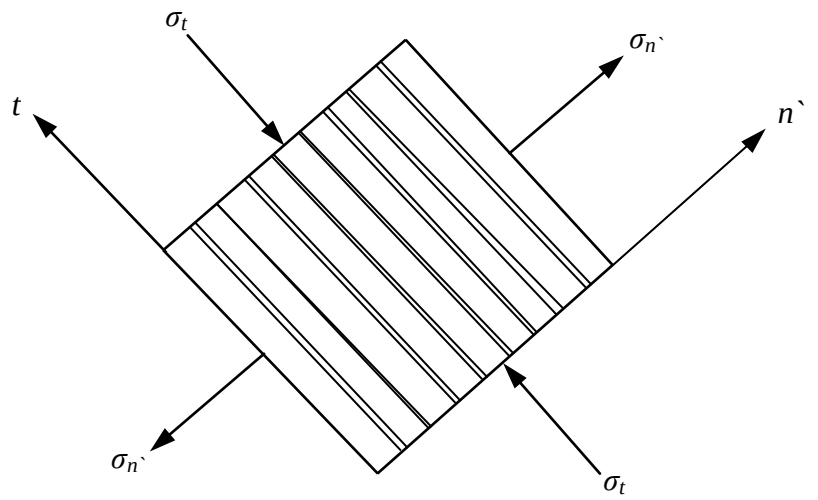

Fig. (٤-٦): Idealization of a Single Smeared Crack [١١]

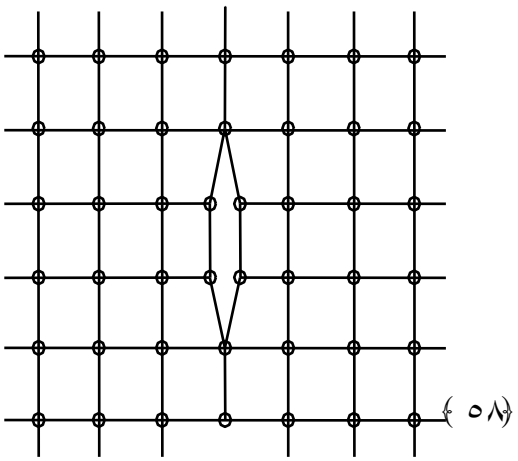

(a): One-Directional Cracking

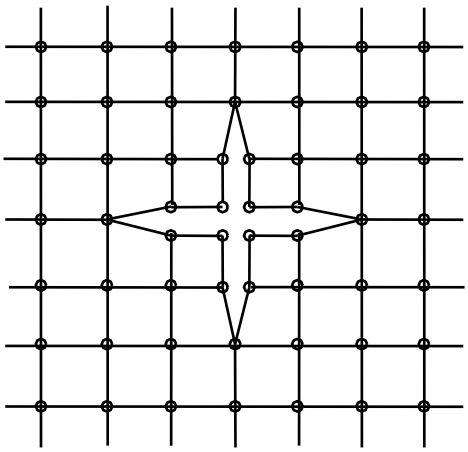

(b): Two-Directional Cracking

٤.٣.٢.١ Cracking Criterion

In the present research, the onset of cracking is controlled by a maximum principal stress criterion. According to this criterion, cracking occurs when the principal tensile stress exceeds the limited tensile strength of concrete f_t, the limited tensile stress required to define the onset of cracking can be calculated for states of triaxial tensile stress and for combination of tension and compression principal stresses as [٧] :

a.) For the triaxial tension zone ($\sigma_1 \geq \sigma_2 \geq \sigma_3 \geq 0$)

$$\sigma_i = \sigma_{cri} = f_t \qquad \text{where } i = ١,٢,٣ \qquad \text{---------- (٤-٣٦)}$$

b.) For tension – tension – compression zone ($\sigma_1 \geq \sigma_2 > 0, \sigma_3 \leq 0$)

$$\sigma_i = \sigma_{cri} = f_t[1.0 + \frac{0.75\sigma_3}{f_c'}] \qquad i = ١,٢ \qquad \text{---------- (٤-٣٧)}$$

c.) For tension – compression – compression ($\sigma_1 > 0, \sigma_3 \leq \sigma_2 \leq 0$)

$$\sigma_i = \sigma_{cri} = f_t[1.0 + \frac{0.75\sigma_2}{f_c'}].[1.0 + \frac{0.75\sigma_3}{f_c'}] \quad i = ١ \qquad \text{---------- (٤-٣٨)}$$

where (σ_{cr}) is the cracking stress and both (*ft*)and ($f`_c$) are the tensile and compressive strengths of concrete substitute in positive values.

The last two equations (٤-٣٧) and (٤-٣٨) indicate that the presence of compressive stress in one direction favors the cracking in other directions and thus reduces the tensile capacity of the material.

After cracking, the modulus of elasticity in the direction of the maximum tensile stress (σ_1) is reduced because of the lack of interaction between orthogonal planes caused by cracking, Poisson's ratio (υ), is set to zero and a reduced shear modulus ($\beta_1 G$) is employed to model the shear strength deterioration. Therefore, the incremental stress – strain relationship in local material axes may be expressed as :

$$\begin{Bmatrix} \Delta\sigma_1 \\ \Delta\sigma_2 \\ \Delta\sigma_3 \\ \Delta\tau_{12} \\ \Delta\tau_{23} \\ \Delta\tau_{31} \end{Bmatrix} = \begin{bmatrix} E_1 & 0 & 0 & 0 & 0 & 0 \\ 0 & E/1-\nu^2 & \nu E/1-\nu^2 & 0 & 0 & 0 \\ 0 & \nu E/1-\nu^2 & E/1-\nu^2 & 0 & 0 & 0 \\ 0 & 0 & 0 & \beta_1 G & 0 & 0 \\ 0 & 0 & 0 & 0 & G & 0 \\ 0 & 0 & 0 & 0 & 0 & \beta_1 G \end{bmatrix} \begin{Bmatrix} \Delta\varepsilon_1 \\ \Delta\varepsilon_2 \\ \Delta\varepsilon_3 \\ \Delta\gamma_{12} \\ \Delta\gamma_{23} \\ \Delta\gamma_{31} \end{Bmatrix} \quad \text{---------- (٤-٣٩)}$$

where (E_1) is the reduced modulus of elasticity in the direction of (σ_1) and (G) is the shear modulus of elasticity. Equation (٤-٣٩) can be written in a compact form as :

$$\{\Delta\sigma\} = [D_{cr}].\{\Delta\varepsilon\} \qquad \text{---------- (٤-٤٠)}$$

where $[D_{cr}]$ is the material stiffness in the local axes. The stress increment in the global axes (x, y, and z) may be obtained by using the coordinate transformation matrix such that

$$\{\Delta\sigma\} = [T]^T.[D_{cr}][T].\{\Delta\varepsilon\} \qquad \text{---------- (٤-٤١)}$$

where $[T]$, is the transformation matrix expressed in terms of the direction cosines as :

$$[T] = \begin{bmatrix} l_1^2 & m_1^2 & n_1^2 & l_1 m_1 & m_1 n_1 & n_1 l_1 \\ l_2^2 & m_2^2 & n_2^2 & l_2 m_2 & m_2 n_2 & n_2 l_2 \\ l_3^2 & m_3^2 & n_3^2 & l_3 m_3 & m_3 n_3 & n_3 l_3 \\ 2l_1 l_2 & 2m_1 m_2 & 2n_1 n_2 & (l_1 m_2 + l_2 m_1) & m_1 n_2 + m_2 n_1 & n_1 l_2 + n_2 l_1 \\ 2l_2 l_3 & 2m_2 m_3 & 2n_2 n_3 & (l_2 m_3 + l_3 m_2) & m_2 n_3 + m_3 n_2 & n_2 l_3 + n_3 l \\ 2l_3 l_1 & 2m_3 m_1 & 2n_3 n_1 & (l_3 m_1 + l_1 m_3) & m_3 n_1 + m_1 n_3 & n_3 l_1 + n_1 l_3 \end{bmatrix} \quad \text{--- (٤-٤٢)}$$

where l_i, m_i, and n_i represent the direction cosines with respect to x,y, and z directions respectively.

For both the tension – tension – compression and the triaxial tension states of stress, the cracking criterion may be violated by the major principal stress (σ_1) and the second principal stress (σ_2) simultaneously. Thus, two sets of orthogonal failure planes develop. These planes are perpendicular to the principal axes ١ and ٢ respectively as in figure (٤-٨ a and b). In this case Poisson's ratio is set to zero in all directions and the constitutive matrix in the local material axis is reduced to the following form :

$$[D_{cr}] = \begin{bmatrix} E_1 & 0 & 0 & 0 & 0 & 0 \\ 0 & E_2 & 0 & 0 & 0 & 0 \\ 0 & 0 & E & 0 & 0 & 0 \\ 0 & 0 & 0 & \beta_1 G & 0 & 0 \\ 0 & 0 & 0 & 0 & \beta_2 G & 0 \\ 0 & 0 & 0 & 0 & 0 & \beta_1 G \end{bmatrix} \qquad \text{---------- (٤-٤٣)}$$

In the current model, a maximum of three sets of cracks are allowed to form at each sampling point. For triaxial tension states, a third crack may appear when the minor principal stress, (σ_3) exceeds the uniaxial tensile strength f'_t in figure (٤-٨c).

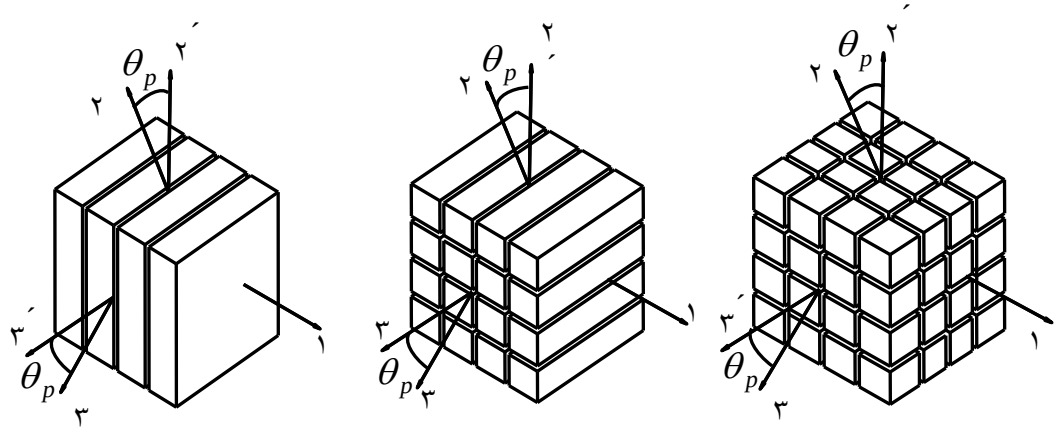

a) Single cracks *b) Double cracks* *c) Triple cracks*

Fig. (٤-٨): Failure Cracking for Triaxially Loaded Concrete [٧]

٤.٣.٢.٢ Post – Cracking Models

After cracking, the stresses normal to the cracked plane are released as the cracks propagate. To simulate this behavior in connection with finite element modeling of reinforced concrete members, the tension – stiffening concept has been used. This concept is based on the fact that some of the tension stresses can be carried by the concrete between the cracks due to the bond action between the steel bar and the surrounding concrete. Two approaches have been suggested to account for the tension – stiffening effects [٤٠]. These are an increase of the steel stiffness and a gradual decrease of the tensile stress in the cracked concrete over a specified strain range. The last approach has been widely used. In this approach, the stress – strain curve for tension stress may be approximated as shown in figure (٤-٩).

The formulation of this approach is described as follows :

a.) For $\varepsilon_{cr} \leq \varepsilon_n \leq \alpha_1 \varepsilon_{cr}$

$$\sigma = \alpha_2 \ \sigma_{cr} \ \frac{(\alpha_1 - \frac{\varepsilon_n}{\varepsilon_{cr}})}{(\alpha_1 - 1.0)} \qquad \text{---------- (٤-٤٤)}$$

b.) For $\varepsilon_n \geq \alpha_1 \varepsilon_{cr}$

$$\sigma_n = 0.0 \qquad \text{---------- (٤-٤٥)}$$

where, (σ_n) and (ε_n) are the stress and strain normal to the cracked plane, ε_{cr} is the cracking strain associated with the cracking stress σ_{cr}, α_1 and α_2 are the tension stiffening parameters, where α_1 represents the rate of the

stress reduction as the cracking widens, and α_2 represents the sudden loss of stress at the instance of cracking.

In the cracked concrete, the secant modulus of elasticity is decreased, when the crack is closed, the effects of any residual strains are neglected. The secant modulus (E_1) can be used to account for the closing and reopening of the crack as [٧] :

$$\sigma_n = E_1.\varepsilon_n \qquad \text{---------- (٤-٤٦)}$$

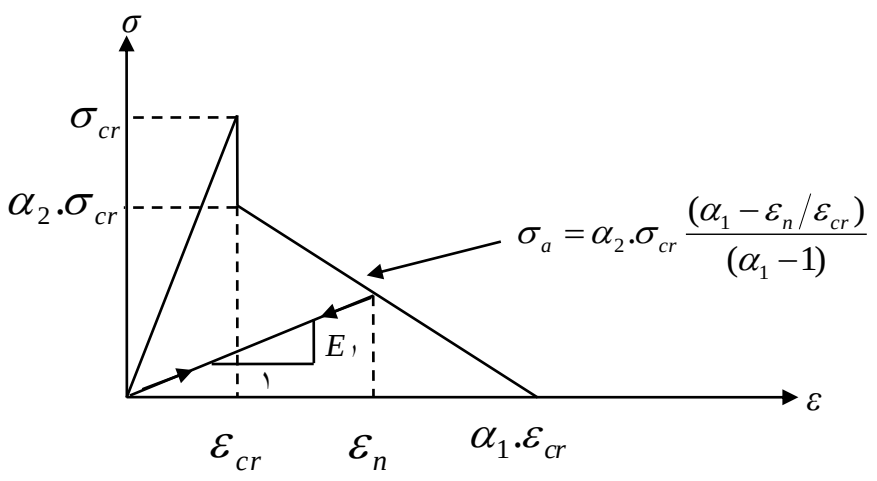

Fig. (٤-٩): Post-Cracking model for Concrete in Tension [٧]

٤.٣.٢.٣ Shear Retention Models

The shear stiffness at a cracked sampling point becomes progressively smaller as the crack widens. The dowel action of the reinforcing steel and aggregate interlocking contribute to produce a considerable residual shear stiffness of cracked concrete. Thus a reduction factor (β) has been used across the cracked planes to reduce the shear stiffness at the cracked

sampling point. Before cracking (β) equal (١.٠), when the cracks propagate the shear reduction factor (β) is assumed to decrease linearly as shown in figure (٤-١٠). When the crack is opened, a constant value of (β) is set to account for the dowel action.

The shear retention model can be expressed as [٧] :

a) For $\varepsilon_n < \varepsilon_{cr}$

$$\beta = ١.٠ \qquad \text{---------- (٤-٤٧)}$$

b) For $\varepsilon_{cr} \le \varepsilon_n \le \gamma_1 \varepsilon_{cr}$

$$\beta = \frac{\gamma_2 - \gamma_3}{\gamma_1 - 1}\left[\gamma_1 - \frac{\varepsilon_n}{\varepsilon_{cr}}\right] + \gamma_3 \qquad \text{---------- (٤-٤٨)}$$

c) For $\varepsilon_n > \gamma_1 \varepsilon_{cr}$

$$\beta = \gamma_٣ \qquad \text{---------- (٤-٤٩)}$$

where $\gamma_١$, $\gamma_٢$, and $\gamma_٣$ are the shear retention parameters, $\gamma_١$ is the rate of decaying of shear stiffness as the crack widens, $\gamma_٢$ is the sudden loss in the shear stiffness at the onset of cracking, and $\gamma_٣$ is the residual shear stiffness due to the dowel action.

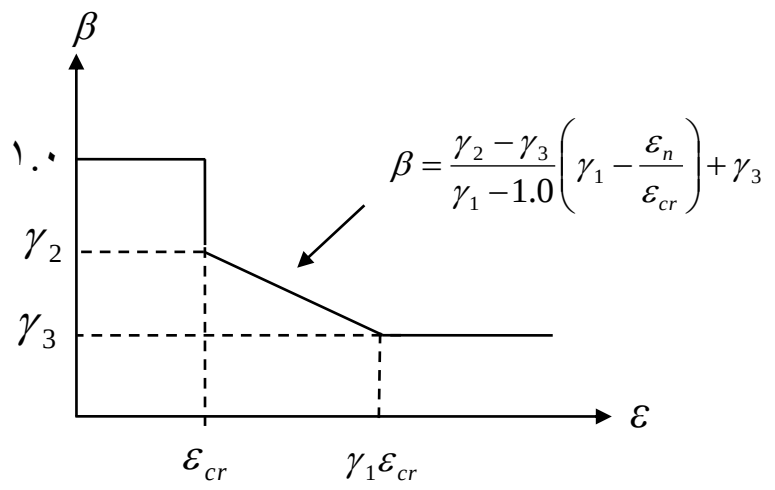

Fig. (٤-١٠): Shear Retention Model for Concrete [٧]

٤.٣.٢.٤ Modeling the Compressive Strength Reduction Due to Orthogonal Cracks

In reinforced concrete members, a significant degradation in compressive strength can result due to the presence of transverse tensile strain after cracking.

In plasticity – based model, effects of transverse tensile strain on the yield criterion and the evolution of the subsequent loading surfaces can be simulated by scaling the equivalent uniaxial stress – strain relationships given by equation (٤-١٦) and (٤-٢١) according to the current value of the compressive strength reduction factor. The model incorporated in the current study is based on the proposals of Cervenka [١٠], which illustrates the use of the reduction factor (λ_1) to reduce both the peak stress and corresponding strain, therefore, from equation (٤-١٣, ٤-١٦, and ٤-٢١).

The modified stress – strain relationship can be written as [٧,١٥] :

a.) For $\sigma \le \lambda_1 C_p . f_c'$

$$\sigma = E.\varepsilon_c \qquad \text{---------- (٤-٥٠)}$$

b.) For $\lambda_1 . C_p . f_c' \le \sigma \le \lambda_1 . f_c'$

$$\sigma = \lambda_1 . C_p . f_c' + E\left[\varepsilon_c - \frac{\lambda_1 . C_p . f_c'}{E}\right] - \frac{E}{2\varepsilon_0'}\left[\varepsilon_c - \frac{\lambda_1 . C_p . f_c'}{E}\right]^2 \qquad \text{---------- (٤-٥١)}$$

c.) For $\varepsilon_c \ge \varepsilon_0'$

$$\sigma = \lambda_1 . f_c' \qquad \text{---------- (٤-٥٢)}$$

where,

$$\varepsilon'_o = \frac{2(1-C_p).\lambda_{.1}\, f'_c}{E} \qquad \text{---------- (٤-٥٣)}$$

consequently, the effective stress – plastic strain relation equation (٤-٢٠) can be modified as :

$$\overline{\sigma} = \lambda_1.C_p.f'_c - E.\varepsilon_p + \sqrt{2.E.\lambda_1.\varepsilon'_0.\varepsilon_p} \qquad \text{---------- (٤-٥٤)}$$

and hence, the hardening parameter can be expressed as :

$$H' = \frac{d\overline{\sigma}}{d\varepsilon_p} E.\left[\left[\frac{\lambda_{.1}\varepsilon'_0}{2.\varepsilon_p}\right]^{\frac{1}{2}} - 1.0\right] \qquad \text{---------- (٤-٥٥)}$$

for a singly cracked sampling point, the compression reduction factor is given by :

$$\lambda_1 = 1.0 - k_1 \frac{\varepsilon}{0.005} \le 1.0 - k_1 \qquad \text{---------- (٤-٥٦)}$$

where, ε_1 is the transverse tensile strain in principal direction ١.

for a doubly cracked sampling point the expression can be taken as :

$$\lambda_1 = 1.0 - k_1 \frac{\sqrt{\varepsilon_1^2 + \varepsilon_2^2}}{0.005} \le 1.0 - k_1 \qquad \text{---------- (٤-٥٧)}$$

where ε_2 is the tensile strain normal to the second crack, and k_1 represents a compression reduction parameter. Cervenka has used values ranging between (٠.٢٧ and ٠.٧٣) for the parameter k_1 [١٠].

٤.٣ Modeling of Reinforcement

The stress – strain curve for a typical prestressing steel bar differs from the ordinary steel reinforcement. The main differences are the much higher proportional elastic limit and strength available in the round wire and alloy bars used for prestressing, and the substantially lower ductility. Figure (٤-١١) shows a typical stress – strain diagram for prestressing steel in comparison with a mild steel bar reinforcement [٣٨].

The ordinary and prestressing steel bars are long and relatively slender; and assumed to be capable of transmitting axial force only. The modeling of ordinary and prestressing steel in connection with the finite element analysis of prestressed concrete beams are much simpler than the modeling of concrete.

In the present study, the uniaxial stress – strain behavior of ordinary and prestressing steel bars has been simulated by an elastic linear work hardening model as shown in figure (٤-١٢) [٧].

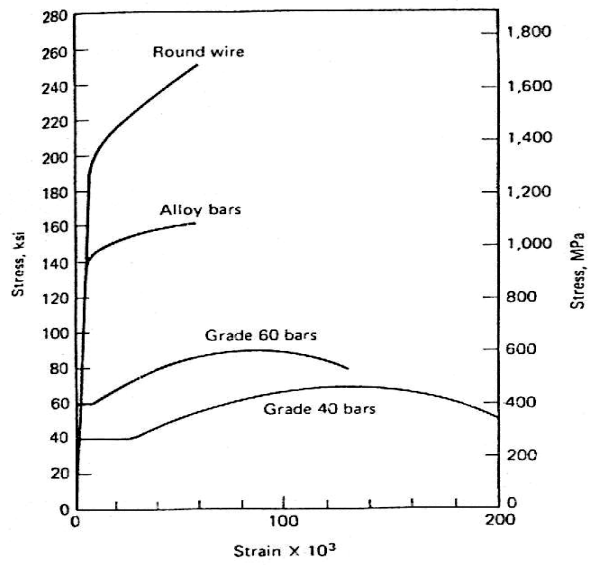

Fig. (٤-١١): Comparative Stress – Strain Curves for Reinforcing and Prestressing Steel [٣٨]

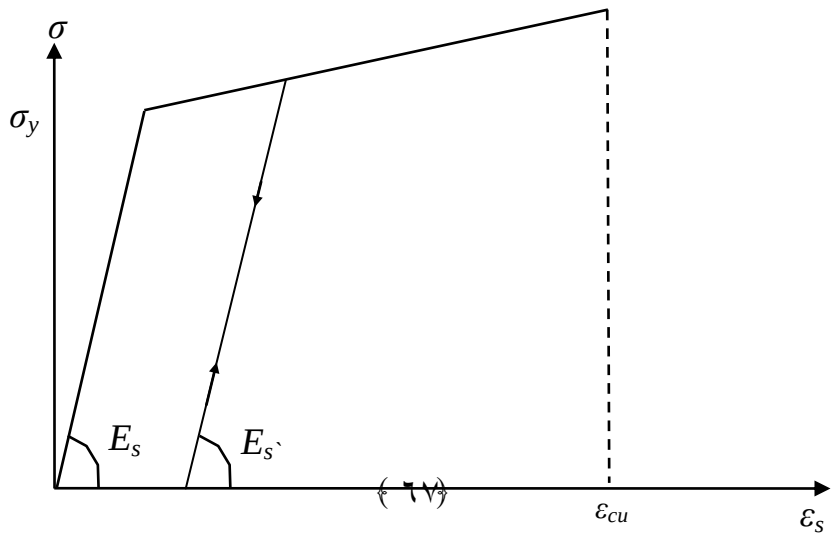


ain

Chapter five

Applications, Results, and Discussion

٥.١ Introduction

In this chapter many examples are considered to verify the validity and accuracy of the proposed three dimensional nonlinear finite element model which is used to investigate the behavior and ultimate capacity of prestressed concrete beams under torsion and combined shear, bending and torsion, and to study the influence of variation of some important material parameters on the behavior and ultimate capacity of beams subjected to combined shear and torsion. The results of analysis are discussed and compared with the experimental results. Also the torque – twist curves of the tested beams that obtained from the finite element analysis are compared with the available experimental torque – twist curves.

Parametric studies have been carried out in this chapter to investigate the effects of some important material parameters, and geometrical parameters on the numerical results as obtained for the considered cases.

٥.٢ Case One : Prestressed Concrete Beams under Pure Torsion

٥.٢.١ Abul Hasanat et.al Prestressed Concrete Beam [PA-٠-RL]

Abul Hasanat et.al (١٩٨٨), tested a series of rectangular prestressed concrete beams under torsion with various properties and detail of reinforcement. Among these tested specimen beams, the beam designated as [PA-٠-RL] which was analyzed by **Shuber** using three dimensional nonlinear finite element analysis is considered in the present study.

٥.٢.١.١ Description and Material Properties of Abul Hasanat et.al Beam [PA-٠-RL]

Beam [PA-٠-RL] was simply supported prestressed concrete beam over (٢١٩٠ mm) span and has an effective span of (١٨٥٠ mm), with (١٠٠ x ٢٥٠) mm rectangular cross sectional dimensions. Figure (٥-١) shows the dimensions and reinforcement details of beam [PA-٠-RL]. The material properties of concrete and reinforcement and the additional material parameters of the tested beam are listed in table (٥-١).

٥.٢.١.٢ Finite Element, Boundary Conditions, and Equivalent Nodal Forces of the Tested Beam

Beam [PA-٠-RL] has a symmetry in loading, geometry and reinforcement layout. Thus only half of the beam has been used in the present finite element analysis. The considered segment was simulated by (١٢) isoparametric ٢٠-noded brick elements. While the reinforcement was modeled as one dimensional axial element embedded within the brick element as shown in figure (٥-١). The effect of prestressing introduced before applying the external torque as effective stress and strain at sampling point of prestressing tendons using (١٠) increments. The

external torque modeled as a set of equivalent nodal forces were applied at both ends of the selected segment as described in section ٣-٧. The ١٥b – point integration rule has been considered as a numerical integration, with a convergence tolerance (٥ %). The modified Newton – Raphson (KT٢a) method has been adopted as a nonlinear solution algorithm.

Table (٥-١) : Material Properties and Material Parameters for Abul Hasanat et.al Beam [PA-٠-RL]

Concrete		
E_c	Young's modulus (N/mm^2)	٢٩٠٠٠
$f`_c$	Compressive strength (N/mm^2)	٤٤.٨٤
f_t	Tensile strength (N/mm^2)	٣.٩
υ	Poisson's ratio*	٠.٢
k_1	Compression reduction parameter*	٠.٦
α_1	Tension stiffening parameters*	١٠
α_2		٠.٥
γ_1	Shear - Retention parameters*	١٠
γ_2		٠.٥
γ_3		٠.١
Prestressing tendons		
E_{ps}	Young's modulus (N/mm^2)	٢٠٠٠٠٠
A_{ps}	Total area prestressing tendons (mm^2)	١٩٨.٤٨
f_{se}	Effective prestressing stress (N/mm^2)	١١٤٠.١
f_{py}	Yield stress (N/mm^2)	١٨١٦
Gp	Number of Gauss points of tendons	٨
Longitudinal and transverse reinforcement		
E_s	Young's modulus (N/mm^2)	٢٠٠٠٠٠
A_l	Total area of longitudinal steel bars (mm^2)	١٢٦.٦٨
Av	Area of ordinary steel bar (mm^2)	٣١.٦٧
f_y	Yield stress (N/mm^2)	٣٧١

** assumed values : selected to obtain the best results in comparing with the experimental results.*

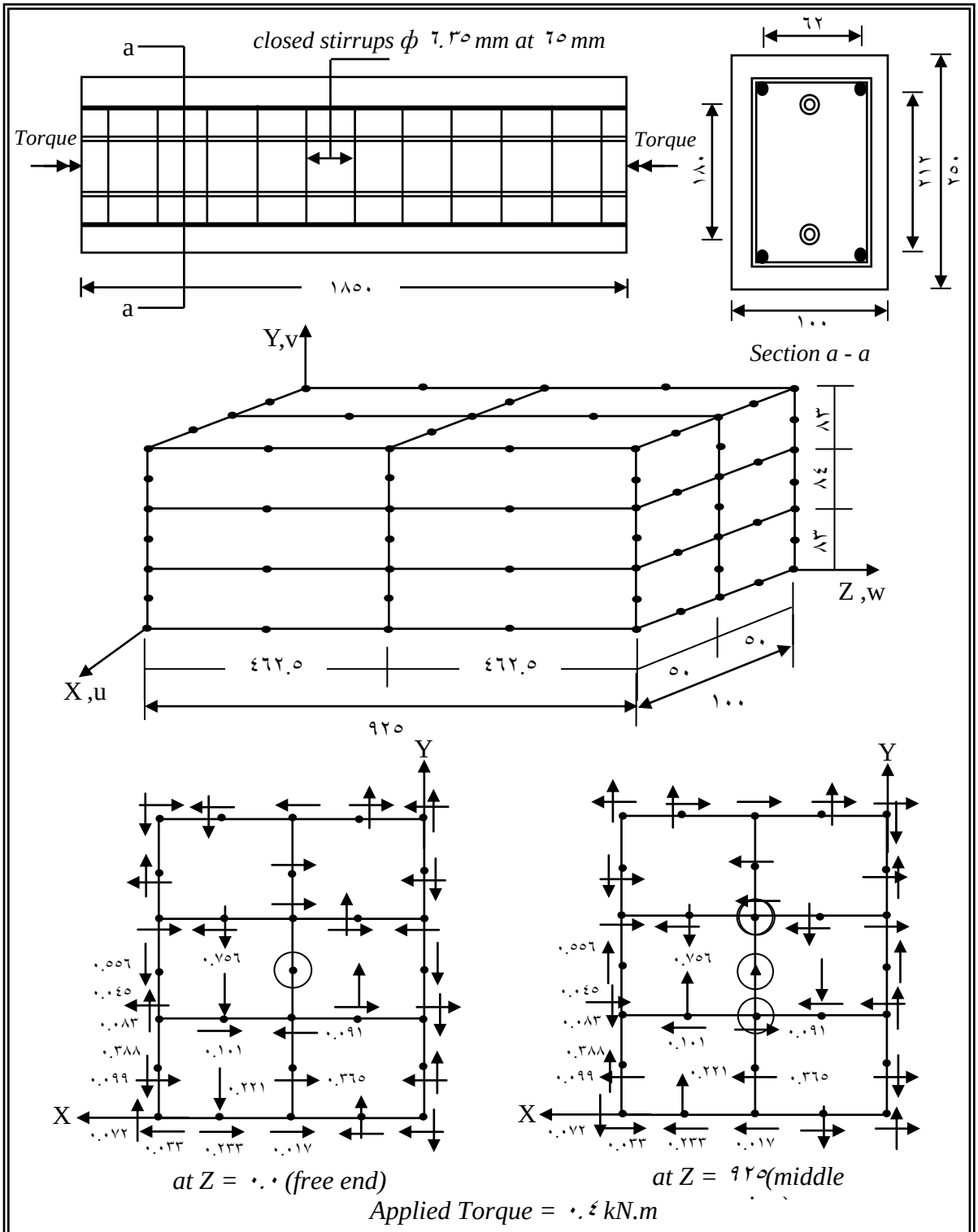

Fig. (٥-١): Finite Element Mesh, Boundary Conditions and Equivalent Nodal Forces for Abul Hasanat et.al Beam [PA-٠-RL]

٥.٢.١.٣ Results of Analysis of Abul Hasanat et.al Beam [PA-٠٠-RL]

Many numerical tests have been considered on the tension stiffening parameters, shear retention parameters and the compression reduction parameter (k_1), to obtain the best values of these parameters, that give the best results as compared with the experimental results. The results of these tests show that the value of these parameters are the same as values that used by **Shuber** except the tension stiffening parameter (α_2) and compression reduction parameter (k_1). Where **Shuber** used (α_2) equal to (٠.٦) and (k_1) equal to (٠.٤), while in the present analysis (α_2) set equal to (٠.٥) and (k_1) equal to (٠.٦).

The results of the tested beam show a good agreement between the experimental results by **Abul Hasanat et.al** and the present finite element analysis. The experimental ultimate torque was (٧.٥ kN.m) while the present numerical torque was (٧.٧٧ kN.m) with a difference (٣.٦ %) between experimental and numerical torque. Also the results show that no significant difference in ultimate torque between the present finite element torque which is (٧.٧٧ kN.m) and the predicted numerical ultimate torque by **Shuber** which was (٧.٨ kN.m).

In the present study the effect of prestressing has been introduced as an effective stress and strain at sampling points of prestressing tendons. While **Shuber** introduced the effect of prestressing as an external prestressing force at the ends of the tested beam.

A comparison between the present torque-twist curve, the torque-twist curve by **Shuber** and the experimental torque-twist curve were shown in figure (٥-٢). Table (٥-٢) listed the experimental and numerical ultimate torque and the comparison between the experimental and numerical ultimate torque.

Table (٥-٢) : Comparison Between the Experimental and Predicted Ultimate Torque of Abul Hasanat et.al Beam [PA-٠-RL]

Beam	T_{exp} (kN.m)	T_N (kN.m)	T_U (kN.m)	$\frac{T_U - T_{exp}}{T_{exp}}$	$\frac{T_U - T_N}{T_N}$	$\frac{T_U}{T_{exp}}$
[PA-٠-RL]	٧.٥	٧.٨	٧.٧٧	٣.٦ %	- ٠.٣٨٪	١.٠٣٦

where :
T_{exp} : The ultimate experimental torque (by Abul Hasanat et.al).
T_N : The ultimate experimental torque (by Shuber).
T_U : The ultimate torque obtained from the present F.E.A.

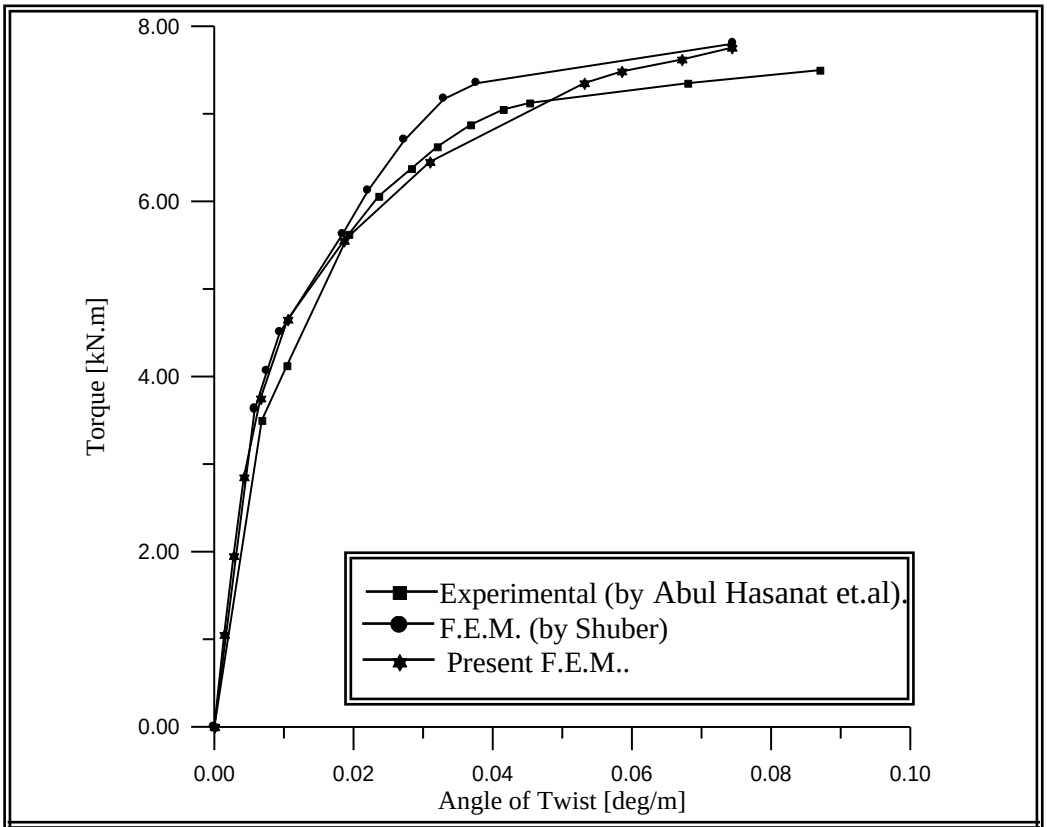

Fig. (٥-٢): Torque – Twist Curve of Beam [PA-٠-RL] (case one)

٥.٢.٢ Mitchell and Collins Prestressed Concrete Beams [P١] and [P٣]

In ١٩٧٨, **Mitchell and Collins**, tested a series of six rectangular prestressed concrete beams under torsion loads to describe the influence of longitudinal prestressing steel on the torsional response of these beams. All beams having the same amount of transverse reinforcement and dimensions but with varying amounts of ordinary longitudinal and prestressing steel. In this study two beams have been analyzed that are designated as [P١] and [P٣], to study the influence of prestressing steel and ordinary longitudinal steel bars on the torque – twist behavior and ultimate torque capacity.

٥.٢.٢.١ Description and Material Properties of Mitchell and Collins Beams [P١] and [P٣]

Beams [P١] and [P٣] have a (٣٠٠٠ mm) length, with (٣٥٥ x ٤٣٠) mm cross sectional dimensions. Beam [P١] is concentrically prestressed by four (ϕ ١٢.٠ mm) prestressing wires, while [P٣] is prestressed by one (ϕ١٢.٠ mm) prestressing wires. The two beams have the same amount of (ϕ ٩.٥ mm) web reinforcement, but beam [P١] has eight (ϕ ٩.٥ mm) ordinary longitudinal reinforcement and beam [P٣] has six (ϕ ٩.٥ mm) ordinary longitudinal steel bars. Figure (٥-٣) shows the dimensions and reinforcement of beams [P١] and [P٣].

The materials properties of concrete and reinforcement and the additional material parameters used in the analysis of the two beams are listed in table (٥-٣).

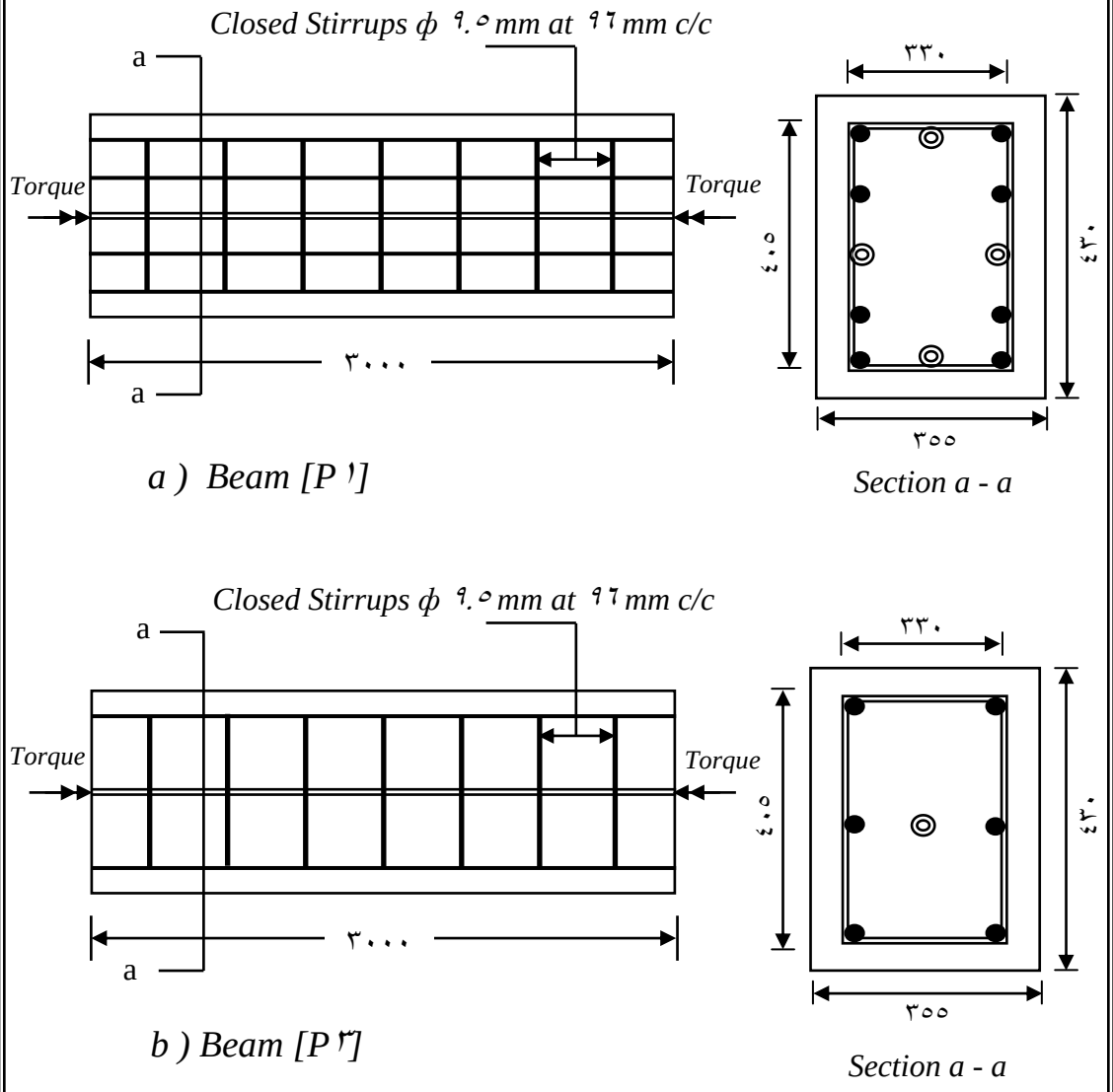

Fig. (٥-٣): Dimensions and Reinforcement Details of Mitchell and Collins Beams [P١] and [P٣]

Table (٥-٣) : Material Properties and Material Parameters for Mitchell and Collins Beams [P١] and [P٣]

Concrete		**[P١]**	**[P٣]**
E_c	Young's modulus (N/mm^2)	٢٧٠٠٠	٢٧٠٠٠
$f`_c$	Compressive strength (N/mm^2)	٣٣	٣٤
f_t	Tensile strength (N/mm^2)	٢.٤	٢.٥
υ	Poisson's ratio*	٠.٢	٠.٢
k_1	Compression reduction parameter*	٠.٥	٠.٦
α_1	Tension stiffening parameters*	١٥	١٥
α_2		٠.٦	٠.٥
γ_1	Shear - Retention parameters*	١٠	١٠
γ_2		٠.٥	٠.٥
γ_3		٠.١	٠.١
Prestressing tendons			
E_{ps}	Young's modulus (N/mm^2)	١٩٧٠٠٠	١٩٧٠٠٠
A_{ps}	Total area of prestressing tendon (mm^2)	٤٦٤	١١٦
f_{se}	Effective prestressing stress (N/mm^2)	١١٤٥	١١٤٥
f_{py}	Yield stress (N/mm^2)	١٤٧٥	١٤٧٥
Gp	Number of Gauss points of tendons	٣٢	٨
Longitudinal steel			
E_s	Young's modulus (N/mm^2)	١٩٧٠٠٠	١٩٧٠٠٠
A_l	Total area of longitudinal steel (mm^2)	٥٦٨	٤٢٦
f_y	Yield stress (N/mm^2)	٣٢٨	٣٢٨
Web reinforcement			
E_s	Young's modulus (N/mm^2)	١٩٧٠٠٠	١٩٧٠٠٠
A_v	Area of web reinforcement (mm^2)	٧١	٧١
f_y	Yield stress (N/mm^2)	٣٢٨	٣٢٨

** assumed values : selected to obtain the best results in comparing with the experimental results.*

٥.٢.٢.٢ Finite Element, Boundary Conditions, and Equivalent Nodal Forces of Mitchell and Collins Beams [P١] and [P٣]

Due to symmetry in loading, geometry, and reinforcement layout only half of the beams will be considered in the analysis. The selected segment has been analyzed with different meshes to study the effect of these meshes on the numerical results. The results of these analysis show that the (٢٤) isoparametric ٢٠-noded brick elements gives closer results to the experimental results. While the reinforcement was modeled as one dimensional element embedded within the ٢٠-noded brick element. The external torque was modeled as a set of equivalent nodal forces were applied at both ends of the selected segment as described in section ٣-٧. The angle of twist was calculated at the free end of the beams (at z = ٠.٠). The imposed boundary conditions maintain the stability of the beams and allow to post cracking extension of the beams in z-direction to occur, the same boundary conditions are used by many researchers who tested prestressed and ordinary beams under pure torsion loads [١٥,٤٤].

The finite element mesh, boundary conditions, and the equivalent nodal forces of beams [P١] and [P٣] are shown in figure (٥-٤).

The effect of prestressing on the beams were introduced before applying the external torque, and was considered as an effective stress and strain at the sampling points of the prestressing tendons using (١٠) increments.

The present finite element analysis has been carried out using ١٥b-point integration rule, with a convergence tolerance (٥٪). The modified Newton – Raphson (KT٢a) method has been adopted as a nonlinear solution algorithm.

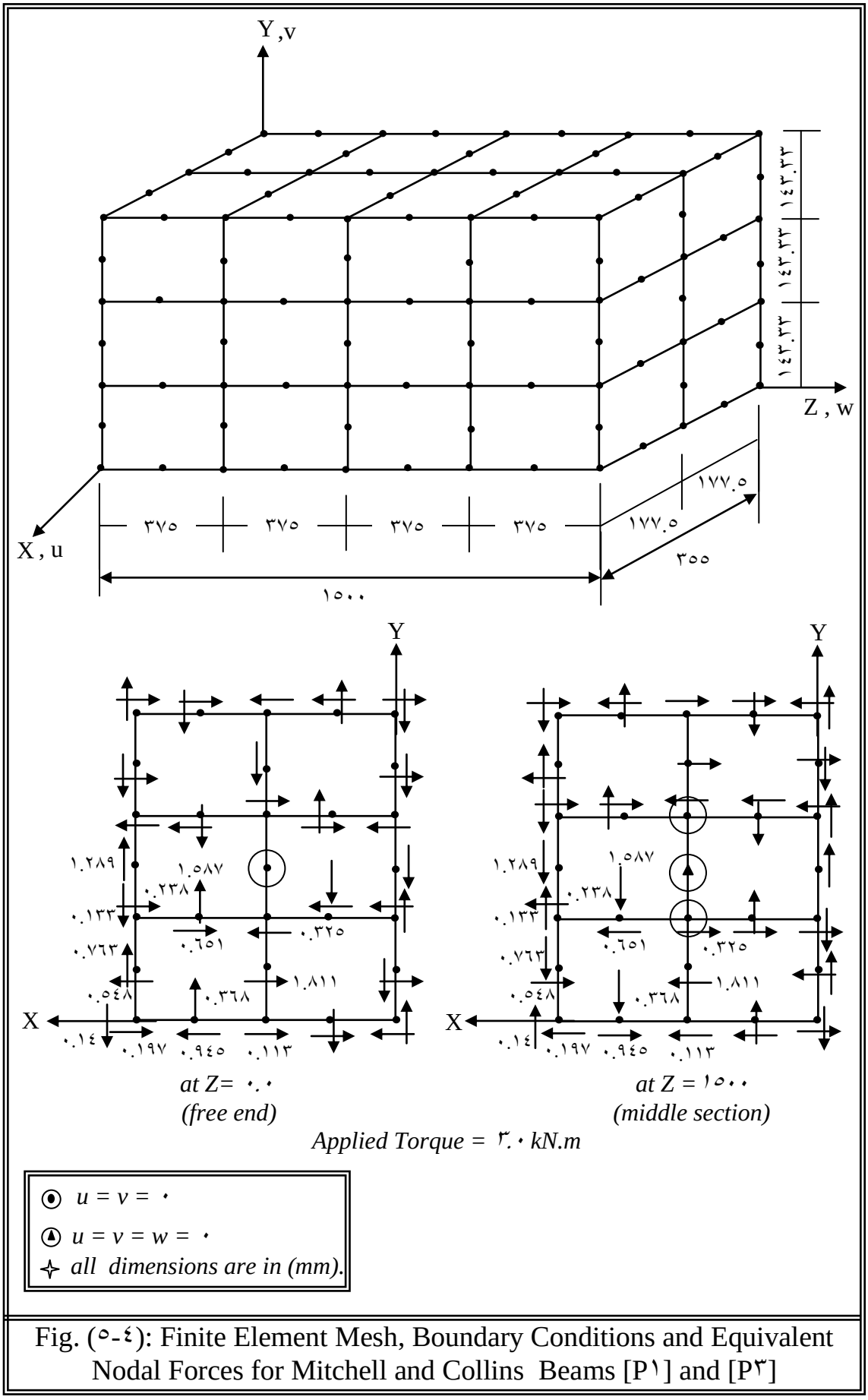

at Z= ٠.٠
(free end)

at Z = ١٥٠٠
(middle section)

Applied Torque = ٣.٠ kN.m

- *u = v = ٠*
- *u = v = w = ٠*
- *all dimensions are in (mm).*

Fig. (٥-٤): Finite Element Mesh, Boundary Conditions and Equivalent Nodal Forces for Mitchell and Collins Beams [P١] and [P٣]

٥.٢.٢.٣ Results of Analysis of Mitchell and Collins Beams [P١] and [P٣]

For beam [P١], figure (٥-٥) shows the experimental (by **Mitchell and Collins**) and present numerical torque – twist curve. This figure shows a good agreement between the numerical results and the experimental results throughout the entire range of loading. The numerical ultimate torque was (٨٤.٦) kN.m, while the experimental ultimate torque was (٨٠.٧١) kN.m. Thus the difference between these results is (٤.٨٢٪).

Figure (٥-٦) shows the experimental by **Mitchell and Collins** and presents numerical torque – twist curve of beam [P٣]. This figure shows an acceptable agreement between the experimental and the present finite element analysis results. The present numerical ultimate torque of beam [P٣] was (٥٤.٦)kN.m, while the experimental ultimate torque was (٥٣.١١)kN.m and the difference between them is equal to (٢.٦٣٪). The results for the two beams ([P١]and [P٣]) explain that when increasing the amount of prestressing and ordinary steel bars, the ultimate and cracking torque will increase.

The ultimate torque which is obtained from the present finite element analysis and the experimental ultimate torque by **Mitchell and Collins** for beams [P١] and [P٣] are presented in table (٥-٤).

Table (٥-٤) : Comparison Between the Experimental and Predicted Ultimate Torque of Mitchell and Collins Beams [P١] and [P٣]

Beam	T_{exp} (kN.m)	T_u (kN.m)	$\frac{T_u}{T_{exp}}$	$\frac{T_u - T_{exp}}{T_{exp}}$
[P١]	٨٠.٧١	٨٤.٦	١.٠٤٨	٤.٨٢ %
[P٣]	٥٣.١١	٥٤.٦	١.٠٢٨	٢.٦٣ %

where :
T_{exp} : The ultimate experimental torque (by Mitchell and Collins).
T_u : The ultimate torque obtained from the present F.E.A.

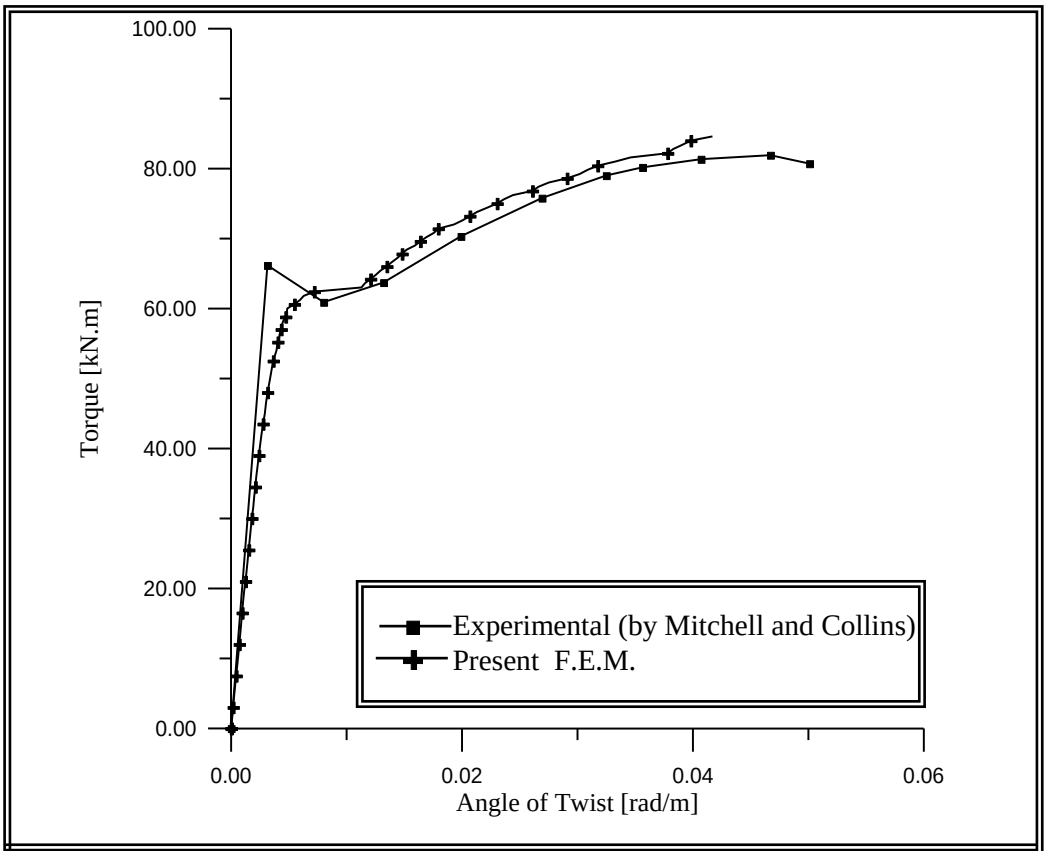

Fig. (٥-٥): Torque – Twist Curve of Beam [P١] (case one)

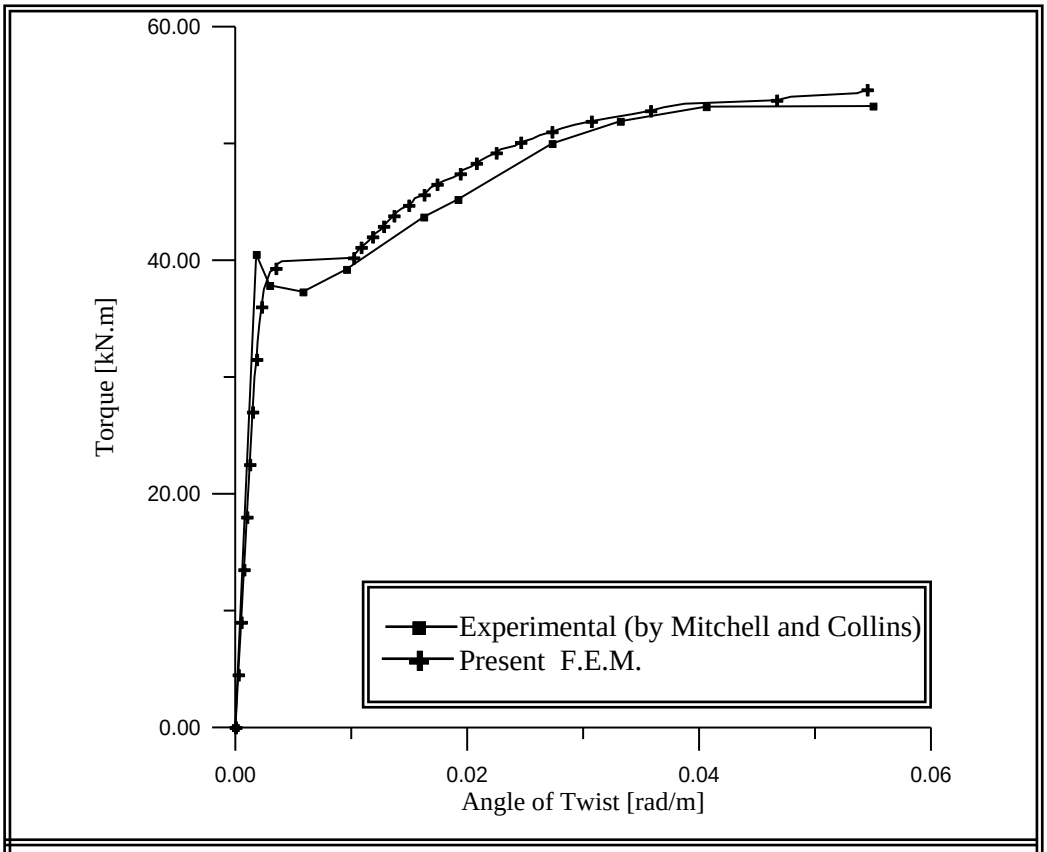

Fig. (٥-٦): Torque – Twist Curve of Beam [P٣] (case one)

٥.٣ Case Two : Prestressed Concrete Beams under Combined Shear, Bending and Torsion

Two groups of prestressed concrete beams have been tested by **Mukherjee and Warwaruk**, the first group consisted of (٢٨) prestressed concrete beams subjected to combined bending and torsion loads. In the second group, (٢٤) prestressed concrete beams were tested under a combination of shear, bending and torsion. These beams were grouped into four series (VA, VB, VC, and VD), among these series the amount of prestressing and its eccentricity were varied. Series (VA) and (VC) were concentrically prestressed and series (VB) and (VD) were eccentrically prestressed. In the present study, beams (V١٠٢, V١٠٣, V١٠٤, V١٠٥, and V١٠٧) from series (VA) and beams (V١٢٢, V١٢٣, V١٢٤, V١٢٥, and V١٢٧) from series (VB) have been considered.

٥.٣.١ Description and Material Properties of Series (VA) and (VB) Beams

Series (VA) and (VB) have the same dimensions and amount of reinforcement. All beams of series (VA) and (VB) have (٣١٢٤ mm) overall length, and (٢٧٤٢ mm) supported length with (١٥٢ x ٣٠٥) mm cross sectional dimensions. Each beam has four (ϕ ٧.٩٥ mm) prestressing wire strand, four (ϕ ٩.٥٢٥ mm) ordinary longitudinal steel bars, and (ϕ ٩.٢٥٢ mm) closed stirrups outside the gage length and (ϕ ٦.٣٥ mm) closed stirrups inside the gage length, as shown in figure (٥-٧). Within each series the beams were tested with different torsion to bending moment ratio (T/B). Figure (٥-٨) shows the shear force diagram, bending moment diagram, torsion moment diagram and the applied torque and loads. The material parameters and material properties of the tested beams are listed in table (٥-٥) and (٥-٦).

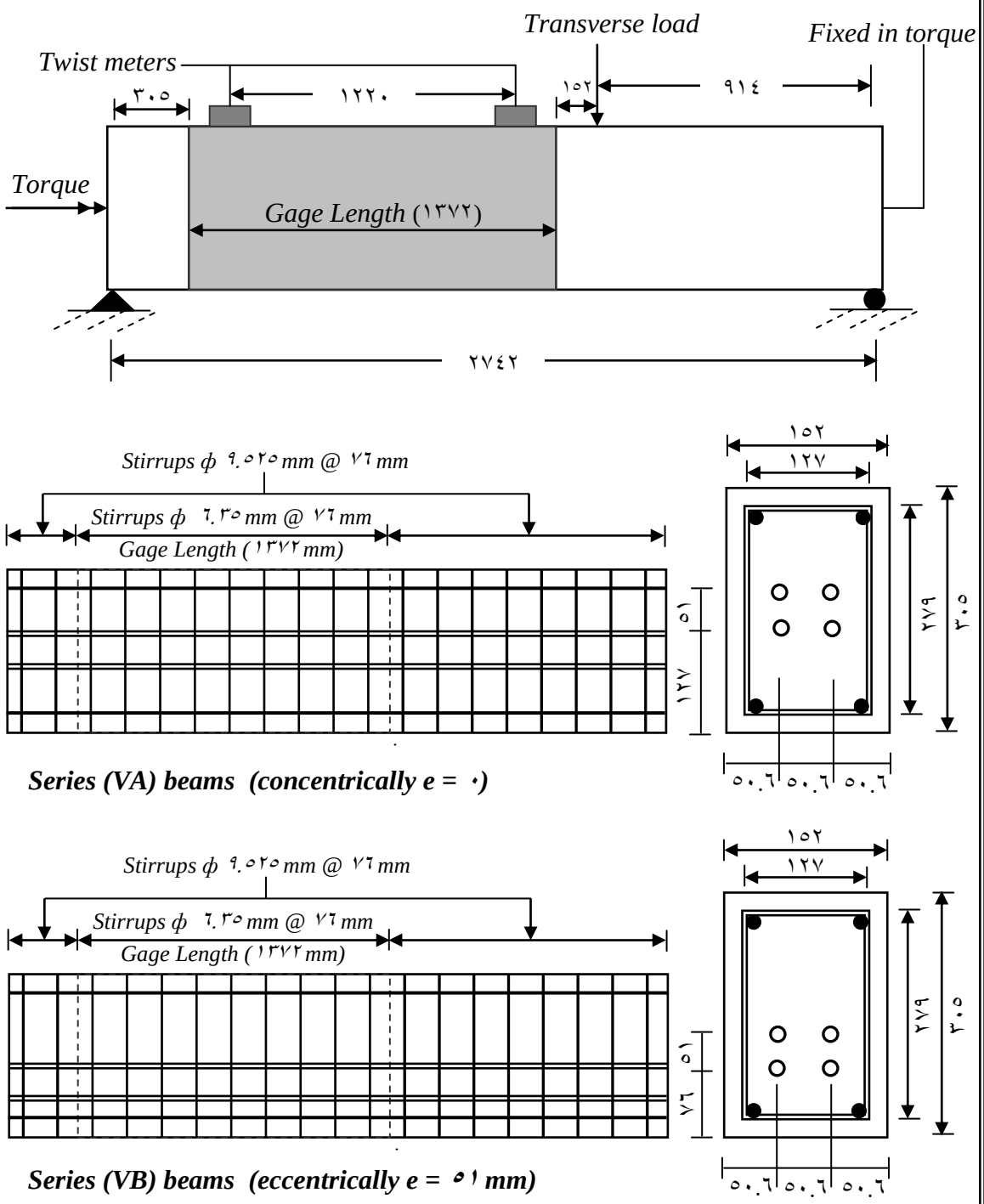

Fig. (٥-٧): Beams Loading, Reinforcement Details and Dimensions of Series (VA) and (VB) Beams (case two)

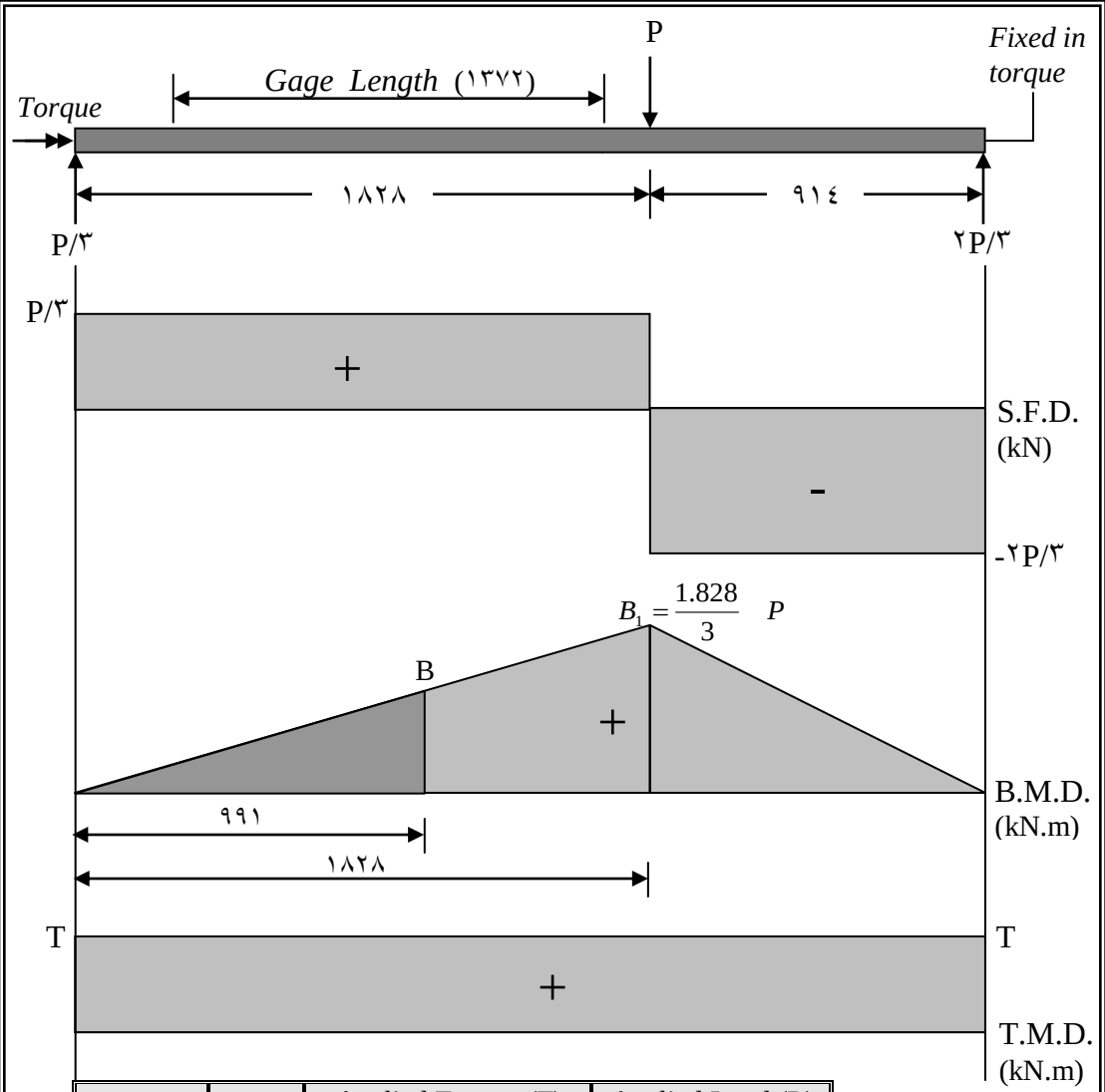

Beam	*T/B*	*Applied Torque (T) (kN.m)*	*Applied Load (P) (kN)*
V١٠٢ V١٢٢	١/٣	١.٥٢	١٣.٨
V١٠٣ V١٢٣	٣/٤	١.٥٢	٦.١٢
V١٠٤ V١٢٤	٤/٣	١.٥٢	٣.٤٥
V١٠٥ V١٢٥	٣	١.٥٢	١.٥٣٤
V١٠٧ V١٢٧	١/٧	١.٥٢	٣٢.٢

$$* \quad \frac{B}{0.991} = \frac{(1.828/3)P}{1.828}, \quad \Rightarrow \quad B = \frac{0.991}{3} P$$

** B_1 = Max. bending moment (kN.m).*
** T = Torsion moment (kN.m).*
** B = Bending moment at the center of gage length (kN.m).*
** all dimensions are in (mm).*

Fig. (٥-٨): Shear Force, Bending Moment, Torsion Moment Diagrams and Applied Loads of Series (VA) and (VB) Beams

Table (٥-٥) : Material Properties and Material Parameters for Mukherjee and Warwaruk Series (VA) Beams

Concrete		***Beam***				
		V١٠٢	**V١٠٣**	**V١٠٤**	**V١٠٥**	**V١٠٧**
E_c	Young's modulus (N/mm^2)	٢٤٩٠٠	٢٥٨٠٠	٢٧٥٠٠	٢٥٣٠٠	٢٣٩٠٠
$f`_c$	Compressive strength (N/mm^2)	٢٧.٥	٢٩.٥	٣٣.٤١	٢٨.٤	٢٥.٤
f_t	Tensile strength (N/mm^2)	٢.٦٢	٢.٧	٢.٨٩	٢.٦٧	٢.٥٢
υ	Poisson's ratio*	٠.٢	٠.٢	٠.٢	٠.٢	٠.٢
k_1	Compression reduction parameter*	٠.٥	٠.٥	٠.٥	٠.٥	٠.٥
α_1	Tension stiffening parameters*	١٠	١٠	١٥	١٥	١٠
α_2		٠.٥	٠.٥	٠.٦	٠.٦	٠.٦
γ_1	Shear - Retention parameters*	١٠	١٠	١٠	١٠	١٠
γ_2		٠.٥	٠.٥	٠.٥	٠.٥	٠.٥
γ_3		٠.١	٠.١	٠.١	٠.١	٠.١
Prestressing tendons						
E_{ps}	Young's modulus (N/mm^2)	١٨٦٠٠٠	١٨٦٠٠٠	١٨٦٠٠٠	١٨٦٠٠٠	١٨٦٠٠٠
A_{ps}	Total area of prestressing tendons (mm^2)	١٥٠	١٥٠	١٥٠	١٥٠	١٥٠
f_{se}	Effective prestressing stress (N/mm^2)	١١٢٢	١١١٩	١٠٠٥	٩٩٠	١٠٧١
f_{py}	Yield stress (N/mm^2)	١٦٠٠	١٦٠٠	١٦٠٠	١٦٠٠	١٦٠٠
Gp	Number of Gauss points of tendons	٨٠	٨٠	٨٠	٨٠	٨٠
Longitudinal steel						
E_s	Young's modulus (N/mm^2)	٢٠٠٠٠٠	٢٠٠٠٠٠	٢٠٠٠٠٠	٢٠٠٠٠٠	٢٠٠٠٠٠
A_l	Total area of longitudinal steel bars (mm^2)	٢٨٨	٢٨٨	٢٨٨	٢٨٨	٢٨٨
f_y	Yield stress (N/mm^2)	٣٤٥	٣٤٥	٣٤٥	٣٤٥	٣٤٥
Web reinforcement						
E_s	Young's modulus (N/mm^2)	٢٠٠٠٠٠	٢٠٠٠٠٠	٢٠٠٠٠٠	٢٠٠٠٠٠	٢٠٠٠٠٠
A_v	Area of web reinforcement (mm^2)	٧٢ ٣٢	٧٢ ٣٢	٧٢ ٣٢	٧٢ ٣٢	٧٢ ٣٢
f_y	Yield stress (N/mm^2)	٣٤٥	٣٤٥	٣٤٥	٣٤٥	٣٤٥
T/B	Torsion to Bending moment ratio	١/٣	٣/٤	٤/٣	٣	١/٧

** assumed values : selected to obtain the best results in comparing with the experimental results*

Table (٥-٦) : Material Properties and Material Parameters for Mukherjee and Warwaruk Series (VB) Beams

Concrete		***Beam***				
		V١٢٢	**V١٢٣**	**V١٢٤**	**V١٢٥**	**V١٢٧**
E_c	Young's modulus (N/mm^2)	٢٥٧٧٠	٢٥٧٥٠	٢٦١٤٠	٢٧٥٣٠	٢٦٨٠٠
$f`_c$	Compressive strength (N/mm^2)	٢٩.٤٣	٢٩.٤	٣٠.٣	٣٣.٦	٣١.٨٥
f_t	Tensile strength (N/mm^2)	٢.٧١	٢.٧	٢.٧٥	٢.٩	٢.٨٢
υ	Poisson's ratio*	٠.٢	٠.٢	٠.٢	٠.٢	٠.٢
k_1	Compression reduction parameter*	٠.٥	٠.٥	٠.٥	٠.٥	٠.٥
α_1	Tension stiffening parameters*	١٥	١٥	١٥	١٥	١٠
α_2		٠.٦	٠.٦	٠.٦	٠.٦	٠.٦
γ_1	Shear - Retention parameters*	١٠	١٠	١٠	١٠	١٠
γ_2		٠.٥	٠.٥	٠.٥	٠.٥	٠.٥
γ_3		٠.١	٠.١	٠.١	٠.١	٠.١
Prestressing tendons						
E_{ps}	Young's modulus (N/mm^2)	١٨٦٠٠٠	١٨٦٠٠٠	١٨٦٠٠٠	١٨٦٠٠٠	١٨٦٠٠٠
A_{ps}	Total area of prestressing tendons (mm^2)	١٥٠	١٥٠	١٥٠	١٥٠	١٥٠
f_{se}	Effective prestressing stress (N/mm^2)	١١٢٢	١١١٩	١٠٠٥	٩٩٠	١٠٧١
f_{py}	Yield stress (N/mm^2)	١٦٠٠	١٦٠٠	١٦٠٠	١٦٠٠	١٦٠٠
Gp	Number of Gauss points of tendons	٨٠	٨٠	٨٠	٨٠	٨٠
Longitudinal steel						
E_s	Young's modulus (N/mm^2)	٢٠٠٠٠٠	٢٠٠٠٠٠	٢٠٠٠٠٠	٢٠٠٠٠٠	٢٠٠٠٠٠
A_l	Total area of longitudinal steel bars (mm^2)	٢٨٨	٢٨٨	٢٨٨	٢٨٨	٢٨٨
f_y	Yield stress (N/mm^2)	٣٤٥	٣٤٥	٣٤٥	٣٤٥	٣٤٥
Web reinforcement						
E_s	Young's modulus (N/mm^2)	٢٠٠٠٠٠	٢٠٠٠٠٠	٢٠٠٠٠٠	٢٠٠٠٠٠	٢٠٠٠٠٠
A_v	Area of web reinforcement (mm^2)	٧٢ ٣٢	٧٢ ٣٢	٧٢ ٣٢	٧٢ ٣٢	٧٢ ٣٢
f_y	Yield stress (N/mm^2)	٣٤٥	٣٤٥	٣٤٥	٣٤٥	٣٤٥
T/B	Torsion to Bending moment ratio	١/٣	٣/٤	٤/٣	٣	١/٧

** assumed values : selected to obtain the best results in comparing with the experimental results*

٥.٣.٢ Effect of Mesh Refinement

To study the effect of mesh refinement on the torque – twist response of Mukherjee and Warwaruk beams, prestressed concrete beam (V١٠٢) has been analyzed using three different finite element meshes as shown in figures (٥-٩). The finite element results for the three meshes are compared in figures (٥-١٠) with the experimental torque – twist curve, this figure shows that the mesh (a) (٢٤ elements) gives a relatively stiffer response as compared with the experimental results. The results of mesh (b) (٣٢ elements) and mesh (c) (٤٠ elements) are relatively similar, but the predicted behavior of the prestressed concrete beam using mesh (c) (٤٠ elements) closer to the experimental response. Therefore, this mesh has been used for all finite element analysis of Mukherjee and Warwaruk prestressed concrete beams throughout the present work.

٥.٣.٣ Effect of Integration Rule

In order to study the accuracy and efficiency of the integration rule, beam (V١٠٢) tested using three different rules. These are ١٥a, ١٥b and ٢٧-point integration rule. The effect of integration rule on the torque – twist response is illustrated in figure (٥-١١). In general, this figure shows that no significant difference are obtained between the effect of type of integration rule on the overall behavior of the tested beams. The ١٥b and ٢٧-Gauss point rules give a similar effect but ١٥b point rule is more close to the experimental results. This rule used in the present study, many research work that dealt with analyzing ordinary and prestressed concrete beams subjected to torsion and combined torsion and bending [٥,٦,١٥,٤٤], adopted ١٥b - point rule.

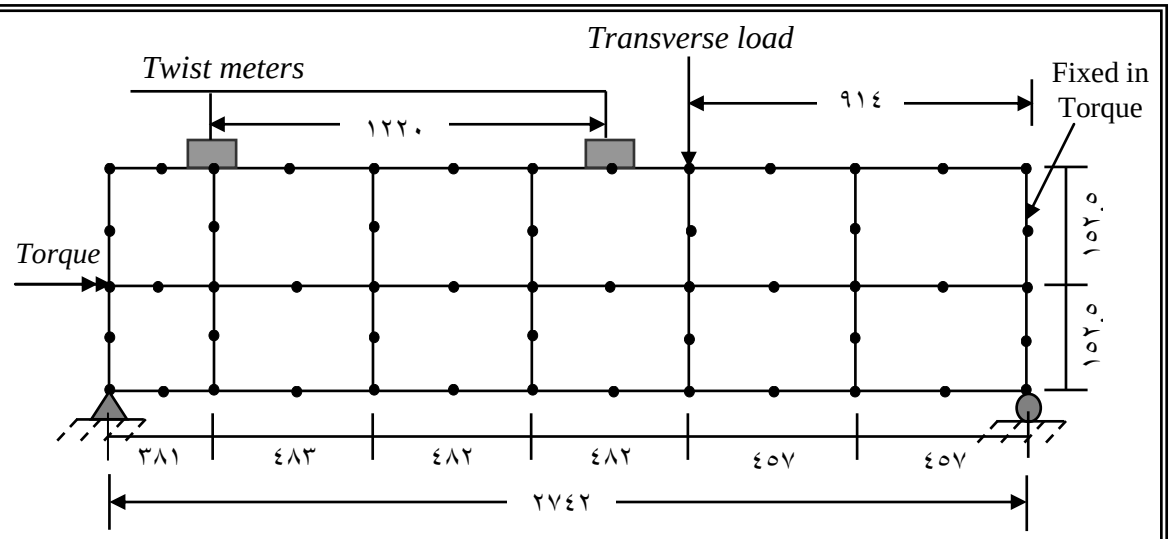

a) ٢٤ - elements

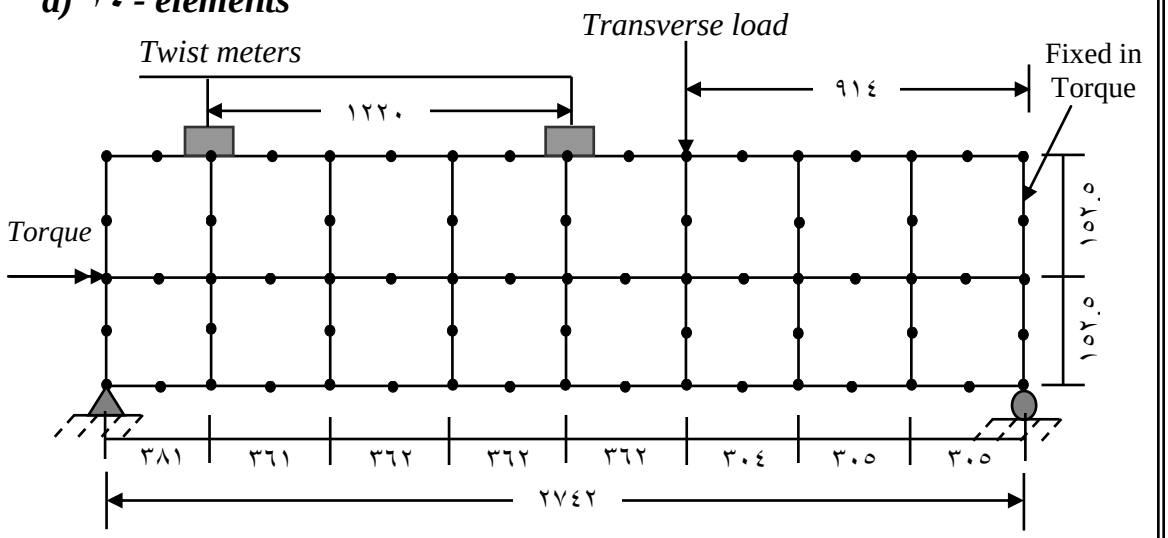

b) ٣٢ - elements

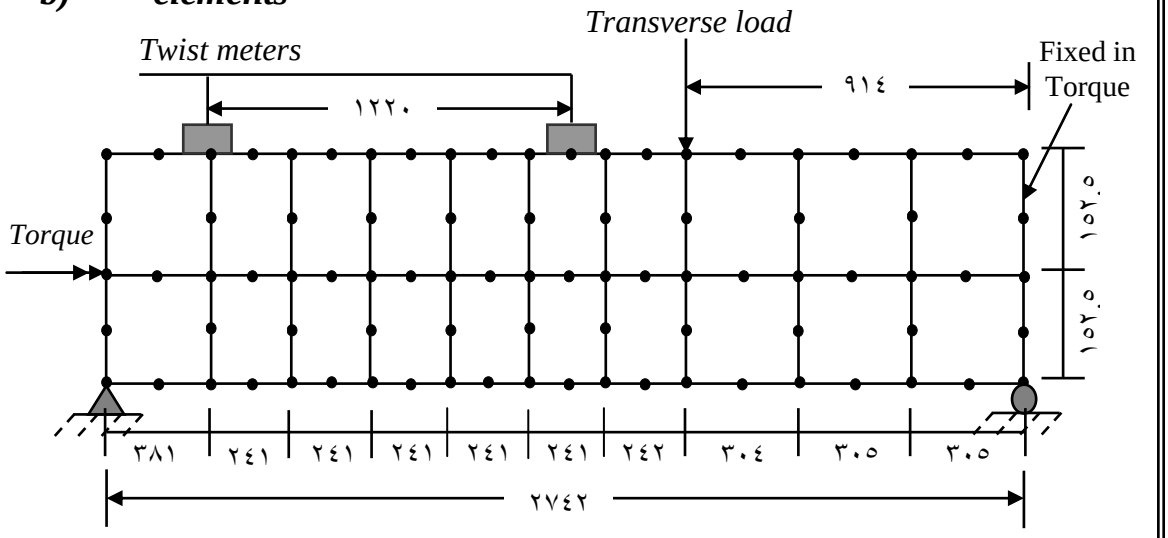

c) ٤٠ – elements

** all dimensions are in (mm).*

Fig. (٥-٩): Different Meshes for Mukherjee and Warwaruk (V١٠٢) Beam (case two)

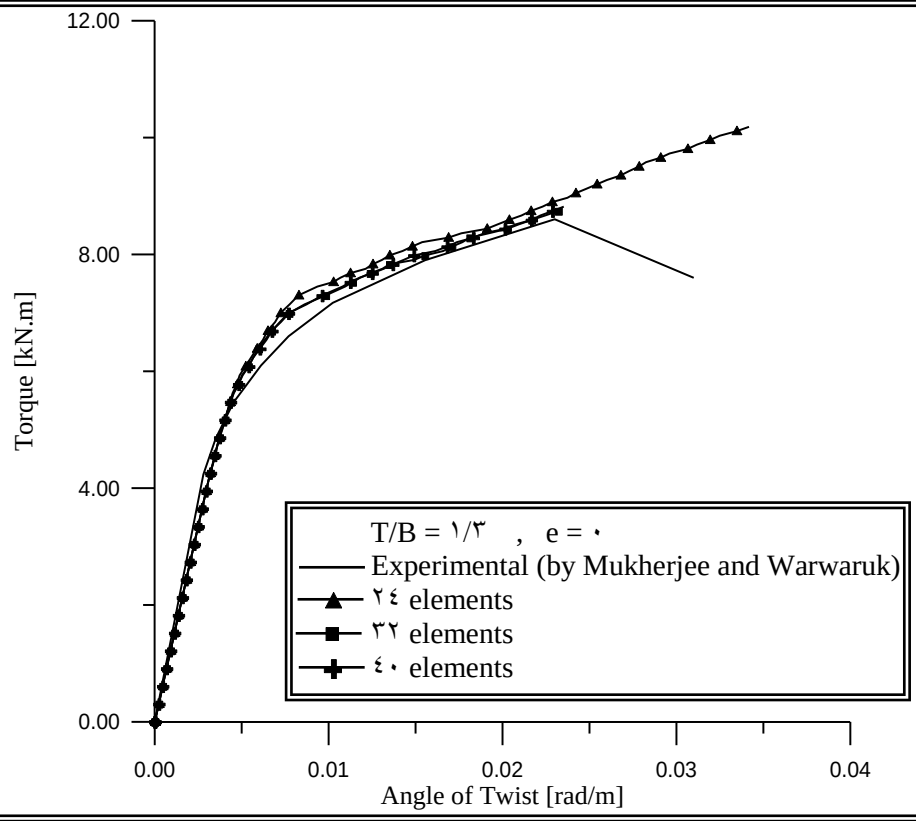

Fig. (٥-١٠): Effect of Mesh Refinement on the Torque – Twist Behavior of Beam (V١٠٢) (case two)

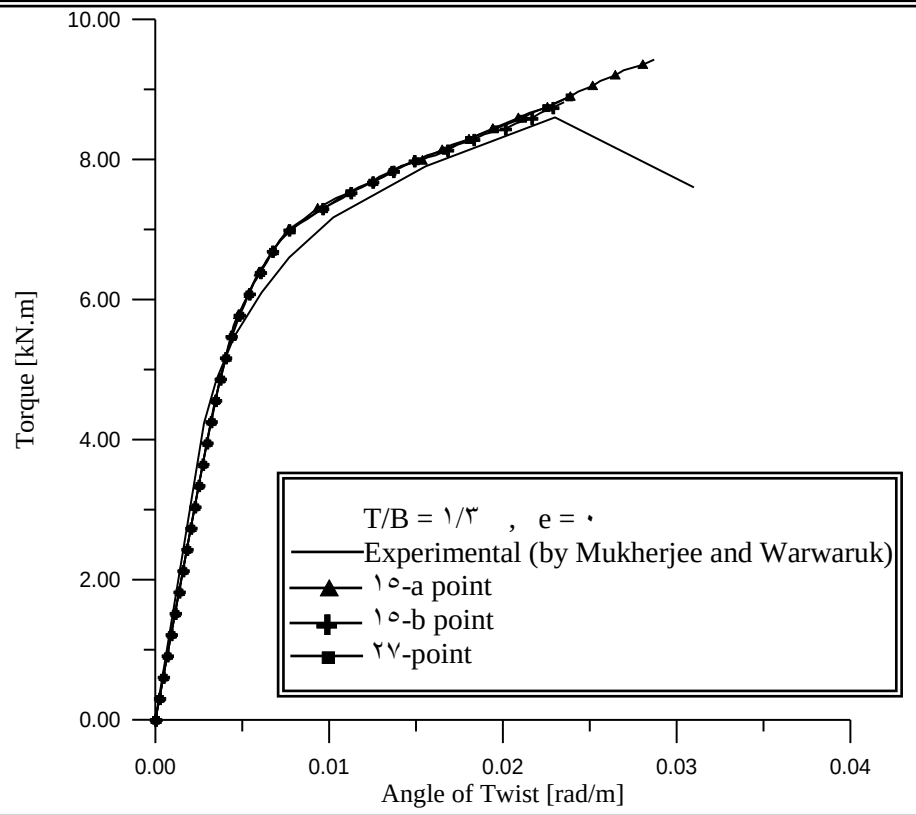

Fig. (٥-١١): Effect of the Integration Rule on the Torque – Twist Behavior of Beam (V١٠٢) (case two)

٥.٣.٤ Finite Element, Boundary Conditions, and Equivalent Nodal Forces of the Tested Beams

Since all the tested beams have the same length and cross sectional dimensions, the same finite element mesh will be used for all beams. Each tested beam was simulated by (٤٠) isoparametric ٢٠-noded brick elements, and the reinforcement modeled as one dimensional element embedded within the ٢٠-noded brick element. The concentrated load (P) was modeled as a line load uniformly distributed across the width of the beam, while the external torque was modeled as a set of equivalent nodal forces applied at the end of the beam (at z = ٠.٠), as described in the section ٣-٧.

The imposed boundary conditions maintain the stability and allow to post cracking extension of the beam in z – direction to occur, the angle of twist was calculated at (z = ٣٨١ mm). Figure (٥-١٢) shows the finite element mesh, boundary conditions, and the equivalent nodal forces of the tested beams.

The effect of prestressing on the beam is introduced before applying the external torque. It is considered as an effective stress and strain at the sampling points of the prestressing tendons using (١٠) increments. The numerical analysis was carried out using the modified Newton Raphson method (KT٢a). Many numerical tests have been considered to study the suitable convergence tolerance and proper integration rule. The results of these tests show that a convergence tolerance (٢٪) and the ١٥b – point integration rule give closer results to the experimental results.

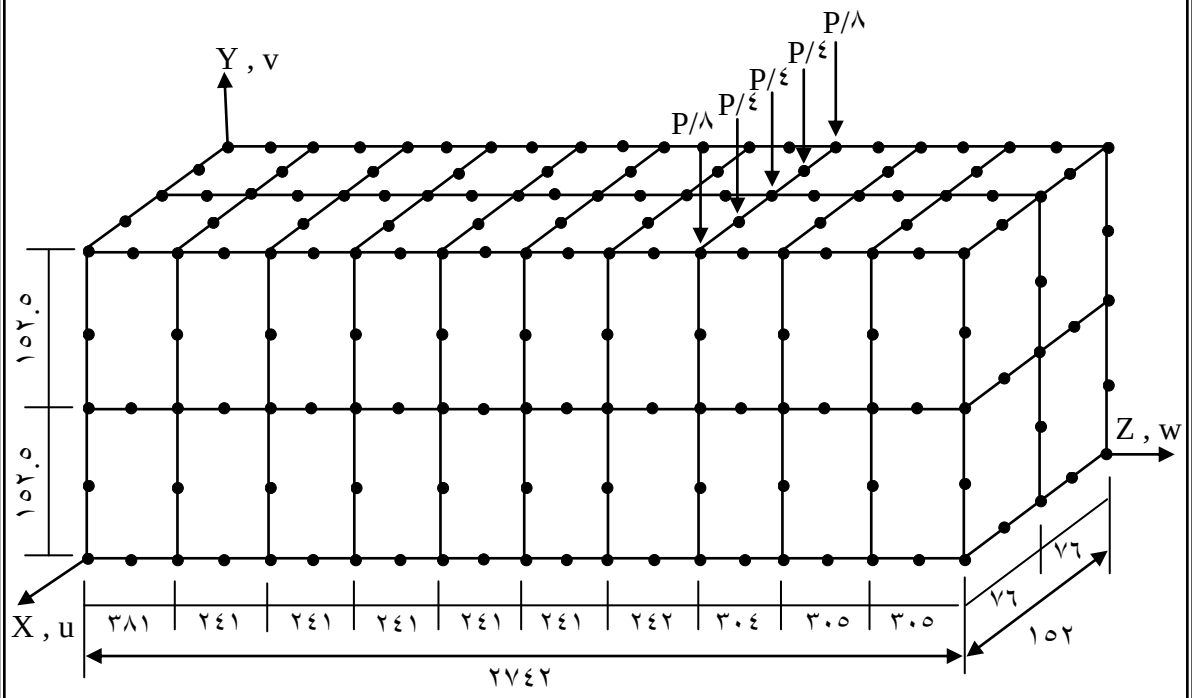

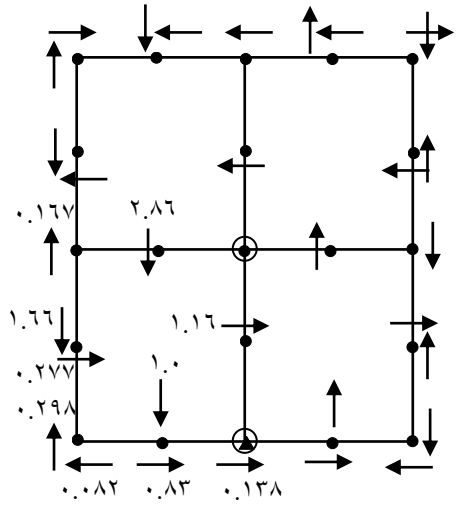

at z = ٠.٠
(Free end for torque)

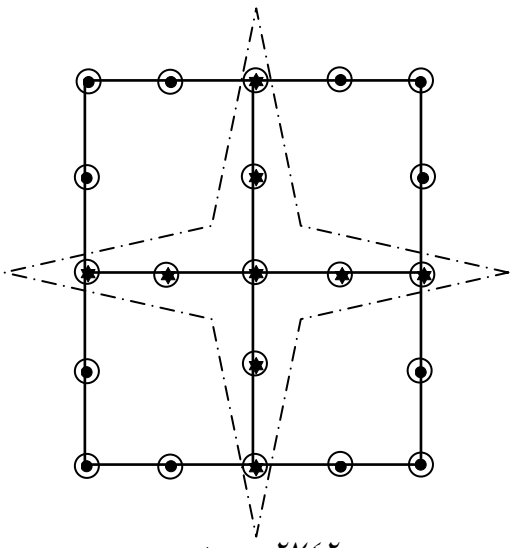

at z = ٢٧٤٢
(Fixed end for torque)

Applied torque
(١.٥٢kN.m)

- *v = ٠*
- *u = v = ٠*
- *u = v = w = ٠*
- *all dimensions are in (mm).*

Fig. (٥-١٢): Finite Element Mesh, Boundary Conditions, and the Equivalent Nodal Forces of Series (VA) and (VB) Beams (case two)

٥.٣.٥ Results of Analysis of the Tested Beams

The results of the present finite element analysis of beams (series VA) V١٠٢, V١٠٣, V١٠٤, V١٠٥, and V١٠٧ give an acceptable agreement with the experimental (by Mukherjee and Warwaruk) results, with a difference range (١.٥٪ - ٨.٤٪) for ultimate torque. Figures (٥-١٣), (٥-١٤), and (٥-١٥) represent a comparison between the experimental (by Mukherjee and Warwaruk) and the present finite element torque-twist curve of the concentrically prestressed concrete beams V١٠٢ (T/B = ١/٣), V١٠٥ (T/B = ٣), and V١٠٧ (T/B = ١/٧) respectively. The results explain that a small difference between the ultimate torque of beams V١٠٤ (T/B = ٤/٣) and V١٠٥ (T/B = ٣), and the increasing in the transverse load causes a significant decreases in the ultimate torque as shown in figure (٥-١٦). The beams of series (VA) analysis without introduced the effect of prestressing (f_{se} = ٠) to study the effect of prestressing on the behavior and ultimate capacity of the beams, the results of this analysis show that the prestressing of the beams increases the ultimate torque with a different percentage and this percentage depends on the torque to bending moment ratio (T/B). The maximum increase in the ultimate torque occurs for beam V١٠٧ (T/B = ١/٧) and the minimum increasing in the ultimate torque occurs for beam V١٠٥ (T/B = ٣), thus the increase in the ultimate torque due to the prestressing increases with decreases the torque to bending moment ratio (T/B).

For beams V١٢٢, V١٢٣, V١٢٤, V١٢٥, and V١٢٧ of series (VB) (concentrically beams e = ٥١mm) the results of the present finite element analysis show a good agreement with the experimental (by Mukherjee and Warwaruk) results, with a different range (٠.٥٪ - ٥.٤٪) for ultimate torque. A comparison between the experimental (by Mukherjee and Warwaruk) and the present finite element analysis torque-twist curve of beams V١٢٣ (T/B = ١/٣), V١٢٥ (T/B = ٣), and V١٢٧ (T/B = ١/٧) are

shown in figure (٥-١٧), (٥-١٨), and (٥-١٩) respectively. Also, a comparison among the beams of series (VB) are illustrated in figure (٥-٢٠) to show the effect of torque to bending moment ratio (T/B) on the ultimate torque. To study the effect of prestressing on the behavior and ultimate capacity of series (VB) beams, analysis these beams without introduced the effect of prestressing (f_{se} = ٠). The results of this analysis explain an increase in the ultimate torque ranging from (١١.٩٪) for beam V١٢٥ (T/B = ٣) to (٤٤.٥٪) for beam V١٢٧ (T/B = ١/٧). By studying the effect of prestressing on series (VA) and (VB) beams, it can be noticed that the prestressing is more effective for series (VB) beams (eccentrically beams). The results of the present finite element analysis, the experimental results (by Mukherjee and Warwaruk), and the comparison between the experimental and numerical results are tabulated in table (٥-٧).

Table (٥-٧) : Comparison Between the Experimental and Predicted Ultimate Torque of Series (VA) and (VB) Beams

	Beam	T/B	$T_{exp.}$	$T_{u١}$	$T_{u٢}$	$\frac{T_{u١}}{T_{exp.}}$	$\frac{T_{u١}-T_{exp.}}{T_{exp.}}$	$\frac{T_{u١}-T_{u٢}}{T_{u٢}}$
Series (VA) (e = ٠)	V١٠٢	١/٣	٨.٦	٨.٨٢	٦.٢	١.٠٢٦	٢.٦ %	٤٢.٣ %
	V١٠٣	٣/٤	١٢.٢٥	١٣.٢٨	١٠.٣٢	١.٠٨٤	٨.٤ %	٢٨.٧ %
	V١٠٤	٤/٣	١٤.٥	١٥.٤٣	١٣.٦	١.٠٦٤	٦.٤ %	١٣.٤٦ %
	V١٠٥	٣	١٤.٥٤	١٥.٣٥	١٤.٢٩	١.٠٥٦	٥.٦ %	٧.٤٢ %
	V١٠٧	١/٧	٤	٤.٠٦	٢.٨٣	١.٠١٥	١.٥ %	٤٣.٥ %
Series (VB) (e = ٥١ mm)	V١٢٢	١/٣	١٠.٧٨	١٠.٨٤	٧.٥٤	١.٠٠٦	٠.٦ %	٤٣.٨ %
	V١٢٣	٣/٤	١٤.٣٣	١٤.٧٧	١١.٤٣	١.٠٣	٣.١ %	٢٩.٢ %
	V١٢٤	٤/٣	١٥.٤٧	١٥.٥٥	١٣.٣٨	١.٠٠٥	٠.٥ %	١٦.٢ %
	V١٢٥	٣	١٥.٤٢	١٦.٢٦	١٤.٥٢	١.٠٥٤	٥.٤ %	١١.٩ %
	V١٢٧	١/٧	٥.٤٦	٥.٥٢	٣.٨٢	١.٠١١	١.١ %	٤٤.٥ %

where :

T_{exp} : The ultimate experimental torque (kN.m) (by Mukherjee and Warwaruk) .

$T_{u١}$: The ultimate torque obtained from the present F.E.A. (kN.m) for prestressing beams .

$T_{u٢}$: The ultimate torque obtained from the present F.E.A. (kN.m) for non-prestressing beams (f_{se} = ٠).

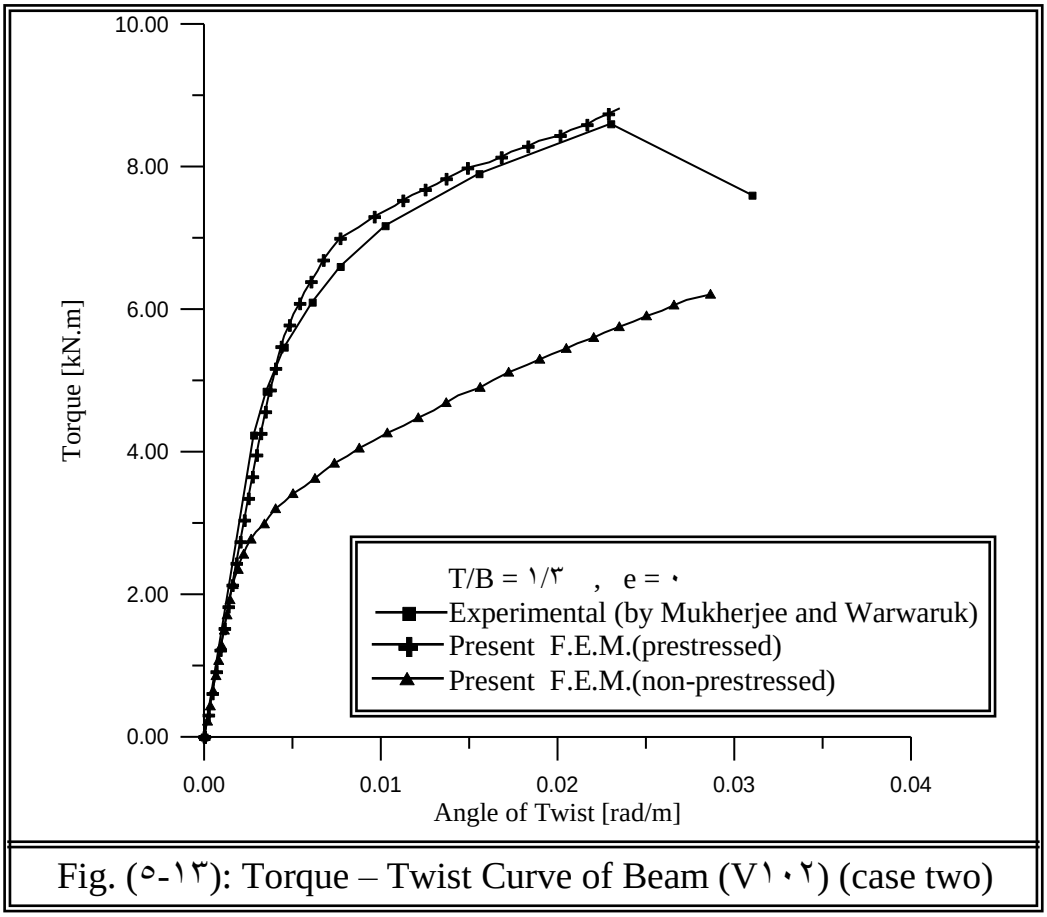

Fig. (٥-١٣): Torque – Twist Curve of Beam (V١٠٢) (case two)

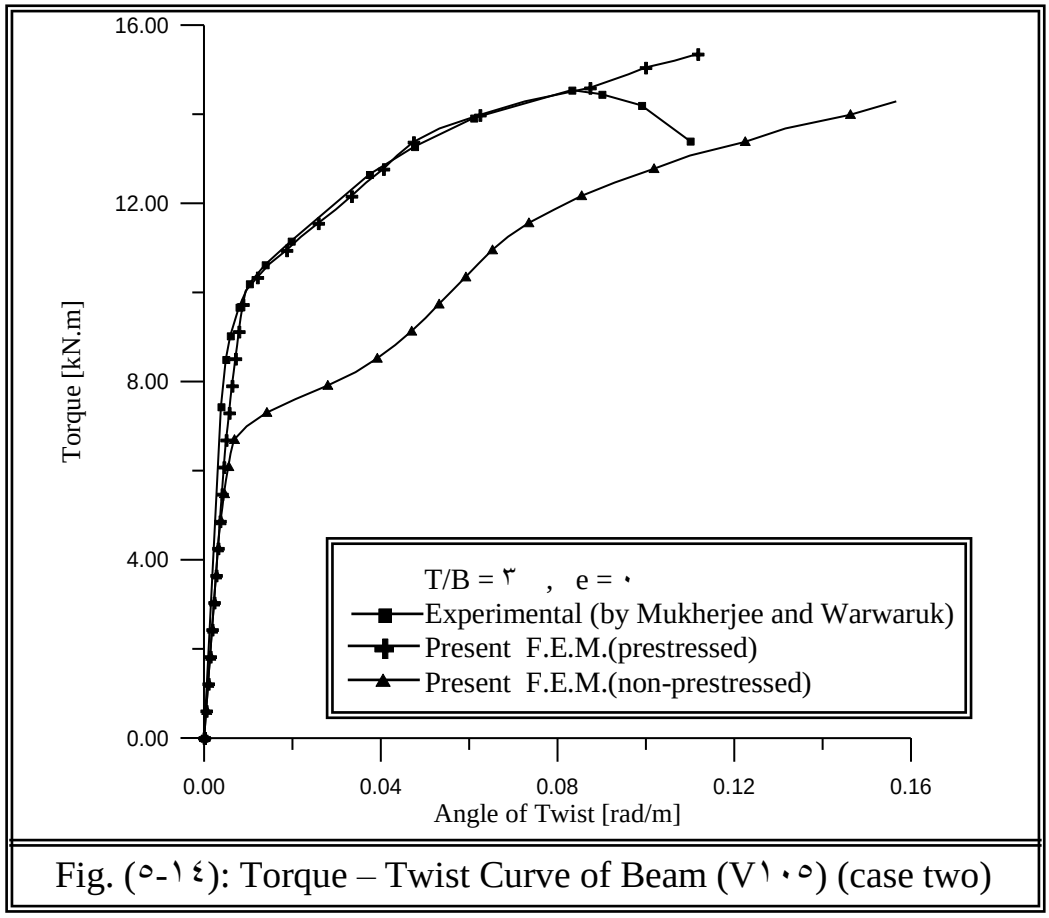

Fig. (٥-١٤): Torque – Twist Curve of Beam (V١٠٥) (case two)

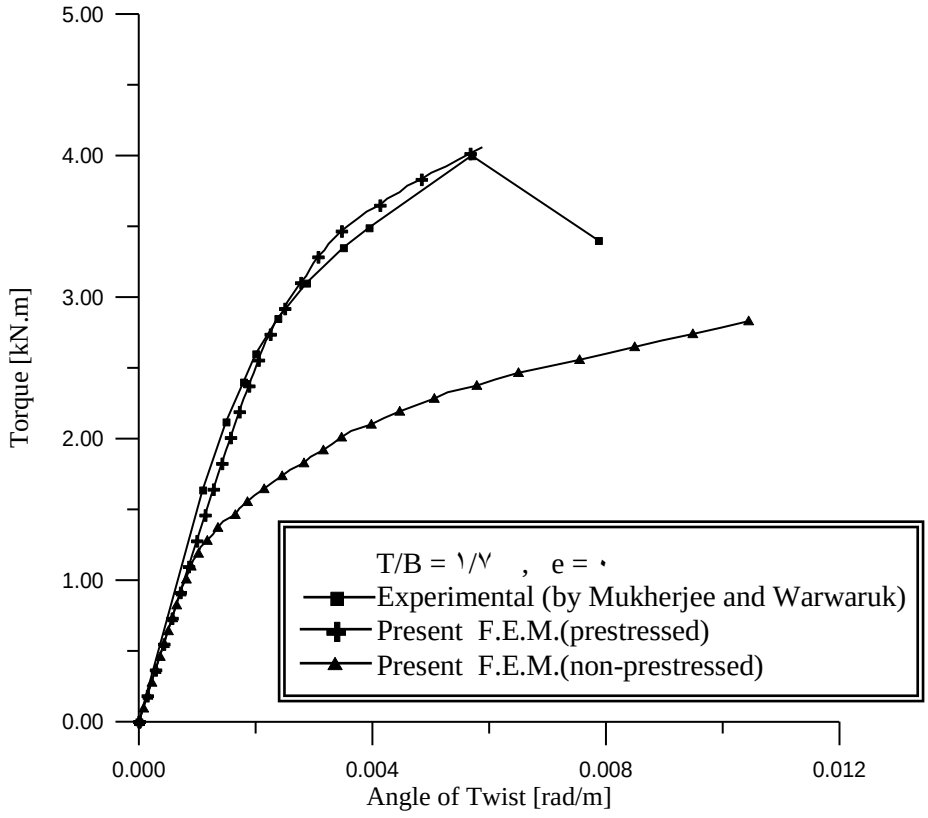

Fig. (٥-١٥): Torque – Twist Curve of Beam (V١٠٧) (case two)

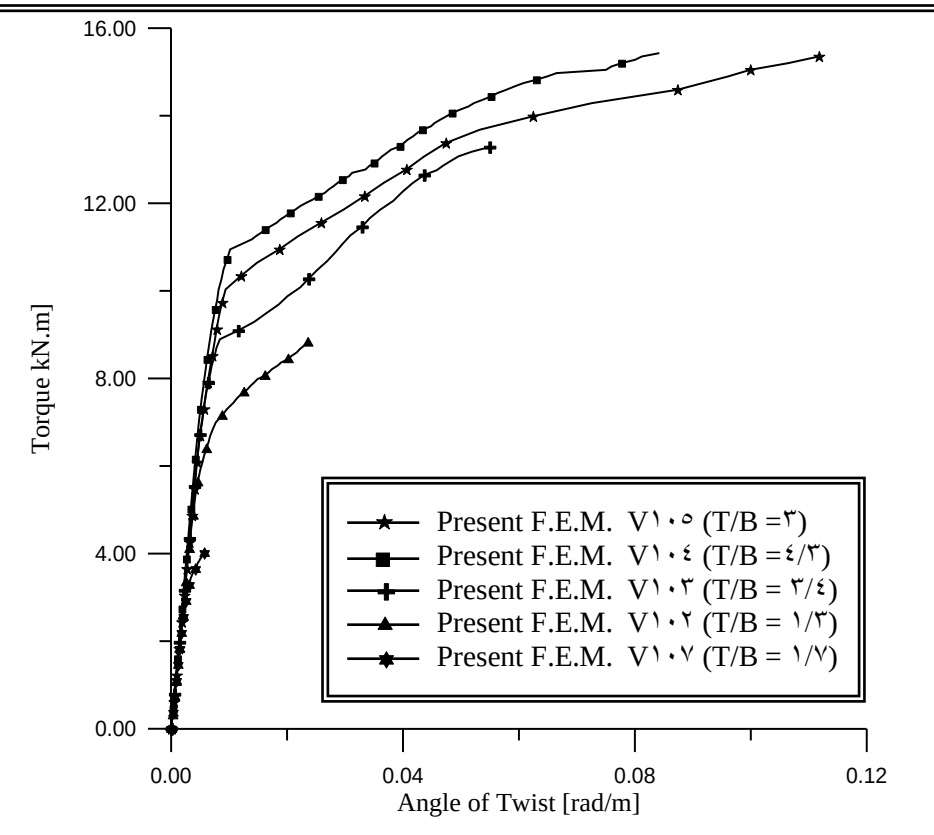

Fig. (٥-١٦): Torque – Twist Curve of Series (VA) Beams (e = ٠)

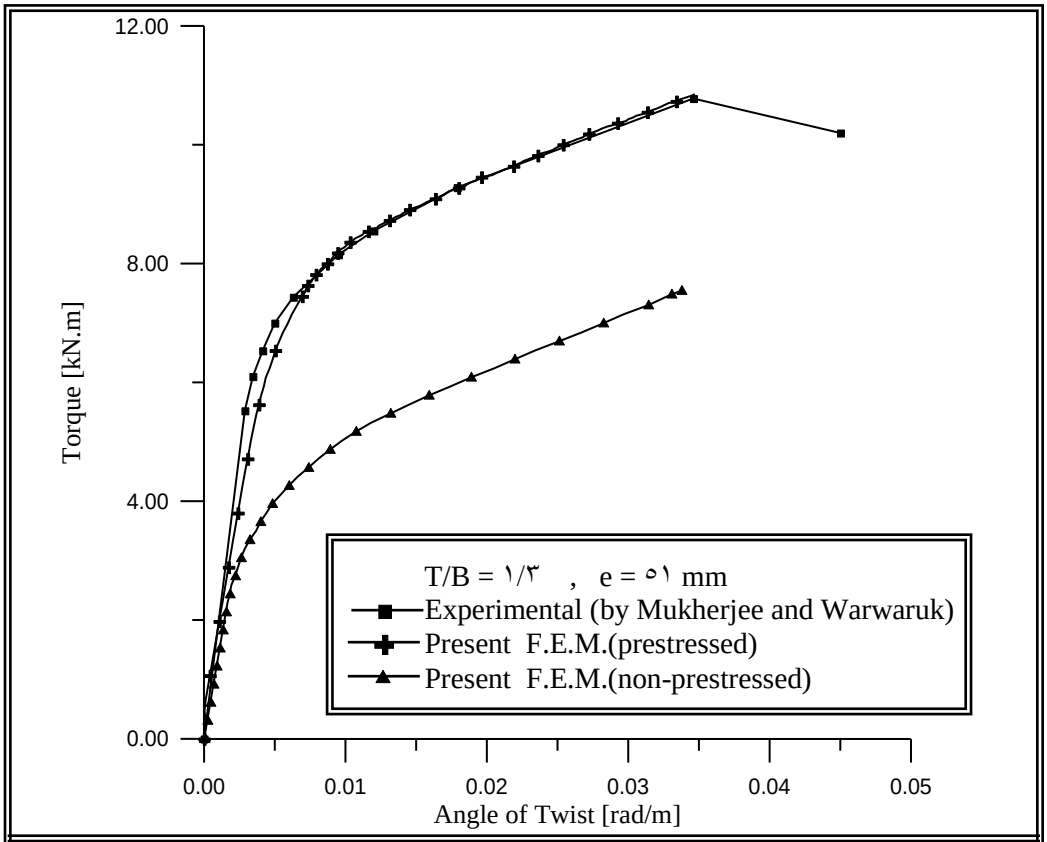

Fig. (٥-١٧): Torque – Twist Curve of Beam (V١٢٢) (case two)

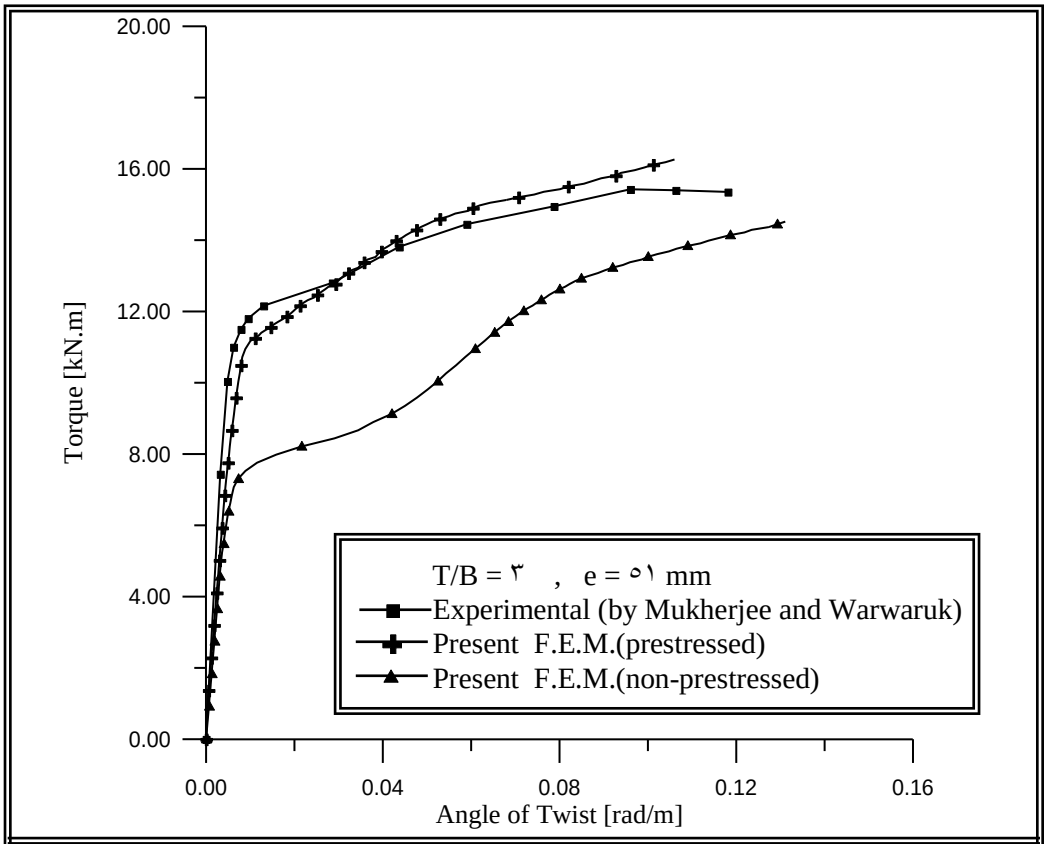

Fig. (٥-١٨): Torque – Twist Curve of Beam (V١٢٥) (case two)

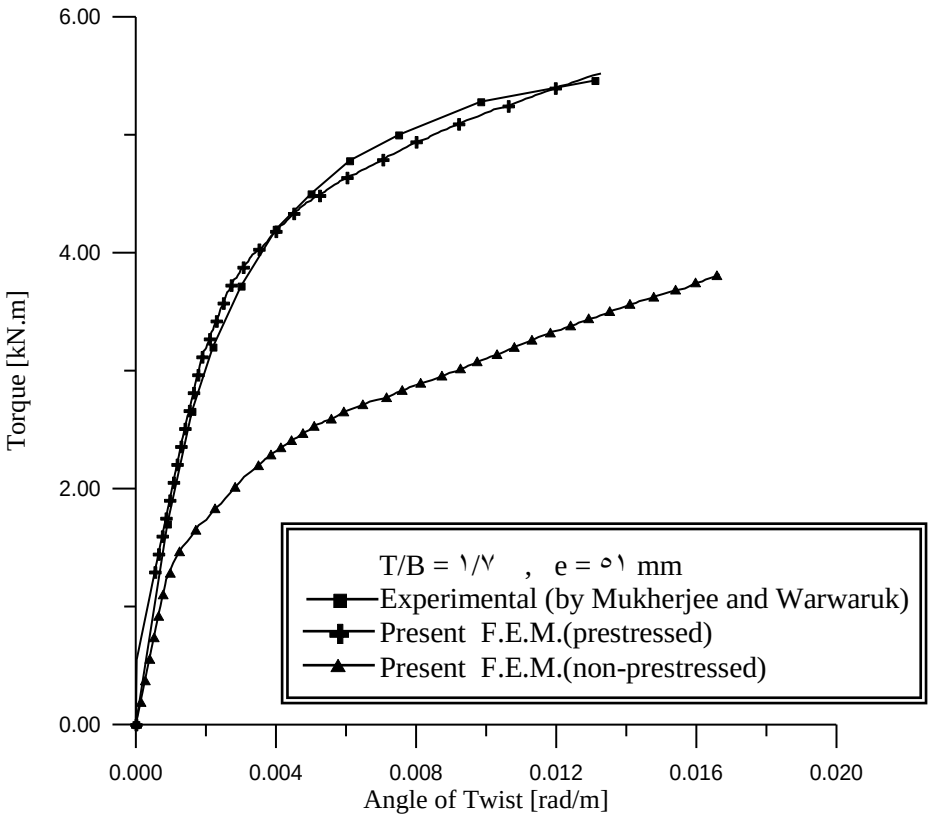

Fig. (٥-١٩): Torque – Twist Curve of Beam (V١٢٧) (case two)

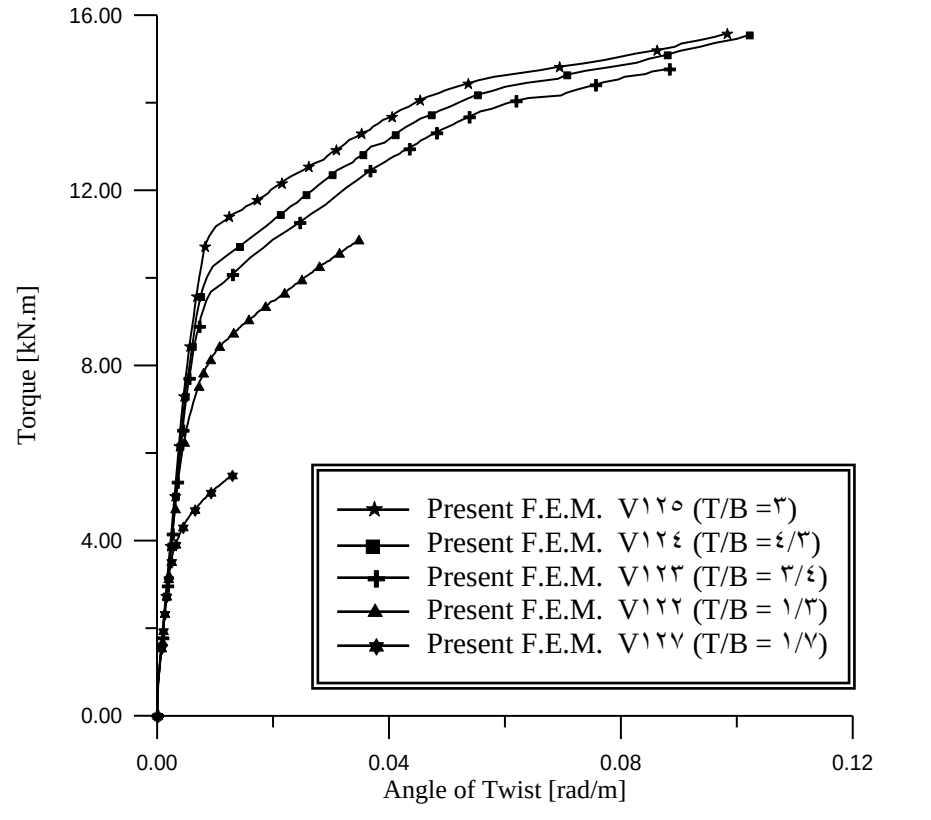

Fig. (٥-٢٠): Torque – Twist Curve of Series (VB) Beams (e = ٥١)

٥.٣.٦ Variation of Warping Displacement

The variation of warping displacement over the section at z = ٠ (applied torque section) and at z = ٢٧٤٢ mm (fixed in torque section) of beams (V١٠٢), (V١٠٣), (V١٠٤), (V١٠٥) and (V١٠٧) at the collapse loads are shown in figures (٥-٢١), (٥-٢٢), (٥-٢٣), (٥-٢٤) and (٥-٢٥) respectively. The warping displacement of beams V١٠٢ (T/B = ١/٣) and (V١٠٧) (T/B = ١/٧) at z = ٠ is similar and the warping surface is plane. The section has a rotating about the neutral axis and small rotating about the longitudinal axis.

While the warping surface of beams V١٠٣ (T/B = ٣/٤), (V١٠٤) (T/B = ٤/٣) and V١٠٥ (T/B = ٣) at z = ٠ is non uniform (non plane); this is due to effect of torsion. Where the torsion to bending moment ratio (T/B) in these beams is high. When the (T/B) ratio is high the warping surface is non plane and when (T/B) is small the warping surface is plane.

The warping displacement At z = ٢٧٤٢ mm (fixed in torque section) the section rotate about the longitudinal and neutral axes in all beams.

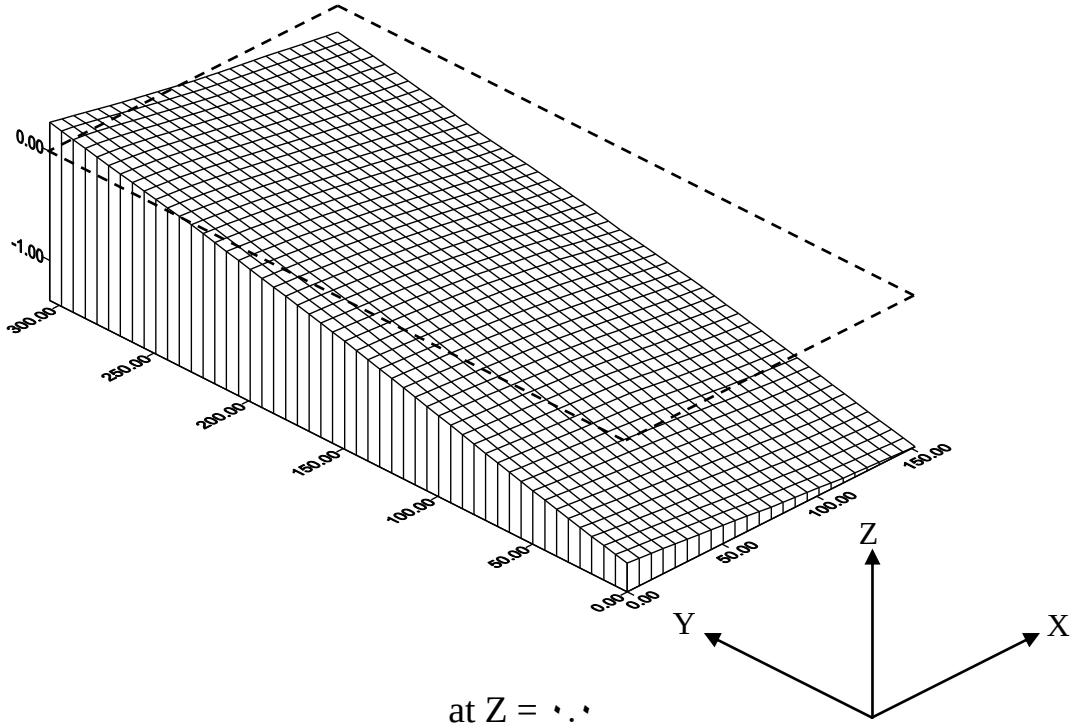

at Z = ٠.٠
(Applied Torque Section)

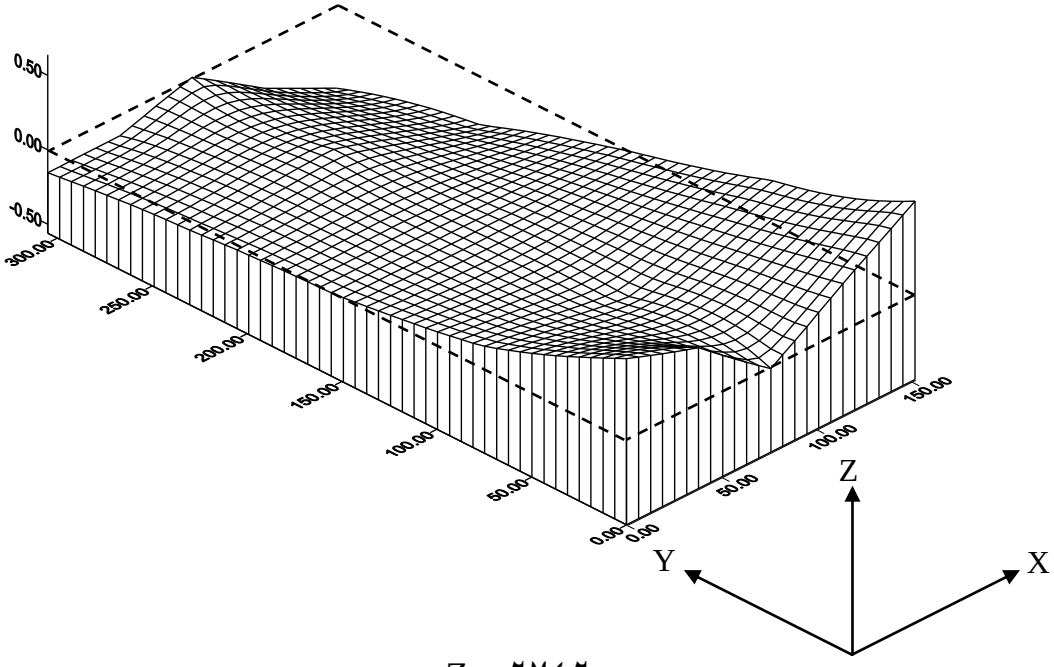

at Z = ٢٧٤٢ mm
(Fixed in Torque Section)

Fig. (٥-٢١): Variation of the Displacement in Z-Direction at Ultimate Torque of Beam (V١٠٢) (T/B = ١/٣ , e = ٠)

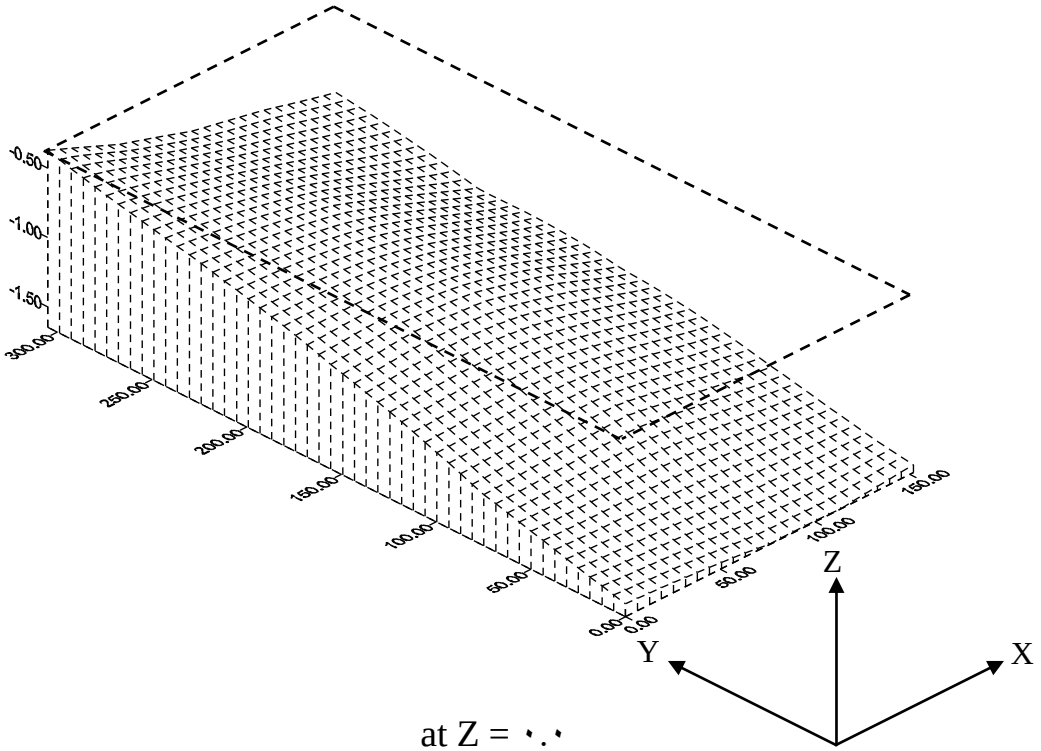

at Z = ٠.٠
(Applied Torque Section)

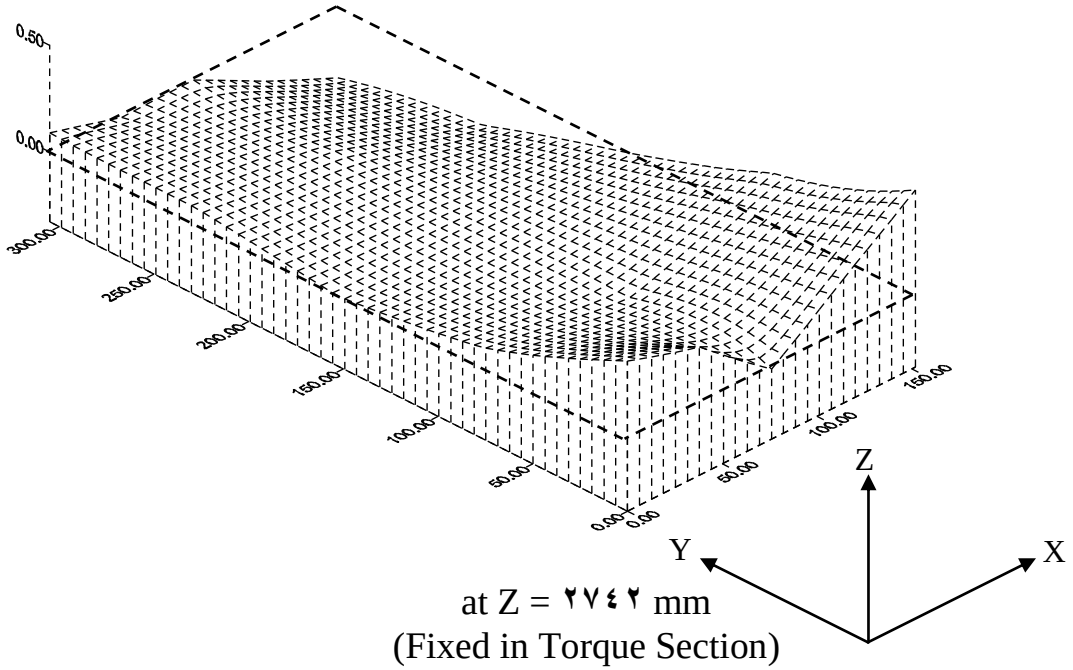

at Z = ٢٧٤٢ mm
(Fixed in Torque Section)

Fig. (٥-٢٢): Variation of the Displacement in Z-Direction at Ultimate Torque of Beam (V١٠٣) (T/B = ٣/٤ , e = ٠)

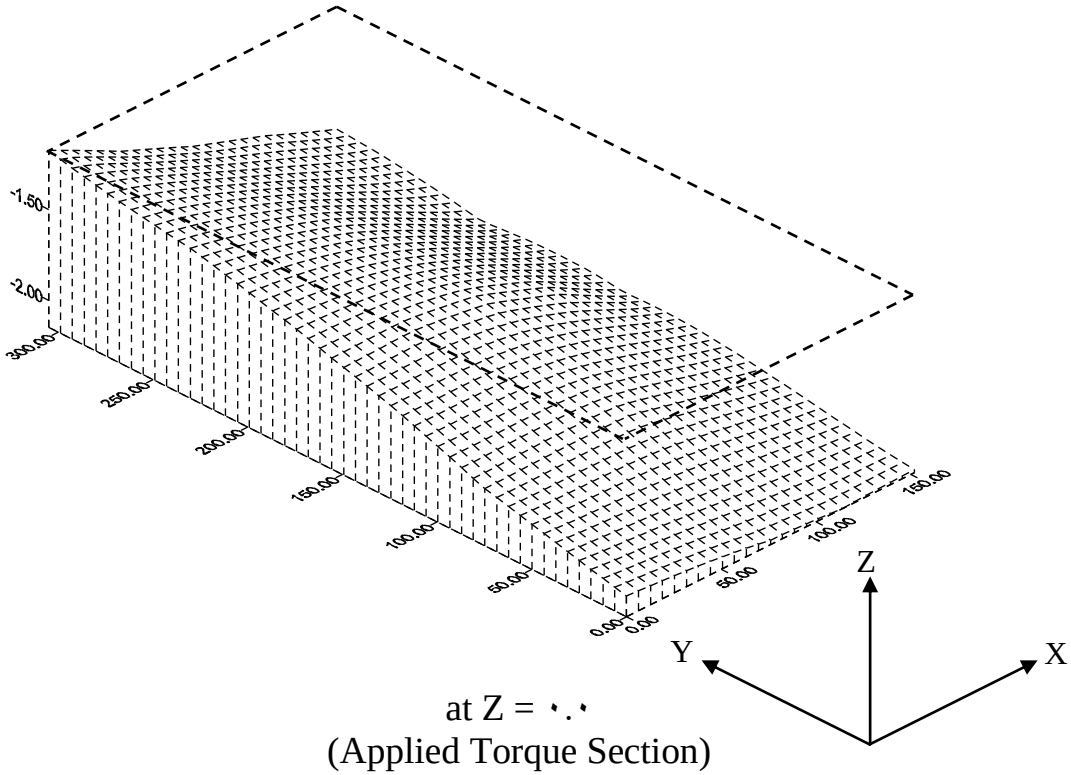

at Z = ٠.٠
(Applied Torque Section)

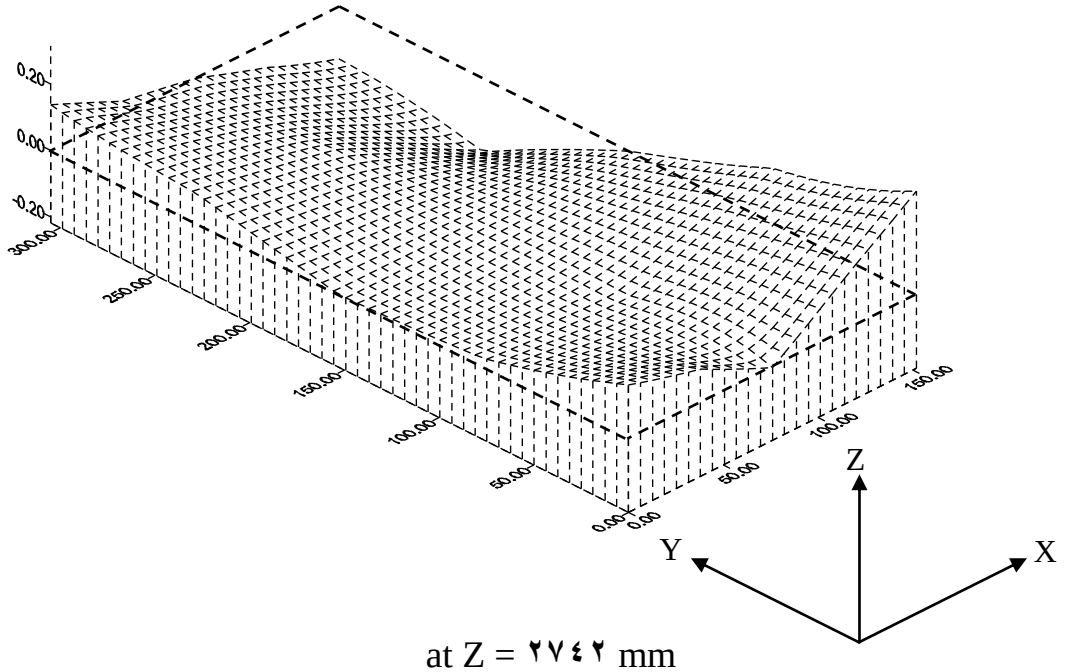

at Z = ٢٧٤٢ mm
(Fixed in Torque Section)

Fig. (٥-٢٣): Variation of the Displacement in Z-Direction at Ultimate Torque of Beam (V١٠٤) (T/B = ٤/٣ , e = ٠)

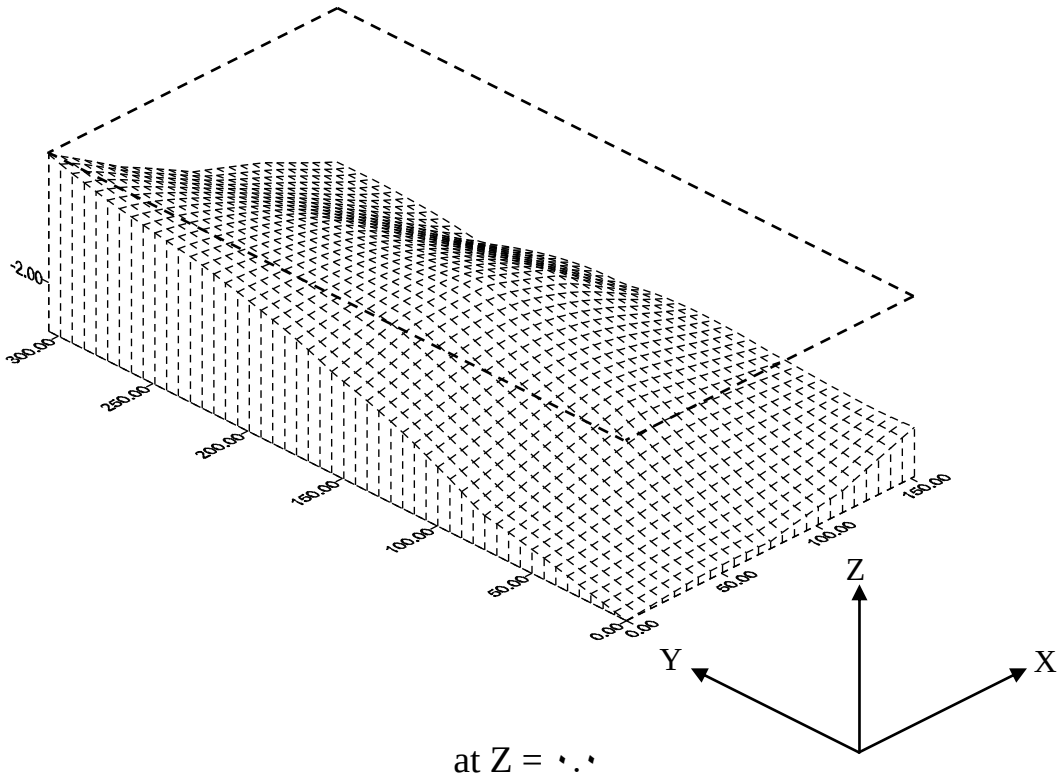

at Z = ٠.٠
(Applied Torque Section)

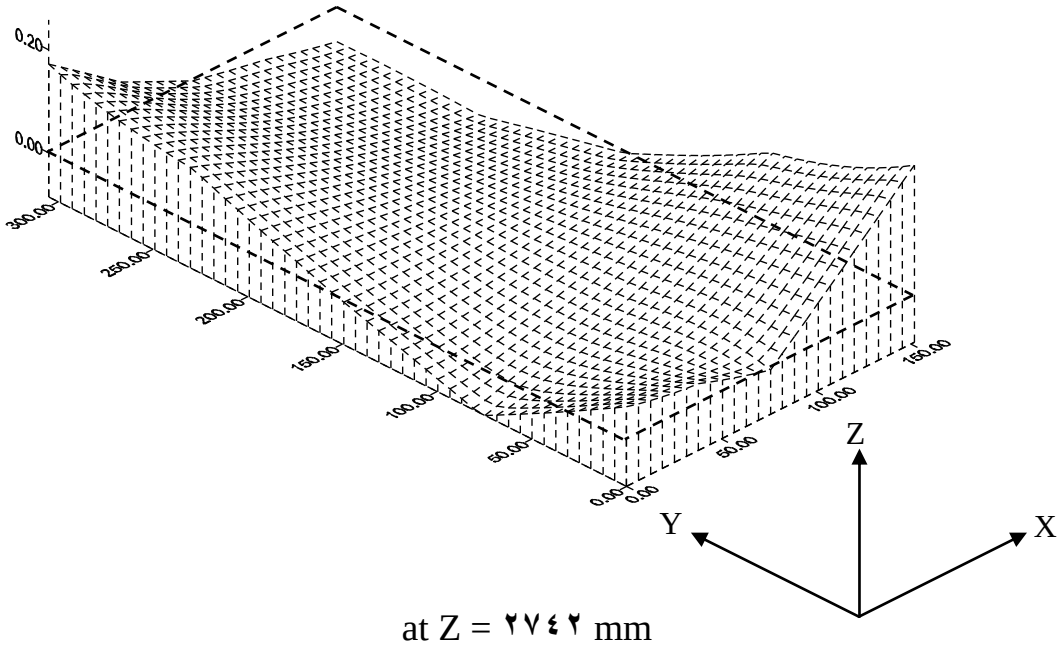

at Z = ٢٧٤٢ mm
(Fixed in Torque Section)

Fig. (٥-٢٤): Variation of the Displacement in Z-Direction at Ultimate Torque of Beam (V١٠٥) (T/B = ٣ , e = ٠)

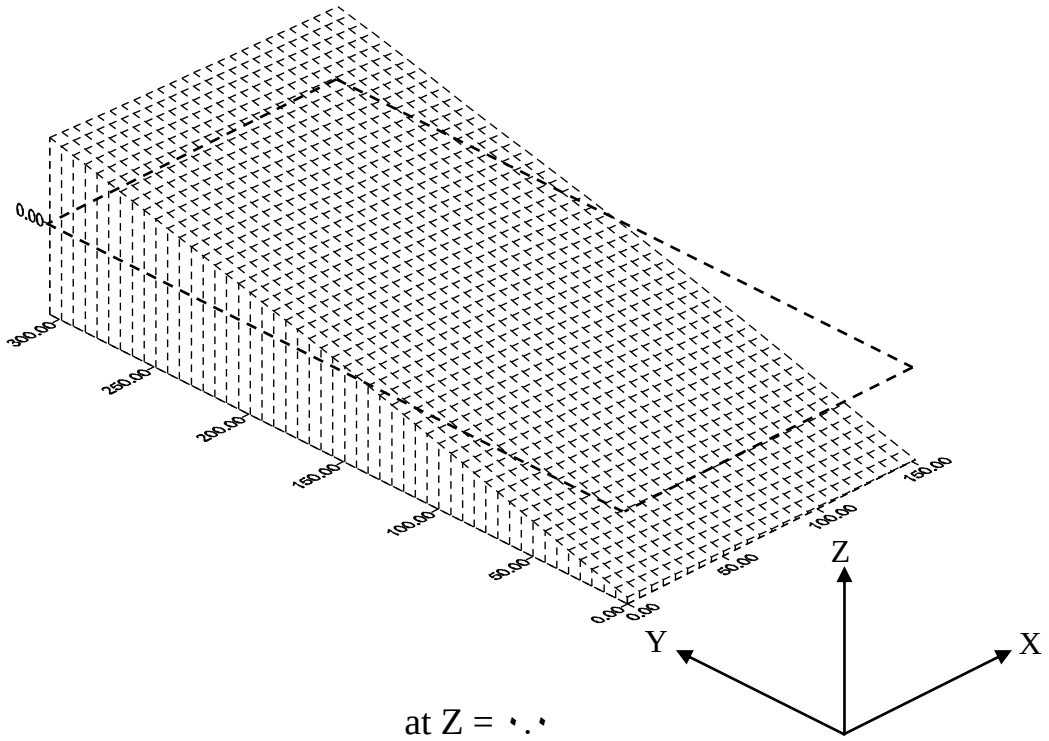

at Z = ٠.٠
(Applied Torque Section)

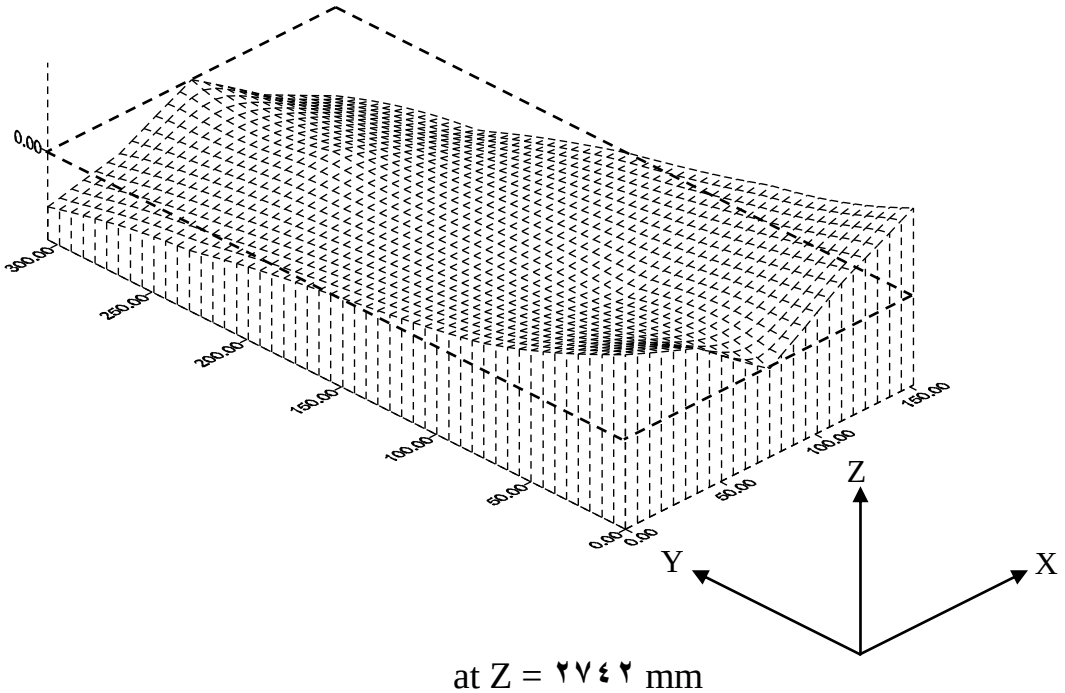

at Z = ٢٧٤٢ mm
(Fixed in Torque Section)

Fig. (٥-٢٥): Variation of the Displacement in Z-Direction at Ultimate Torque of Beam (V١٠٧) (T/B = ١/٧ , e = ٠)

٥.٤ Parametric Study

The effect of tension stiffening parameters, shear retention parameters, Poison's ratio, and effect of torque to transverse load (T/P) ratio have been studied on beam (V١٠٢) (T/B = ١/٣) which was subjected to combined shear, bending and torsion. The effect of reduction in compressive strength ($k_١$), the effect of variation of amount of prestressing steel and the amount of longitudinal and transverse reinforcement have been studied on beams (V١٠٢), (V١٠٣), (V١٠٤), (V١٠٥), and (V١٠٧) that were subjected to combined shear, bending and torsion. In these numerical tests one parameter was selected to be vary and all the other parameters were kept constant.

٥.٤.١ Effect of Tension Stiffening Parameters ($\alpha_١$ and $\alpha_٢$):

To study the effect of tension stiffening parameters ($\alpha_١$ and $\alpha_٢$) on the behavior and ultimate capacity of beams subjected to combined shear, bending and torsion loads, beam (V١٠٢) has been analyzed with different values of ($\alpha_١$) and ($\alpha_٢$).

Numerical tests of beam V١٠٢ with values of ($\alpha_١$) equal to (٥ , ١٠ , ١٥ and ٣٠) have been carried out, in these tests ($\alpha_٢$) was set to (٠.٥) for beam V١٠٢. Throughout the numerical tests of beam V١٠٢ the tension stiffening parameter ($\alpha_١$), which represents the rate of stress release as the crack widens, has a strongly effect on the post cracking behavior of the tested beam. Figure (٥-٢٦) show that the effect of ($\alpha_١$) is largely influence on the post cracking response and the ultimate capacity of the beam. The higher value of ($\alpha_١$ = ٣٠) causes slightly stiffer response while the lower

value (α_1 = ٥) shows a softer response. The best fit to the experimental results of beam V١٠٢ was obtained when (α_1) set is equal to (١٠).

To study the effect of the tension stiffening parameter (α_2), which represents the sudden loss in the tensile stress at instant of cracking, numerical tests on beam (V١٠٢) with values of (α_2) equal to (٠.٢, ٠.٥, ٠.٧ and ١.٠) have been carried out, in these tests (α_1) was set equal to (١٠) during the analysis. The parameter (α_2) has a significant effect on the post cracking torque-twist response and a small effect on the ultimate capacity of the tested beam as shown in figure (٥-٢٧). The best fit to the experimental results was obtained when (α_2) is equal to (٠.٥). Similar analysis has been carried out on beams of series (VA) and (VB) to choose the best values of tension stiffening parameters as listed in table (٥-٥) and (٥-٦).

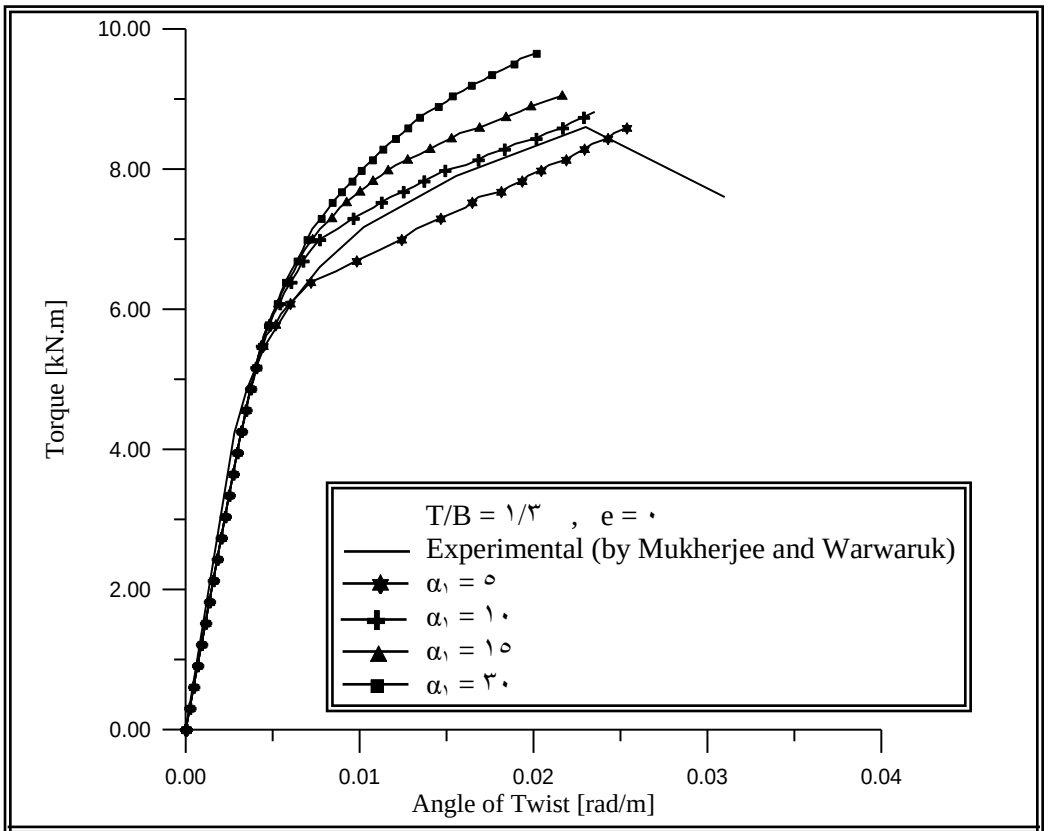

Fig. (٥-٢٦): Effect of Tension Stiffening Parameter (α_1) on the Torque – Twist Behavior of Beam (V١٠٢) (case two)

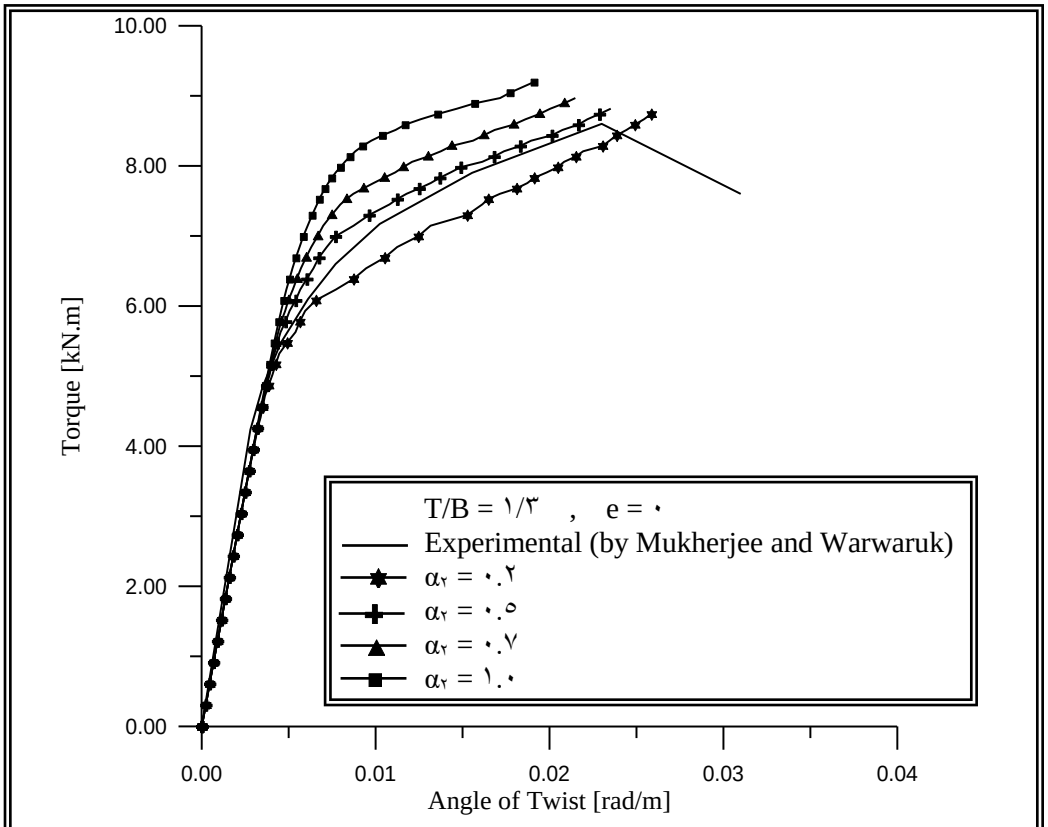

Fig. (٥-٢٧) : Effect of Tension Stiffening Parameter (α_2) on the Torque – Twist Behavior of Beam (V١٠٢) (case two)

٥.٤.٢ Effect of Shear Retention Parameters (γ_1, γ_2 and γ_3)

Different values of shear retention parameters (γ_1, γ_2, and γ_3) have been used in a numerical tests of beam (V١٠٢) to study the effect of shear retention parameters on the torque – twist response and ultimate capacity of the tested beam. Numerical tests with values of (γ_1) which represents the rate of decay of the shear stiffness as the crack widens equal to (٥, ١٠, ١٥ and ٣٠) and (γ_2) equals to (٠.٥) and (γ_3) equals to (٠.١) were carried out. A slightly stiff response was obtained for (γ_1) equal to (٣٠), as shown in figure (٥-٢٨) . The best fit to the experimental results of the tested beams is obtained when (γ_1) is equal to (١٠). Three numerical tests on beams (V١٠٢) with (γ_2) equal to (٠.٢, ٠.٥, and ٠.٧), the parameters (γ_1) and (γ_2) were set equal to (١٠) and (٠.١) respectively in all tests have been considered to study the effect of shear retention parameter (γ_2) which

represents the sudden loss in shear stiffness at instant of cracking. The results of these tests show that no significant effect of (γ_2) on the torque-twist curve of the tested beam as shown in figure (٥-٢٩). The best value of (γ_2) for the tested beams was set equal to (٠.٥). The effect of shear retention parameter (γ_3) which represents the residual shear stiffness due to dowel action is examined by four numerical tests of beams (V١٠٢) with (γ_3) equals to (٠.٠٥, ٠.١, ٠.١٥, and ٠.٣). Figure (٥-٣٠) show that (γ_3) has a small effect on the behavior and slightly effect on the ultimate capacity of the tested beam, the best value of the parameter (γ_3) has been taken equal to (٠.١). From the results of the above testes of parameters (γ_1, γ_2 and γ_3) it is clear that a small effect of these parameters on the behavior and ultimate capacity of the tested beam. Thus, for beams of series (VA) and (VB) can use values (١٠, ٠.٥, and ٠.١) for parameters (γ_1, γ_2 and γ_3) respectively.

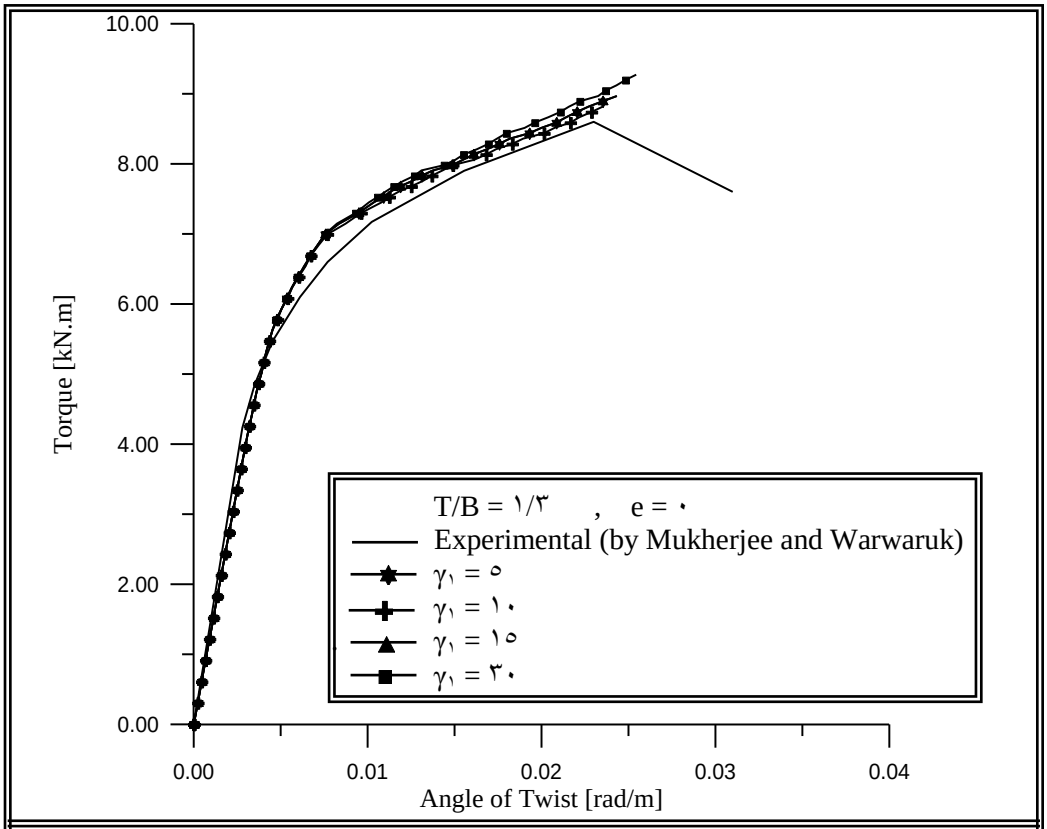

Fig. (٥-٢٨): Effect of Tension Stiffening Parameter (γ_1) on the Torque – Twist Behavior of Beam (V١٠٢) (case two)

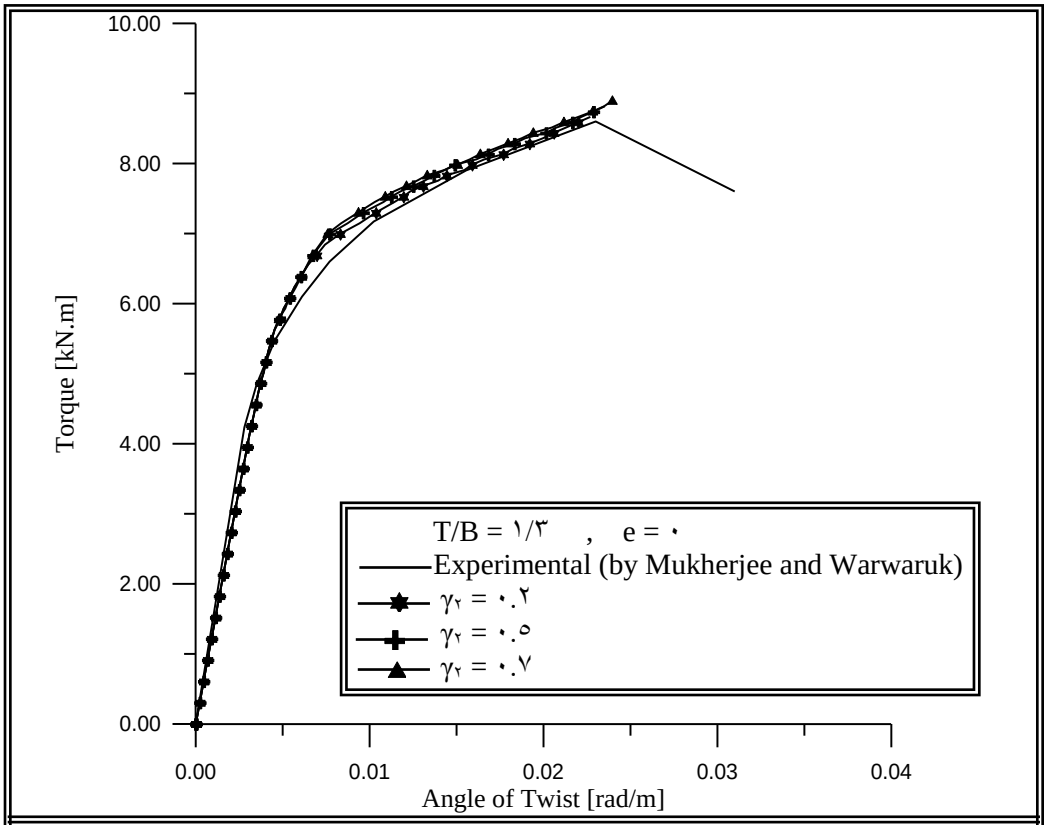

Fig. (٥-٢٩): Effect of Tension Stiffening Parameter (γ_2) on the Torque – Twist Behavior of Beam (V١٠٢) (case two)

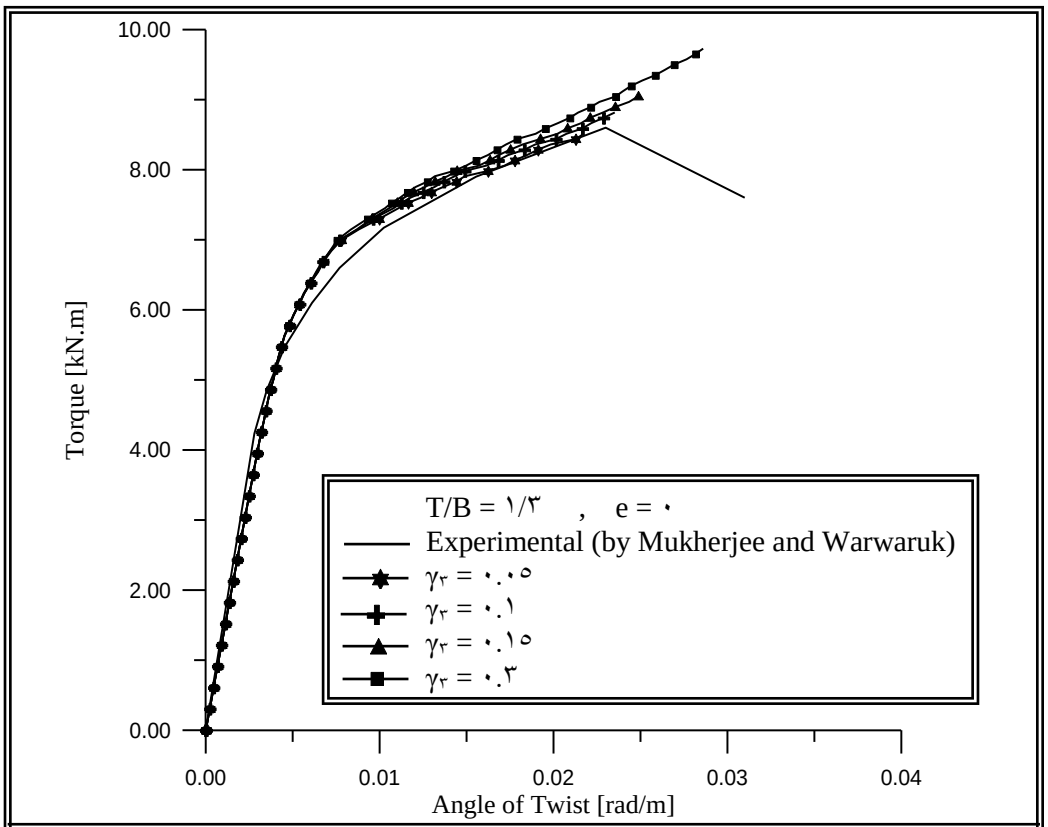

Fig. (٥-٣٠): Effect of Tension Stiffening Parameter (γ_3) on the Torque – Twist Behavior of Beam (V١٠٢) (case two)

٥.٤.٣ Effect of Poisson's Ratio (υ)

The beam (V١٠٢) was analyzed using three different values of Poisson's ratio. These values are (٠.١٥, ٠.٢, and ٠.٣). Figure (٥-٣١) shows that no considerable difference is noticed in torque-twist response and ultimate capacity of the tested beam for Poisson's ratio equal to (٠.١٥ and ٠.٢) but the value (٠.٣) gives decreasing ultimate capacity of the tested beam. The best value of Poisson's ratio was set equal to (٠.٢) for beams of series (VA) and (VB). The same value of Poisson's ratio was used by many researchers who analyzed reinforced and prestressed concrete beams under torsion and combined bending and torsion [٥,٦,١٥,٤٤].

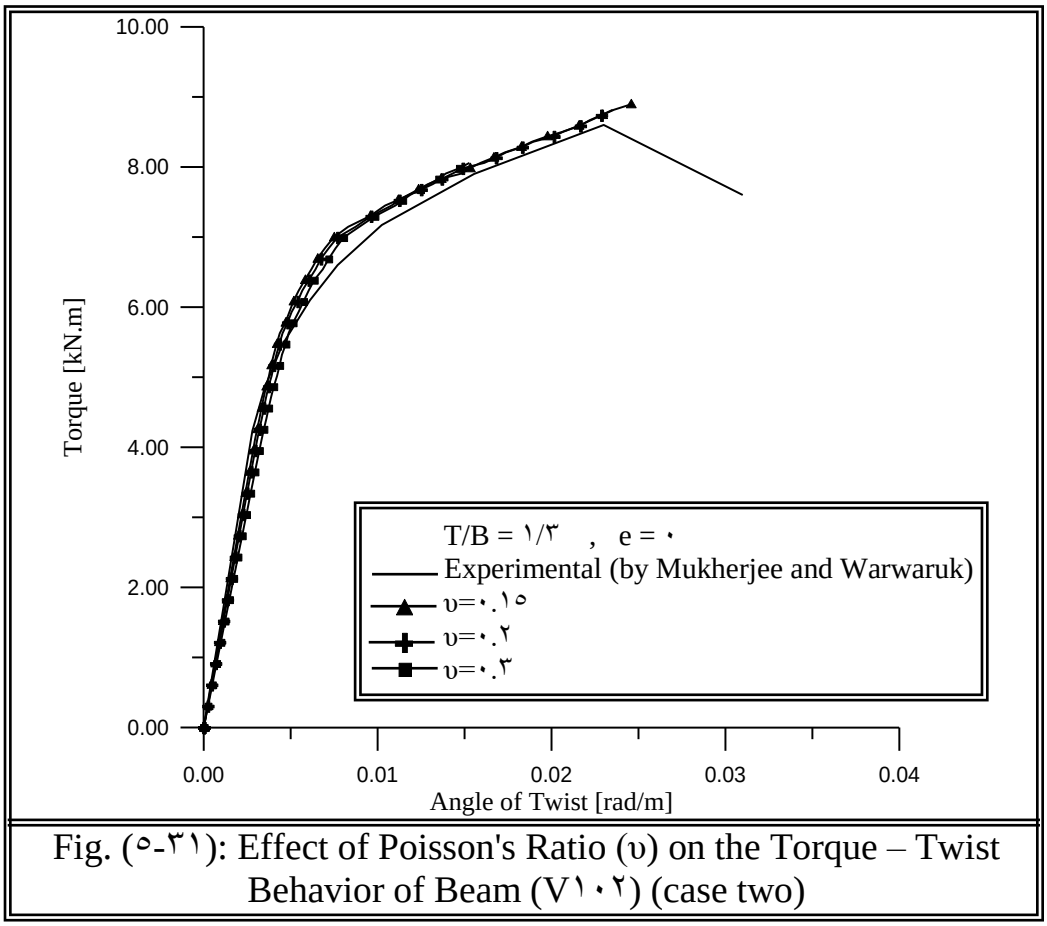

Fig. (٥-٣١): Effect of Poisson's Ratio (υ) on the Torque – Twist Behavior of Beam (V١٠٢) (case two)

٥.٤.٤ Effect of Compressive Strength Reduction Parameter ($k_١$)

Four numerical tests have been carried out on the beams (V١٠٢), (V١٠٣), (V١٠٤), (V١٠٥), and (V١٠٧) with different values of ($k_١$) in order to study the effect of compressive strength reduction parameter ($k_١$). For each test the parameter ($k_١$) was set equal to (٠.٧), (٠.٥), (٠.٣), and (٠.٠) (i.e. The compressive strength reduction phenomena is not activated). Figure (٥-٣٢) shows no considerable effect of ($k_١$) on the overall torque – twist response and small effect on the ultimate torsional capacity of beam (V١٠٢). The best fit of beam (V١٠٢) to the experimental results is obtained when ($k_١$) set equal to (٠.٥). The results of analysis to study the effect of the parameter ($k_١$) on the torque – twist behavior of beam (V١٠٣) explain that the parameter ($k_١$) has more effect on the torque – twist response and ultimate torsional capacity than in beam (V١٠٢), and the best value of the parameter ($k_١$) equal to (٠.٧). The effect of the parameter ($k_١$) increased in beams (V١٠٤) and (V١٠٥) that were tested with four different values of ($k_١$). The result of the (V١٠٥) beam is illustrated in figure (٥-٣٣), which shows a strongly effect of the parameter ($k_١$) on the post cracking response and ultimate torsional capacity of beam (V١٠٥). The best fit of the parameter ($k_١$) to the experimental torque – twist curve is obtained for ($k_١$) equals to (٠.٥) for the two beams. No significant effect of the parameter ($k_١$) on the ultimate torque of beam (V١٠٧). The best fit to the experimental results is obtained when the parameter ($k_١$) set equal to (٠.٥). The results of the tested beams to study the effect of the reduction compressive strength parameter ($k_١$) indicated that the parameter ($k_١$) is more effective for beam with high (T/B) ratio, and can be used a reduction compressive strength parameters ($k_١$) equal to (٠.٥) with an acceptable error for all beams of series (VA) and (VB).

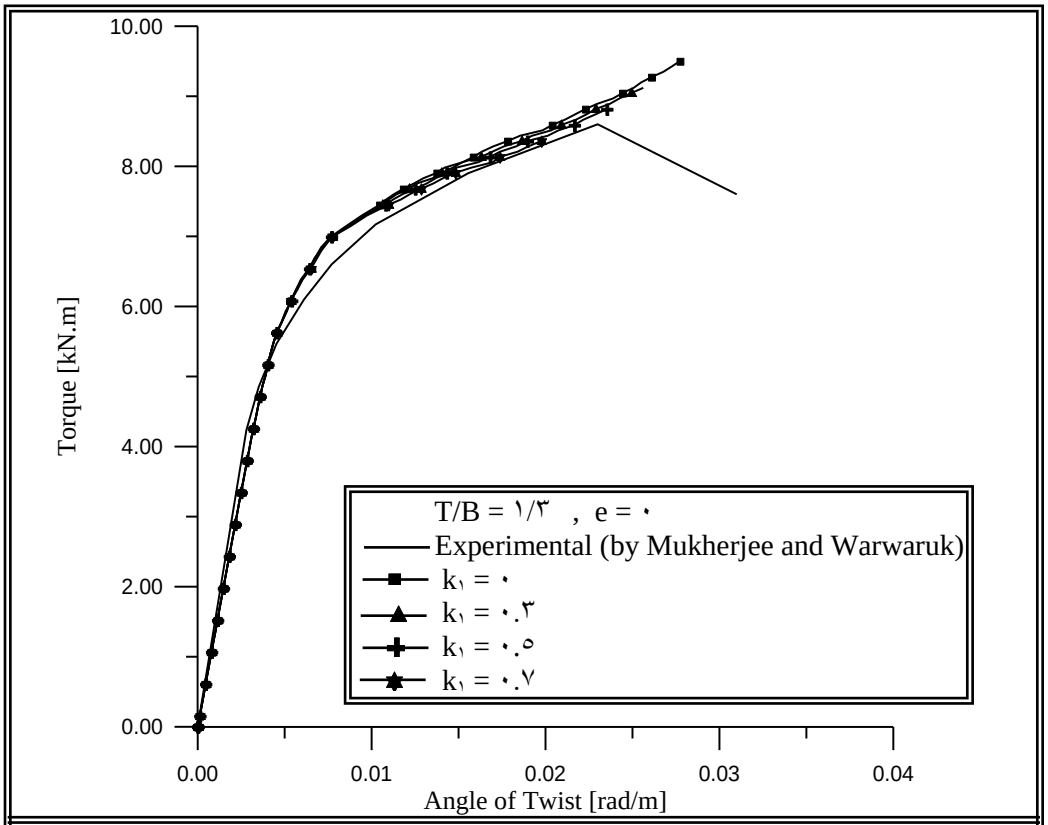

Fig. (٥-٣٢): Effect of the Degradation of Concrete Compressive Strength (k١) on the Torque–Twist Behavior of Beam (V١٠٢)

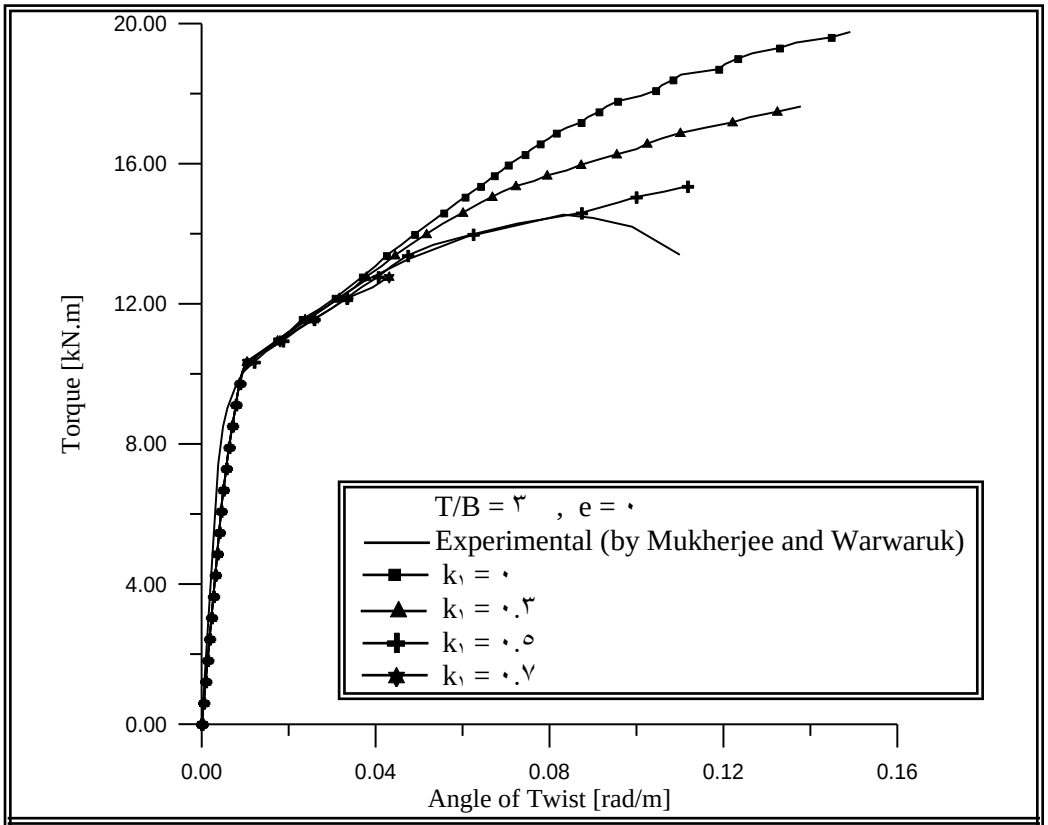

Fig. (٥-٣٣): Effect of the Degradation of Concrete Compressive Strength (k١) on the Torque –Twist Behavior of Beam (V١٠٥)

٥.٤.٥ Effect of Amount of Prestressing Steel (A_{ps})

The effect of the amount of prestressing steel (A_{ps}) on the torque-twist behavior of beams (V١٠٢), (V١٠٣), (V١٠٤), (V١٠٥), and (V١٠٧) are examined by three numerical tests for each beam. These tests contain different values of amount of prestressing steel (A_{ps}), these values are (٥١.٦, ٧٠, and ٩٣) mm^2 in addition to the original area of prestressing steel (٣٧.٥) mm^2. The increasing of amount of prestressing steel causes an increasing in prestressing forces with the same allowable stress ($f_{se} = \frac{p_e}{A_{ps}}$). The figures (٥-٣٤), and (٥-٣٥) that represent the torque – twist curve of beams (V١٠٢), and (V١٠٥) respectively show that increase the amount of prestressing steel increases the stiffness, the cracking loads and the ultimate capacities of the tested beams. The results and the increasing ratio in the ultimate torsional capacity are listed in table (٥-٨). From the results, it is clear that increase the amount of prestressing steel is more effective for beams with low torsion to bending moment ratio (T/B) as shown in figure (٥-٣٦).

Table (٥-٨) : Predicted Ultimate Torque for Different Amount of Prestressing Steel for (VA) Series Beams

Beam	T/B	Ultimate Torque (kN.m)				$\frac{T_{51.6}-T_{37.5}}{T_{37.5}}$	$\frac{T_{70}-T_{37.5}}{T_{37.5}}$	$\frac{T_{93}-T_{37.5}}{T_{37.5}}$
		$T_{٣٧.٥}$	$T_{٥١.٦}$	$T_{٧٠}$	$T_{٩٣}$			
V١٠٢	١/٣	٨.٨٢	٩.٥	١٠.١٩	١٠.٦٤	٧.٧١ %	١٥.٥٣ %	٢٠.٦٣ %
V١٠٣	٣/٤	١٣.٢٨	١٤.١٤	١٤.٨٨	١٥.٢٥	٦.٤٨ %	١٢.٠٥ %	١٤.٨٣ %
V١٠٤	٤/٣	١٥.٤٣	١٦.١١	١٦.٩٥	١٧.٧٩	٤.٤١ %	٩.٨٥ %	١٤.٧١ %
V١٠٥	٣	١٥.٣٥	١٥.٦٦	١٥.٩٦	١٦.٨٧	٢.٠٢ %	٣.٩٧ %	٩.٩ %
V١٠٧	١/٧	٤.٠٦	٤.٤٣	٤.٧٢	٤.٧٩	٩.١١ %	١٦.٢٥ %	١٨ %

where :
$T_{٣٧.٥}$: ultimate torque when using area of prestressing steel equal to ٣٧.٥mm^2.
$T_{٥١.٦}$: ultimate torque when using area of prestressing steel equal to ٥١.٦mm^2.
$T_{٧٠}$: ultimate torque when using area of prestressing steel equal to ٧٠ mm^2 .

$T_{٩٣}$: ultimate torque when using area of prestressing steel equal to ٩٣ $mm^{٢}$.

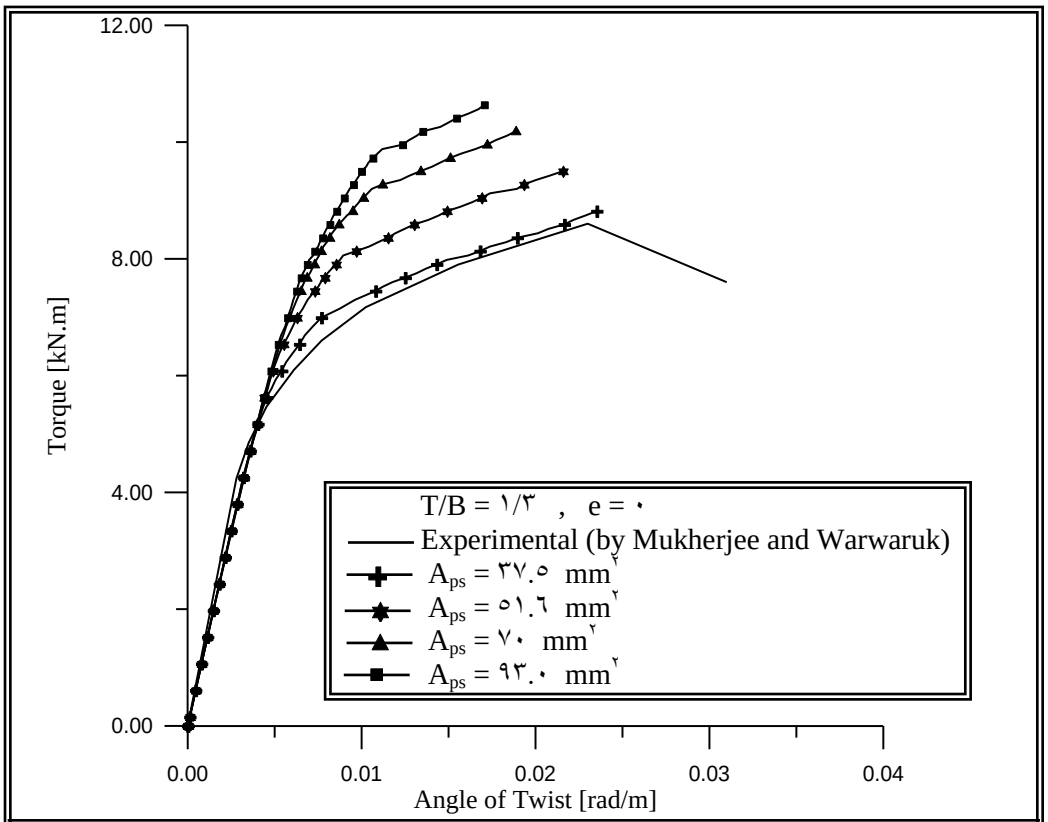

Fig. (٥-٣٤): Effect of the Amount of Prestressing Steel on the Torque–Twist Behavior of Beam (V١٠٢)

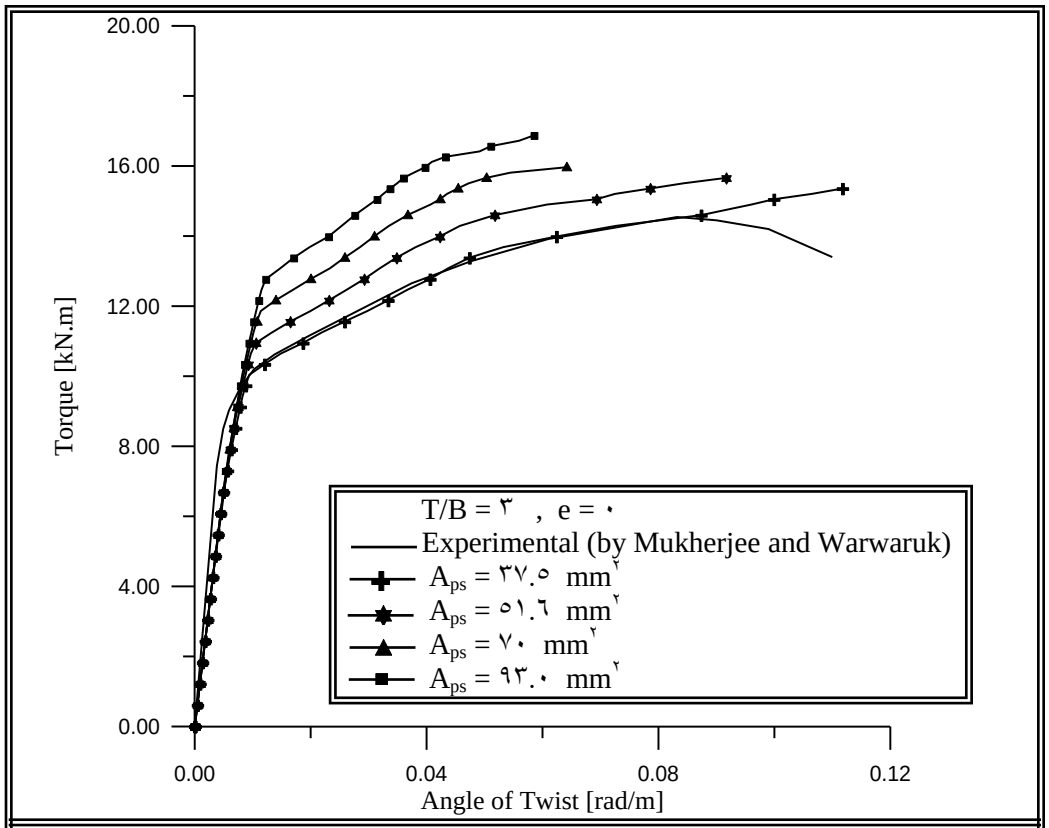

Fig. (٥-٣٥): Effect of the Amount of Prestressing Steel on the Torque–Twist Behavior of Beam (V١٠٥)

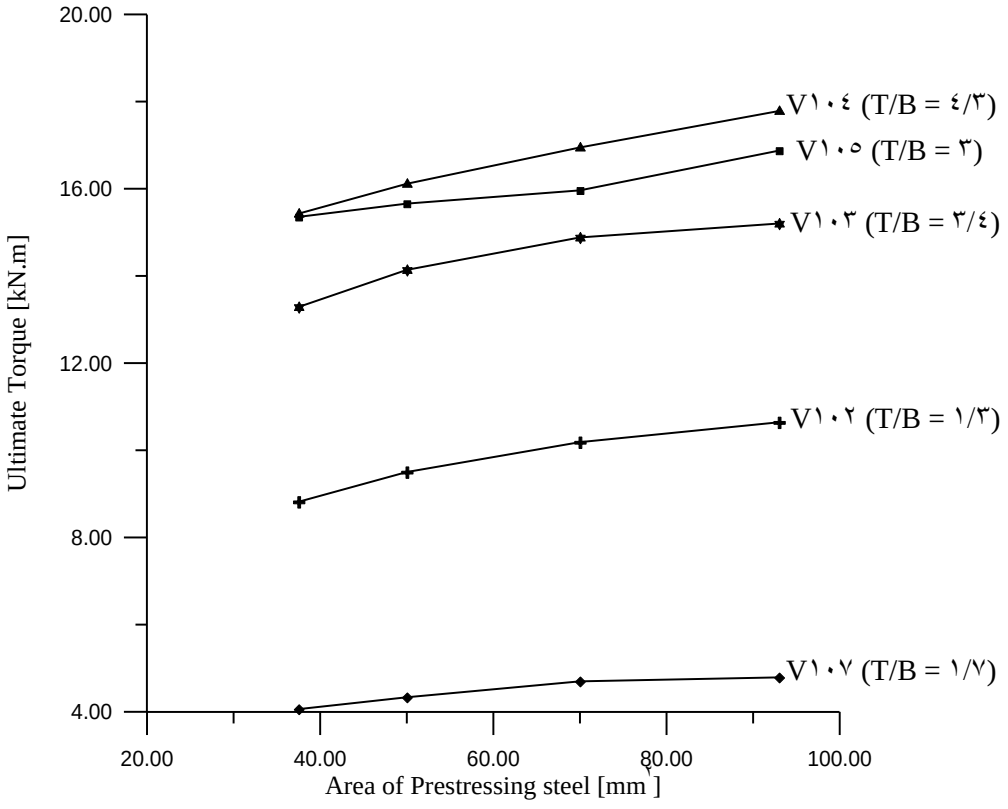

Fig. (٥-٣٦): Effect of the Amount of Prestressing Steel on the Ultimate Torque of Series (VA) Beams (e = ٠)

٥.٤.٦ Effect of Amount of Longitudinal and Transverse Reinforcement

The beams (V١٠٢), (V١٠٣), (V١٠٤), (V١٠٥), and (V١٠٧) are tested under different amounts of longitudinal reinforcement to study the influence of longitudinal reinforcement on the torque – twist behavior and ultimate torque capacity of the tested beams. In each beam, the amount of longitudinal reinforcement (A_l) increases in a uniform percentage (١.٢٥A_l (٩٠ mm^2), ١.٥A_l (١٠٨ mm^2) and ٢A_l (١٤٤ mm^2)), in addition to the actual amount of longitudinal reinforcement (A_l = ٧٢ mm^2). Figures (٥-٣٧) and (٥-٣٨) illustrate the effect of the longitudinal reinforcement on the

torque – twist curve of beams V١٠٢(T/B = ١/٣) and V١٠٥(T/B = ٣) respectively.

The results of all tests of the selected beams are listed in table (٥-٩). These results show that the effect of increasing the longitudinal reinforcement is more effective in ultimate torque capacity for beams (V١٠٢) and (V١٠٧) (in these beams torsion to bending moment ratio is low).

Also, it is noted that a small increase in torsional capacity for beam (V١٠٥) which has a high torsion to bending moment ratio (T/B = ٣). Thus, the effect of the longitudinal reinforcement on the ultimate torque capacity is not constant for all beams of series (VA). figure (٥-٣٩) shows that the increasing in the ultimate torque depend on the (T/B) ratio.

Four numerical tests with amount of transverse reinforcement (A_v) equal to (١.٢٥A_v, ١.٥A_v, ٢A_v, and ٢.٥A_v) have been carried out in order to explain the effect of transverse reinforcement.

Figures (٥-٤٠) and (٥-٤١) show the effect of the variation of the amount of transverse reinforcement on the torque – twist curve of beams (V١٠٢) and (V١٠٥) respectively. The results of the numerical tests that are listed in table (٥-١٠), show that a high increasing in the ultimate torque for beams (V١٠٤) and (V١٠٥) where these beams having a high torsion to bending moment ratio (T/B), and this increase in torsional capacity decreases when the torsion decreases to bending moment ratio. The effect of the amount of transverse steel bars on the ultimate torque is shown in figure (٥-٤٢).

Beam	T/B	Ultimate Torque (kN.m)				$\frac{T_{90}-T_{72}}{T_{72}}$	$\frac{T_{108}-T_{72}}{T_{72}}$	$\frac{T_{144}-T_{72}}{T_{72}}$
		$T_{٧٢}$	$T_{٩٠}$	$T_{١٠٨}$	$T_{١٤٤}$			
V١٠٢	١/٣	٨.٨٢	٩.٠٥	٩.٣٥	٩.٨٨	٢.٦١ %	٦ %	١٢.٠١ %
V١٠٣	٣/٤	١٣.٢٨	١٣.٦١	١٣.٩٢	١٤.٠٣	٢.٤٨ %	٤.٨٢ %	٥.٦٥ %
V١٠٤	٤/٣	١٥.٤٣	١٥.٧٣	١٥.٩٦	١٦.٢٢	١.٩٤ %	٣.٤٣ %	٥.١٢ %
V١٠٥	٣	١٥.٣٥	١٥.٦١	١٥.٧٥	١٥.٨١	١.٦٩ %	٢.٦ %	٣ %
V١٠٧	١/٧	٤.٠٦	٤.١٧	٤.٣٢	٤.٥٧	٢.٧١ %	٦.٤ %	١٢.٥٦ %

Table (٥-٩) : Predicted Ultimate Torque for Different Amount of Longitudinal Steel for (VA) Series Beams

where :
$T_{٧٢}$: ultimate torque when use area of longitudinal steel equal to ٧٢ mm^2.
$T_{٩٠}$: ultimate torque when use area of longitudinal steel equal to ٩٠ mm^2.
$T_{١٠٨}$: ultimate torque when use area of longitudinal steel equal to ١٠٨ mm^2.
$T_{١٢٦}$: ultimate torque when use area of longitudinal steel equal to ١٤٤ mm^2.

Table (٥-١٠) : Predicted Ultimate Torque for Different Amount of Transverse Steel for (VA) Series Beams

Beam	T/B	Ultimate Torque (kN.m)					$\frac{T_1-T_o}{T_o}$	$\frac{T_2-T_o}{T_o}$	$\frac{T_3-T_o}{T_o}$	$\frac{T_4-T_o}{T_o}$
		T_o	$T_١$	$T_٢$	$T_٣$	$T_٤$				
V١٠٢	١/٣	٨.٨٢	٨.٩٧	٩.١٢	٩.٣٥	٩.٥٨	١.٧ %	٣.٤ %	٦ %	٨.٦٢ %
V١٠٣	٣/٤	١٣.٢٨	١٣.٨٢	١٤.٠٣	١٤.٥٦	١٤.٧٨	٤.١ %	٥.٦٥ %	٩.٦٤ %	١١.٣ %
V١٠٤	٤/٣	١٥.٤٣	١٦.٤٩	١٧.٧٩	١٩.٦٩	٢٠.٢٩	٦.٨٧ %	١٥.٣ %	٢٧.٦ %	٣١.٥ %
V١٠٥	٣	١٥.٣٥	١٦.٥٧	١٧.١٣	١٩.٣٧	٢٠.٨٣	٧.٩٥ %	١١.٦ %	٢٦.٢ %	٣٥.٧ %

where :
T_o : ultimate torque when use area of transverse steel equal to (٣٢ and ٧٢) mm^2 inside and outside the gage length respectively.
$T_١$: ultimate torque when use area of transverse steel equal to (٤٠ and ٩٠) mm^2 inside and outside the gage length respectively.
$T_٢$: ultimate torque when use area of transverse steel equal (٤٨ and ١٠٨) mm^2 inside and outside the gage length respectively.

T_3 : ultimate torque when use area of transverse steel equal to (٦٤ and ١٤٤) mm^2 inside and outside the gage length respectively.

T_4 : ultimate torque when use area of transverse steel equal to (٨٠ and ١٨٠) mm^2 inside and outside the gage length respectively.

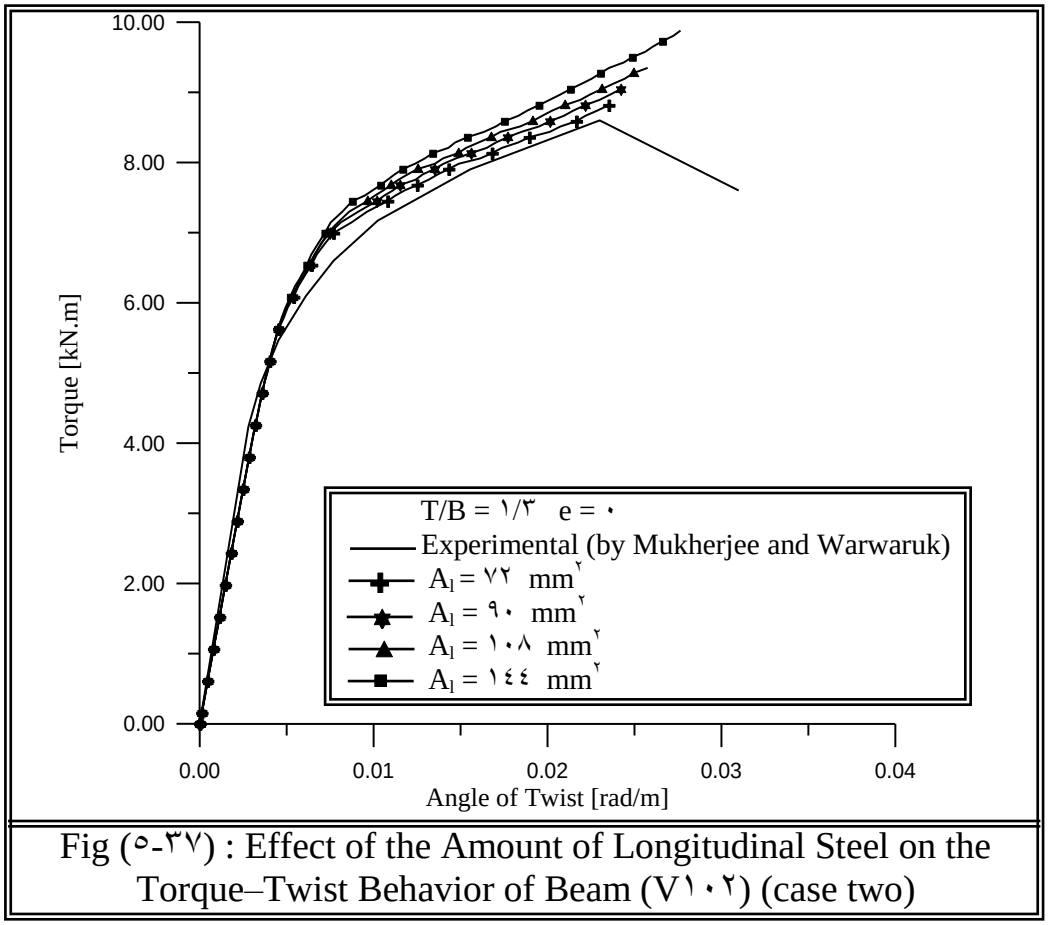

Fig (٥-٣٧) : Effect of the Amount of Longitudinal Steel on the Torque–Twist Behavior of Beam (V١٠٢) (case two)

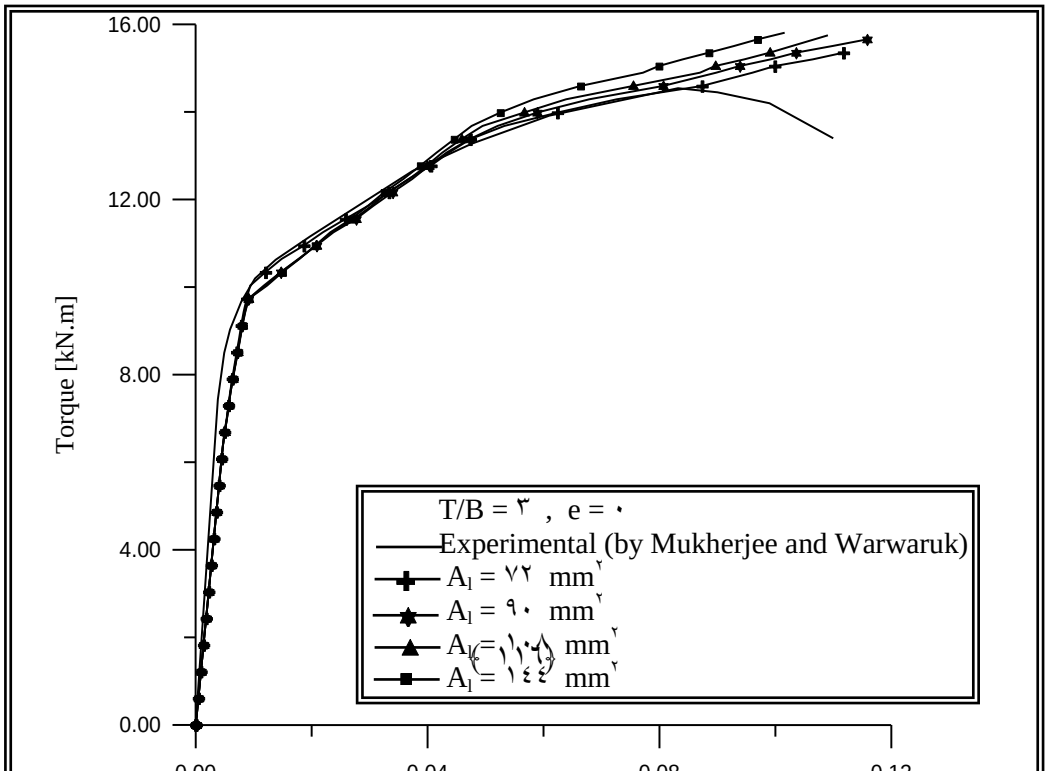

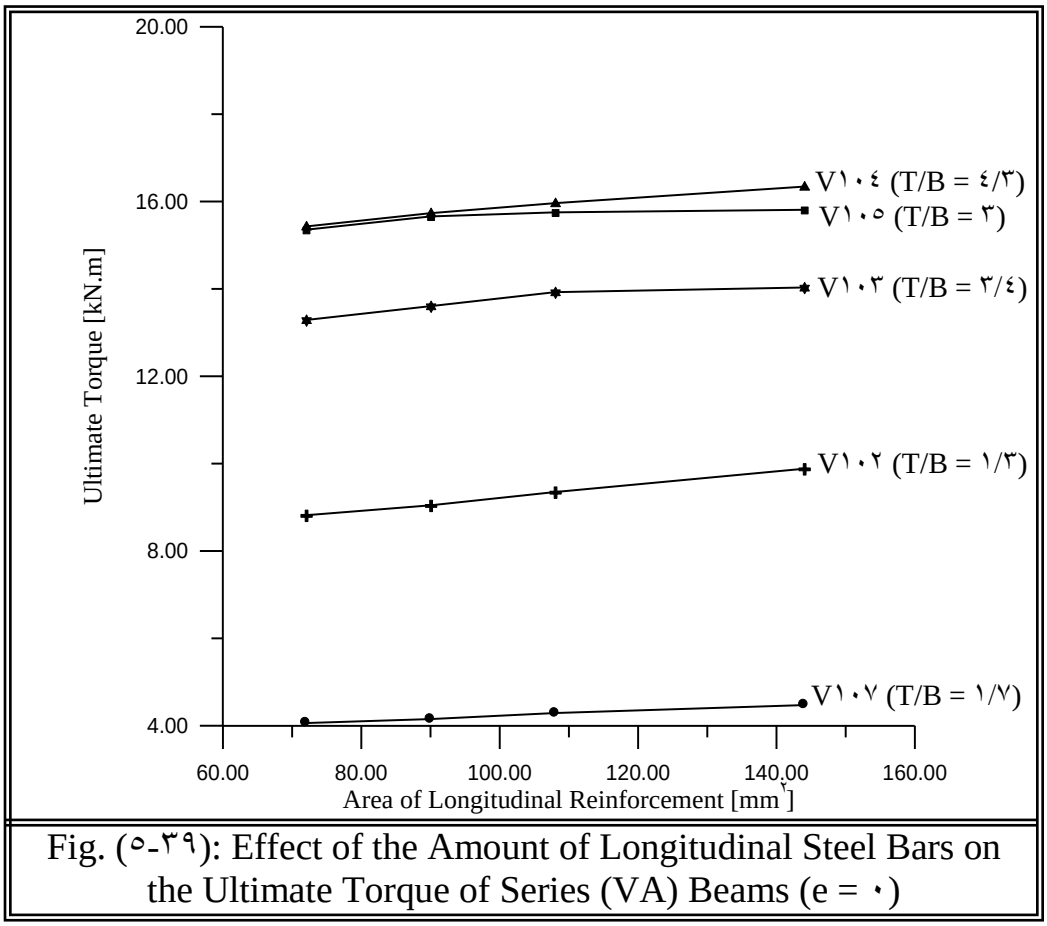

Fig. (٥-٣٩): Effect of the Amount of Longitudinal Steel Bars on the Ultimate Torque of Series (VA) Beams (e = ٠)

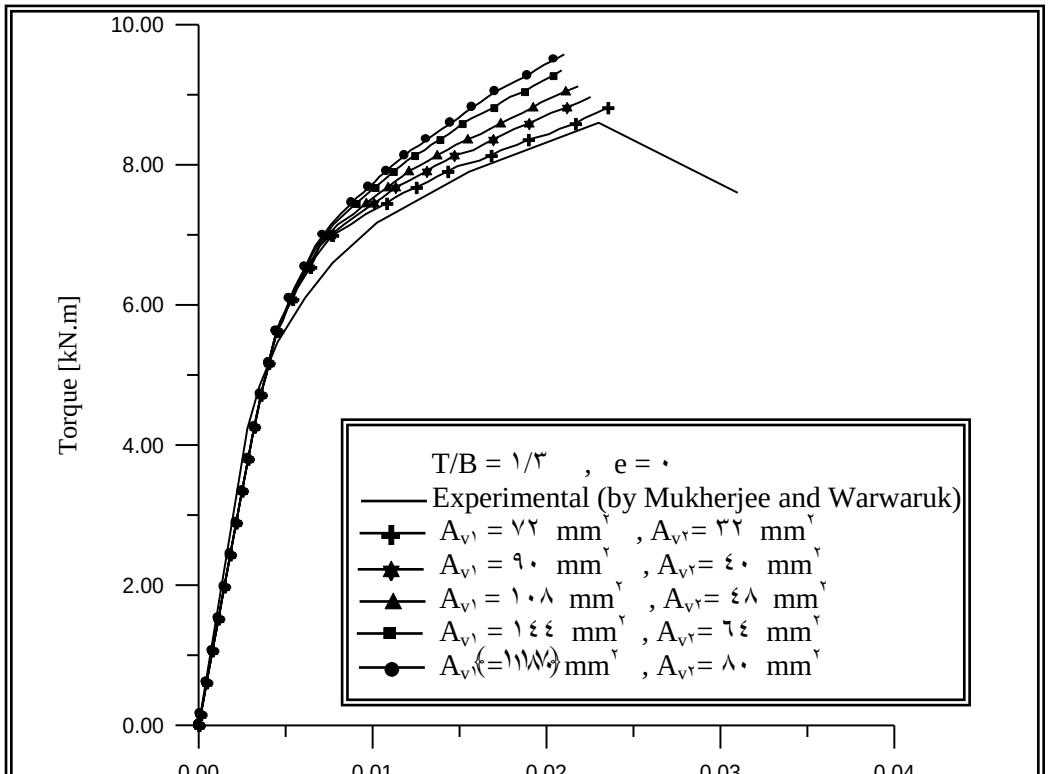

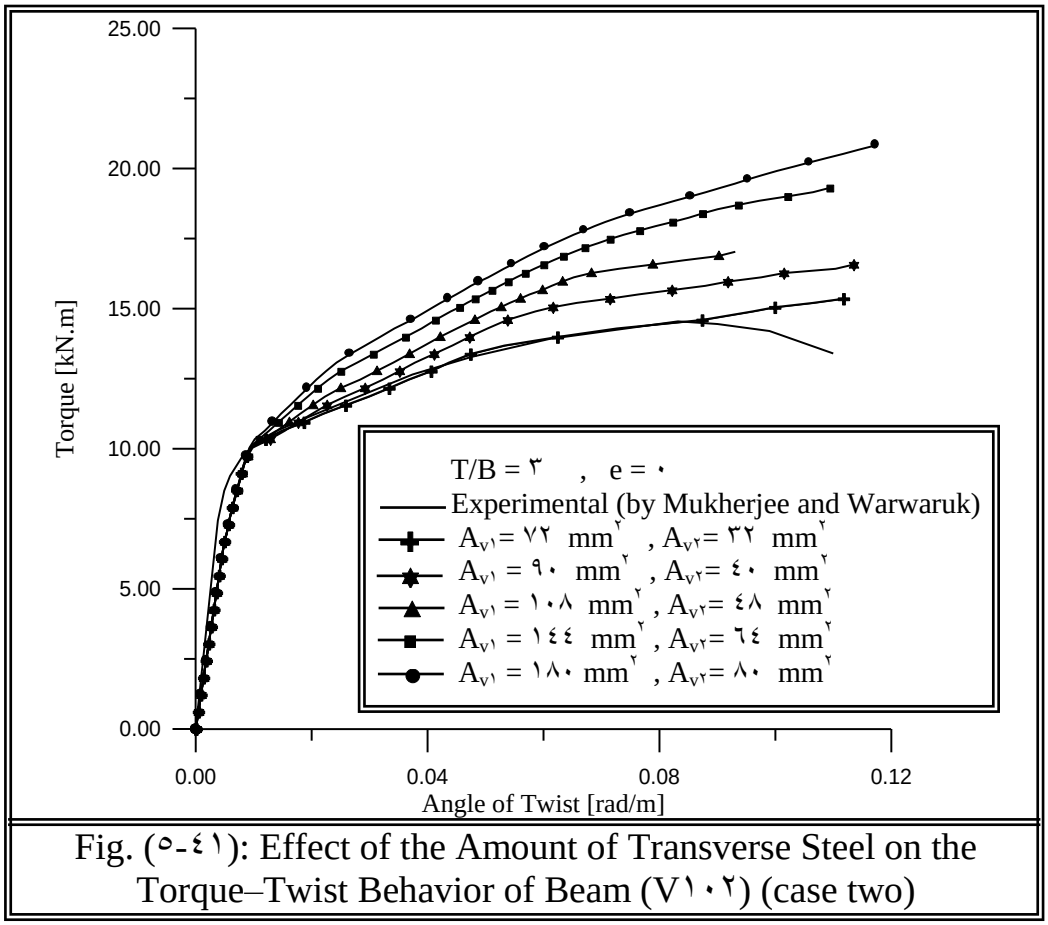

Fig. (٥-٤١): Effect of the Amount of Transverse Steel on the Torque–Twist Behavior of Beam (V١٠٢) (case two)

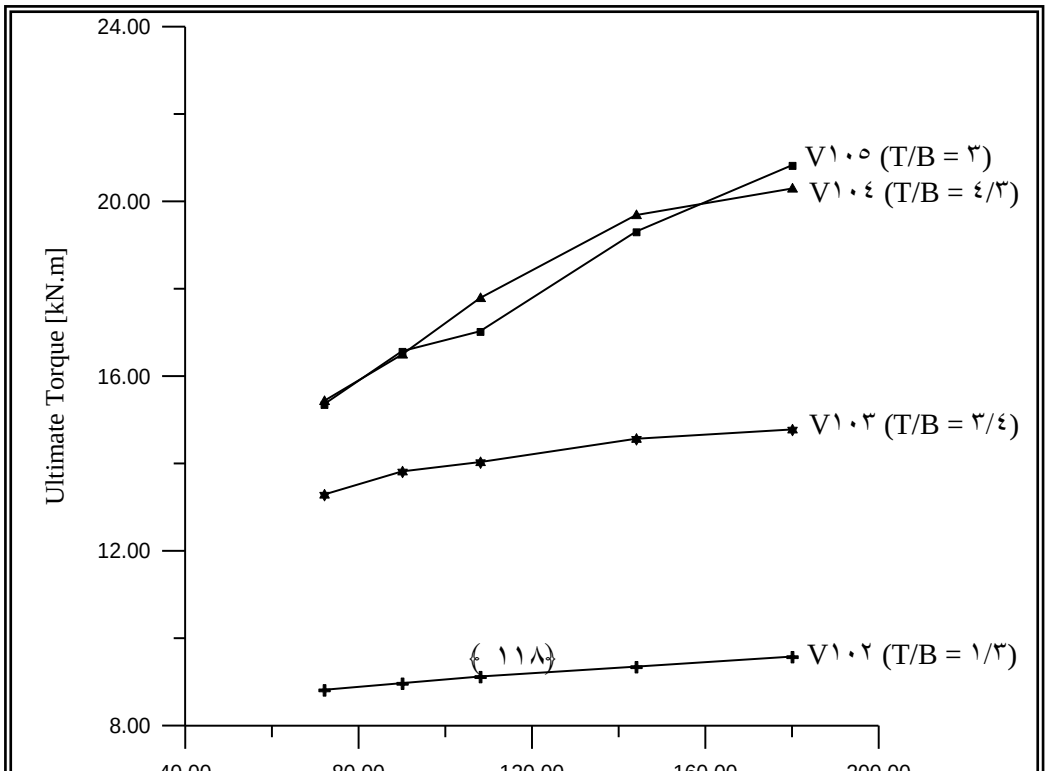

٥.٤.٧ Effect of (T/P) Ratio on the Ultimate Capacity

In order to study the effect of torque to transverse load (T/P) ratio on the ultimate capacity of concentrically beam (V١٠٢) which was subjected to combined shear, bending and torsion, many values of the ratio (T/P) have been considered. The results of the analysis are tabulated in table (٥-١١), these results explain that no considerable difference in the ultimate torque when the torque to transverse load (T/P) ratio is equal or above (٢) as shown in figure (٥-٤٣). The effect of (T/P) ratio on the ultimate load of beam (V١٠٢) is illustrated in figure (٥-٤٤). This figure shows a small difference in the ultimate load for (T/P) ratio range from (٢) to (٩). Below (T/P) ratio of (٢), a high increase in the ultimate load is noticed with decreasing (T/P) ratio . From the results it is clear that the effect of concentrated load (P) on the ultimate torque is negligible for a combination load (T/P) equal or above (٢), and the torque (T) has a small effect on the ultimate load for a combination load (T/P) range from (٢) to (٩).

Table (٥-١١) : Ultimate Torque, and Ultimate Load for Different Values of (T/P) Ratio of Beam (V١٠٢)

T/P [kN.m/kN]	T [kN.m]	P[kN]
١/١٠	٨.٢٤	٨٢.٤
١/٩	٨.٨٩	٨٠.٠١
١/٨	٩.٦٤	٧٧.١٢
١/٧	١٠.٥٤	٧٣.٧٨
١/٦	١١.٦١	٦٩.٦٦
١/٥	١٢.٧٧	٦٣.٨٥
١/٤	١٤.١٤	٥٦.٥٦
١/٣	١٤.٤٤	٤٣.٣٢
١/٢	١٥.١	٣٠.٢
١	١٥.٢١	١٥.٢١
٢	(١٥١.٠٣)	٧.٥١
٣	١٤.٩٨	٤.٩٩
٤	١٤.٩٨	٣.٧٥

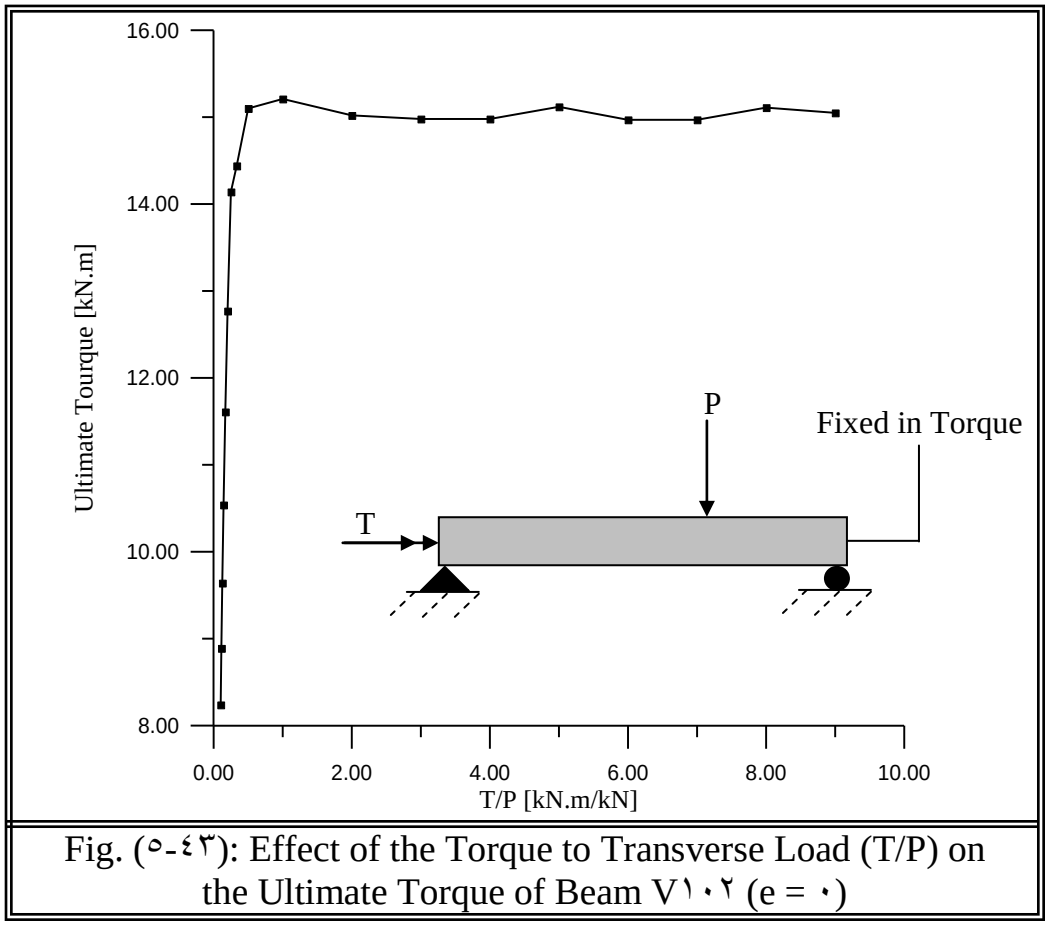

Fig. (٥-٤٣): Effect of the Torque to Transverse Load (T/P) on the Ultimate Torque of Beam V١٠٢ (e = ٠)

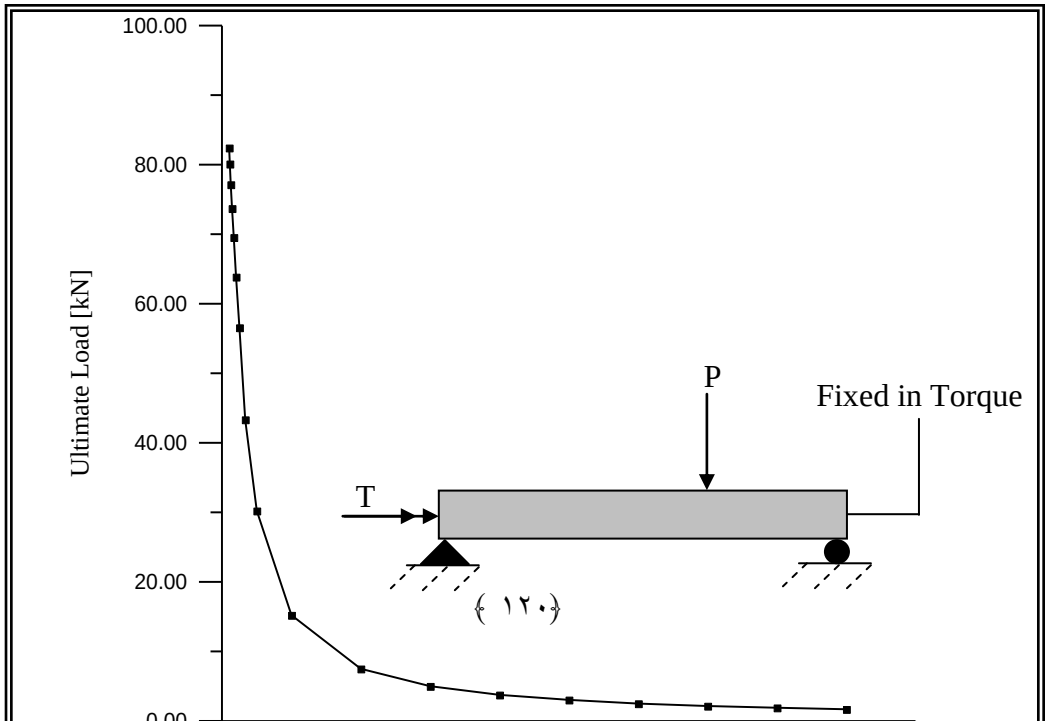

Chapter Six

Conclusions and Recommendations for Future Works

٦.١ Introduction

The following conclusions are drawn with regard to the results of the present finite element analysis of prestessed concrete beams subjected to pure torsion and combined loads of shear, bending and torsion described in the previous chapter, are presented in this chapter. The suggestions for the future works are also presented in this chapter.

٦.٢ Conclusions

١. The effect of transverse load (P) on the ultimate torque capacity (T) is negligible for torque to transverse load ratio (T/P) equal to or above (٢).

٢. It was found that the existing of prestressing force on reinforced concrete beams subjected to combined shear, bending and torsion increases the torsional stiffness and the ultimate torque capacity of these beams. The increasing in the ultimate torque capacity depends on the torque to bending moment ratio (T/B). The prestressing force causes an increasing in the ultimate torque to about (٤٣.٥٪) for (T/B = ١/٧), while for (T/B = ٣) the increasing in the ultimate torque is about (٧.٤٢ %).

٣. The increasing of the amount of prestressing steel decreases the ductility and increases the ultimate torque of prestressed concrete beams subjected to combined shear, bending and torsion in different range and this depends on the torque to bending moment ratio (T/B). The increasing in ultimate torque was (٢٠.٦٣٪) for (T/B = ١/٣) and (٩.٩٪) for (T/B = ٣) for the considered cases.

٤. For beams with low torque to bending moment ratio (T/B), the increase in the longitudinal reinforcement increase the ductility and the ultimate torque capacity. However, for beams with high (T/B) ratio, the change in the amount of longitudinal reinforcement has a small effect on the ultimate torque capacity and ductility. The increase in the ultimate torque capacity is about (١٢.٥٦٪ - ٣٪) for (T/B = ١/٧) and (T/B = ٣) respectively, when the amount of ordinary longitudinal reinforcement is twice.

٥. The transverse reinforcement has a significant effect for beams with high torque to bending moment ratio (T/B). When the amount of transverse reinforcement increases to twice, the ultimate torque capacity increase to about (٣٥.٧٪) for beam with (T/B = ٣) for the considered cases.

٦. The results of finite element analysis indicate that the tension stiffening parameters ($\alpha_١$ and $\alpha_٢$) have a large effect on the torque – twist behavior and the ultimate torque capacity of prestressed concrete beams under pure torsion and combined shear, bending and torsion. While, the shear retention parameters ($\gamma_١$, $\gamma_٢$, and $\gamma_٣$) have small effects on the behavior and ultimate torque capacity.

٧. The best value of the reduction compressive strength parameter ($k_١$) is (٠.٥) for prestressed concrete beams subjected to combined shear, bending and torsion. So, it is recommended to be used for other similar cases.

٨. The three dimensional nonlinear finite element model and the proposed simulation of the prestressing as effective stress and strain at sampling points along the prestressing tendons that used in the present study are capable to predict the behavior of prestressed concrete beams subjected to pure torsion and for combined shear, bending and torsion. The results of the analysis are in good agreement with the experimental results, with a difference range of (٠.٥٪ - ٨.٤٪) for ultimate torque.

٦.٣ Recommendations for Future Works

١. Analysis of prestressed concrete beams containing steel fiber under combined shear and torsion could be carried out by modifying the material model used in the present study.

٢. Analysis of prestressed concrete beams under combined shear and torsion with inclusion of the effect of shrinkage, creep of concrete and the relaxation of prestressing steel.

٣. Studying the effect of transverse opening in prestressed concrete beams subjected to combined shear, bending, and torsion.

٤. More numerical research works are required for studying the interaction between shear, bending, and torsion for different shapes of prestressed concrete beams.

LIST OF FIGURES

List of Tables

References

١) Abdel-Rahman, H.H., and Hinton, E., ***"Nonlinear Finite Element Analysis of Reinforced Concrete Stiffened and Cellular Slabs"***, Journal of Computer and Structures, Vol.٢٣, No. ٣, ١٩٨٦, pp. ٣٣٣-٣٥٠.

٢) Abul Hasanat, Wafa, F.F., and Akhtaruzzaman, A.A., ***"Prestressed Concrete Beams with Small Opening under Torsion"***, ASCE, Journal of Structural Engineering, Vol. ١١٤, No. ٧, July ١٩٨٨, pp. ١٦٢٦-١٦٤١.

٣) ACI Committee ٣١٨-٨٩, ***"Building Code Requirements for Reinforced Concrete"***, ACI Committee ٣١٨, American Concrete Institute, Detroit ١٩٨٩, ٣٥٣ pp.

٤) ACI Committee ٣١٨-٠٢, ***"Building Code Requirements for Structural Concrete (ACI ٣١٨M-٠٢) and Commentary (ACI ٣١٨RM-٠٢)"***, American Concrete Institute, Detroit ٢٠٠٢, ٤٤٣ pp.

٥) Al-Mousely, B.S.T., ***"Three Dimensional Nonlinear Finite Element Analysis for Steel Fiber Reinforced Concrete Beams Subjected to Combined Bending and Torsion"***, M.Sc. Thesis, University of Technology , ١٩٩٨.

٦) Al-Radi, S.N., ***"Three Dimensional Nonlinear Analysis of Reinforced Concrete Beams Subjected to Combined Shear and Torsion using Finite Element Method"***, M.Sc. Thesis, University of Basrah, ٢٠٠٢.

٧) Al-Shaarbaf, I.A.S., ***"Three Dimensional Non-Linear Finite Element Analysis of Reinforced Concrete Beam in Torsion"***, Ph.D. Thesis, University of Bradford, ١٩٩٠, ٣٢٠ pp.

٨) Belarbi, A., and Hsu, T.T., ***"Constitutive Laws of Softened Concrete in Biaxial Tension – Compression"***, ACI Structural J., Sec.-Oct. ١٩٩٥, pp. ٥٦٢-٥٧٣.

٩) Bishara, A., ***"Prestressed Concrete Beams under Combined Torsion, Bending and Shear"***, ACI Journal, July ١٩٦٩, pp. ٥٢٥-٥٣٨.

١٠) Cervenka, V., ***"A Constitutive Model for Reinforced Concrete"***, Journal of ACI, Vol. ٨٢, Nov.-Des. ١٩٨٥, pp. ٨٧٧-٨٨٢.

١١) Chen, W., ***"Plasticity in Reinforced Concrete"***, Mc Graw-Hill, New York, ١٩٨٢, ٤٦٣ pp.

١٢) Collins, M.P., and Mitchell, D., ***"Shear and Torsion Design of Prestressed and Non-Prestressed Concrete Beams"***, PCI Journal, September-October ١٩٨٠, pp. ٣٢-١٠٠.

١٣) Cowan, H.J., and Armstrong, S., ***"The Torsional Strength of Prestressed Concrete"***, Proceedings, World conference on prestressed concrete, University of California, Ags. ١٩٥٧, pp. ١٨-١-١٨-١٢.

١٤) Dawe, D.J., ***"Matrix and Finite Element Displacement Analysis of Structures"***, Claredon Press, Oxford, U.K. ١٩٨٤.

١٥) Diab, M.I.M., ***"Three-Dimensional Non-Linear Finite Element Analysis of High Strength Concrete Panels under Combined Loadings and Beams in Torsion"***, Ph.D. Thesis, University of Technology, ١٩٩٨, ١٨٢ pp.

١٦) Elwi, A.E., and Hrudey, T.M., ***"Finite Element Model for Curved Embedded Reinforcement"***, Journal of Engineering Mechanics, ASCE, April ١٩٨٩, pp. ٧٤٠-٧٥٤.

١٧) Gesund, H., Schnette, F.J., Buchana, G., and Gray, G., ***"Ultimate Strength in Combined Bending and Torsion in Concrete Beams Containing both Longitudinal and Transverse Reinforcement"***, Journal of ACI, Proceedings, Vlo.٦١, Dec.١٩٦٤, pp. ١٥٠٩-١٥٢١.

١٨) Ghalib, A.M.,***"Inelastic Finite Element Analysis of Prestressed Concrete Multi-Planer System"***, M.Sc. Thesis, University of Baghdad, ١٩٩٠.

١٩) Grace, N.F., and Abdel-Sayed, G., ***"Ductility of Prestressed Concrete Bridge Using CFRP Tendons"***, concrete int., Vol. ٢٠, No. ٦, ١٩٩٨, pp. ٢٥-٣٠.

٢٠) Grestle, K.H., ***"Behavior of Concrete under Multiaxial Stress State"***, Journal of the Engineering Mechanics Divisions, ASCE, Vol. ١٠٦, No. EM٦, December, ١٩٨٠, pp. ١٣٨٣-١٤٠٣.

٢١) Hartl, H., and Engamal, A., ***"Nonlinear Modeling of Prestressed Structures Based on a Continuum Mechanics Approach"***, Heft٤٥/September ٢٠٠٠, Vienna, pp. ٨٧-٩٦.

٢٢) Henry, L., and Zia, P., ***"Prestressed Beams in Torsion, Bending, and Shear"***, Journal of the Structural Division, Proceedings of the American Society of Civil Engineering, Vol.١٠٠, No. ST٥, May ١٩٧٤, pp. ٩٣٣-٩٥٢.

٢٣) Hinton, E., ***"Numerical Methods and Software for Dynamic Analysis of Plates and Shells"***, Pineridge Press, Swansea, U.K. ١٩٨٨, ٢٦٠ pp.

٢٤) Hsu, T.T.C., ***"Softening of Concrete in Torsional Members-Prestrssed Concrete"***, Journal of American Concrete Institute, September-October ١٩٨٥, pp. ٦٠٣-٦١٥.

٢٥) Hsu, T.T.C., ***"Torsion of Structural Concrete-Behavior of Plain Concrete Sections",*** Torsion of Structural Concrete, SP-١٨, American Concrete Institute, Detroit, ١٩٦٨, pp. ٢٠٣-٢٣٨.

٢٦) Hsu, T.T.C., ***"Torsion of Structural Concrete-Behavior of Reinforced Concrete Rectangular Members"***, Torsion of Structural Concrete, SP-١٨, American Concrete Institute, Detroit, ١٩٦٨, pp. ٢٦١-٣٠٦.

٢٧) Humphreys, R., ***"Torsion of Prestressed Concrete"***, the Structural Engineer (London), Vol.٣٥, No. ٦, June ١٩٥٧, pp. ٢١٣-٢٢٤.

٢٨) Irons, B.M., ***"Quadrature Rules for Brick Based Finite Elements"***, Int. J. of Numerical Method In Eng., Vol.٣, ١٩٧١, pp. ٢٩٣-٢٩٤.

٢٩) Janney, J.R., Hognestad, E., and McHenry, D., ***"Ultimate Flexure Strength of Prestressed and Conventionally Reinforced Concrete Beams"***, ACI Journal, Vol.٢٧, No. ٦, February, ١٩٥٦, pp. ٦٠١-٦٢٠.

٣٠) Kang Young-Jin and Scordelis Alexander, C., ***"Nonlinear Analysis of Reinforced Concrete Frames"***, Journal of Structural Division ASCE, Vol. ١٠٦, No. ST٢, February ١٩٨٠, pp. ٤٢-٥٥.

٣١) Kupfer, H.B., Hilsdorf, H.K., and Rusch, H., ***"Behavior of Concrete under Biaxial Stresses"***, Journal of ACI, Vol. ٦٦, No. ٨, August ١٩٦٩, pp. ٦٥٦-٦٦٦.

٣٢) Kwak, H.G., and Filippou, F.C., ***"Nonlinear F.E. Analysis of R/C Structures under Monotonic Loads"***, Journal of Computers and Structures, Vol. ٦٥, No. ١, ١٩٩٧, pp. ١-١٦.

٣٣) Lampert, P., and Thurliman, B., ***"Torsional Tests of Reinforced Concrete Beams"***, Report No. ٦٥٠٦-٢, Institute for Baustatik, Zurich, June ١٩٦٨.

٣٤) Lessig, N.N., ***"Determination of Carrying Capacity of Reinforced Concrete Elements with Rectangular Cross-Section Subjected to Flexural with Torsion"***, Concrete and Reinforced Concrete Institute, Moscow, No.٥, ١٩٥٩, pp. ٥-٢٨.

٣٥) Mattock, A.H., and Wyss, A.N., ***"Full-Scale Torsion, Shear, and Bending Tests of Prestressed I-Girders"***, PCI Journal, March-April ١٩٧٨, pp. ٢٢-٤١.

٣٦) Mitchell, D., and Collins, M.P., ***"Influence of Prestressing on Torsional Response of Concrete Beams"***, PCI Journal, May-June ١٩٧٨, pp. ٥٤-٧٣.

٣٧) Mukherjee, P.R., and Warwaruk, J., ***"Torsion, Bending, And Shear In Prestressed Concrete"***, Journal Of The Structural Division ASCE, Vol. ٩٧, No. ST٤, April ١٩٧١, pp. ١٠٦٣-١٠٧٩.

٣٨) Nilson, A.H., ***"Design of Prestressed Concrete"***, John Wiley and Sons, ١٩٨٧, ٥٨٥ pp.

٣٩) Pognani, T., Slater, J., Ameur-Mousa, R., and Boyukozturk, O., ***"A Nonlinear Three – Dimensional Analysis of Reinforced Concrete Based on Boundary Surface Model"***, Computer and Structure, Vol. ٤٣, No. ١, ١٩٩٢, pp. ١-١٢.

٤٠) Rahal, K.N., and Collins, M.P., ***"Effect of Thickness of Concrete Cover on Shear – Torsion Interaction"*** ACI Structural Journal, Vol. ٩٢, No. ٣, May-June ١٩٩٥, pp. ٣٣٤-٣٤٢.

٤١) Rausch, E., ***"Design of Reinforced Concrete in Torsion"***, Techniche Hochschule, Berlin, ١٩٢٩, Second Edition, ١٩٣٨, ٥٣ pp.

٤٢) Reeves, J.S., ***"Prestressed Concrete Tee Beams under Combined Bending and Torsion"***, Report TRA ٣٤٦, Cement and Concrete Association, London, Dec. ١٩٦٢, pp. ١-٢٥.

٤٣) Shaikh, A.F., and Branson, D.E., ***"Non-Tensioned Steel in Prestressed Concrete Beams"***, PCI Journal, February ١٩٧٠, pp. ١٤-٣٦.

٤٤) Shuber, M.S., ***"Nonlinear Finite Element Analysis of Prestressed Concrete Members under Torsion"***, M.Sc. Thesis, University of Kufa, ٢٠٠٢.

٤٥) Tasuji, M.E., Slate, F.O., and Nilson, A.H., ***"Stress – Strain Response and Fractured of Concrete in Biaxial Loading"***, J. of ACI, Vol. ٧٥, No. ٧, July ١٩٧٨, pp. ٣٠٦-٣١٢.

٤٦) Tawfieq, A.M., ***"Nonlinear Finite Element Analysis of Prestressed Concrete Beams"***, M.Sc. Thesis, University of Al-Nehrain, ٢٠٠٢.

٤٧) Yamaguchi, E., and Chen, W.F., ***"On Micro-Mechanics of Fracture and Constitutive Modeling of Concrete Materials"***, in Constitutive Laws for Engineering Materials: Theory and Application, Edited by Desai, C.S., Elsevier Science Publishing Co. , ١٩٨٧, pp. ٩٣٩-٩٤٧.

٤٨) Yan, X., Myers, J.J., and Nanni, A.,***"Assessment of Flexural Behavior of CFRP Prestressed Beams Subjected to Incremental Static Loading"***, ASCE Structure Congress ٢٠٠٠, Philadelphia, PA, ٢٠٠٠.

٤٩) Zia, P., ***"Torsional Strength of Prestressed Concrete Members"***, Journal of the American Concrete Institute, Proc. Vol. ٥٧, No. ١٠, April ١٩٦١, pp. ١٣٣٧-١٣٥٩.